Atmos. Chem. Phys., 21, 14789–14814, 2021 https://doi.org/10.5194/acp-21-14789-2021 © Author(s) 2021. This work is distributed under the Creative Commons Attribution 4.0 License.





Formation of condensable organic vapors from anthropogenic and biogenic volatile organic compounds (VOCs) is strongly perturbed by NO_x in eastern China

Yuliang Liu 1,2 , Wei Nie 1,2 , Yuanyuan Li 1,2 , Dafeng Ge 1,2 , Chong Liu 1,2 , Zhengning Xu 1,2,5 , Liangduo Chen 1,2 , Tianyi Wang 1,2,10 , Lei Wang 1,2 , Peng Sun 1,2 , Ximeng Qi 1,2 , Jiaping Wang 1,2 , Zheng Xu 1,2 , Jian Yuan 1,2 , Chao Yan 3 , Yanjun Zhang 3,9 , Dandan Huang 4 , Zhe Wang 6 , Neil M. Donahue 7 , Douglas Worsnop 8 , Xuguang Chi 1,2 , Mikael Ehn 3 , and Aijun Ding 1,2

Correspondence: Wei Nie (niewei@nju.edu.cn)

Received: 30 April 2021 – Discussion started: 4 May 2021

Revised: 21 August 2021 – Accepted: 29 August 2021 – Published: 6 October 2021

Abstract. Oxygenated organic molecules (OOMs) are the crucial intermediates linking volatile organic compounds (VOCs) to secondary organic aerosols (SOAs) in the atmosphere, but comprehensive understanding of the characteristics of OOMs and their formation from VOCs is still missing. Ambient observations of OOMs using recently developed mass spectrometry techniques are still limited, especially in polluted urban atmospheres where VOCs and oxidants are extremely variable and complex. Here, we investigate OOMs, measured by a nitrate-ion-based chemical ionization mass spectrometer at Nanjing in eastern China, through performing positive matrix factorization on binned mass spectra (binPMF). The binPMF analysis reveals three factors about anthropogenic VOC (AVOC) daytime chemistry, three isoprene-related factors, three factors about biogenic VOC (BVOC) nighttime chemistry, and three factors about nitrated phenols. All factors are influenced by NO_x in different ways and to different extents. Over 1000 nonnitro molecules have been identified and then reconstructed from the selected solution of binPMF, and about 72 % of the total signals are contributed by nitrogen-containing OOMs, mostly regarded as organic nitrates formed through peroxy radicals terminated by nitric oxide or nitrate-radical-initiated oxidations. Moreover, multi-nitrates account for about 24 % of the total signals, indicating the significant presence of multiple generations, especially for isoprene (e.g., C₅H₁₀O₈N₂ and C₅H₉O₁₀N₃). Additionally, the distribution of OOM concentration on the carbon number confirms their precursors are driven by AVOCs mixed with enhanced BVOCs during summer. Our results highlight the decisive role of NO_x in OOM formation in densely populated areas, and we encourage more studies on the dramatic interactions between anthropogenic and biogenic emissions.

¹Joint International Research Laboratory of Atmospheric and Earth System Sciences, School of Atmospheric Sciences, Nanjing University, Nanjing, China

²Jiangsu Provincial Collaborative Innovation Center of Climate Change, Nanjing, China

³Institute for Atmospheric and Earth System Research/Physics, Faculty of Science, University of Helsinki, Helsinki, Finland ⁴State Environmental Protection Key Laboratory of Formation and Prevention of Urban Air Pollution Complex, Shanghai

Academy of Environmental Sciences, Shanghai, China

⁵College of Environmental and Resource Sciences, Zhejiang University, Zhejiang, China

⁶Department of Civil and Environmental Engineering, The Hong Kong Polytechnic University, Hong Kong SAR, China

⁷Center for Atmospheric Particle Studies, Carnegie Mellon University, Pittsburgh, PA, USA

⁸Center for Aerosol and Cloud Chemistry, Aerodyne Research Inc., Billerica, MA, USA

⁹Univ. Lyon, Université Claude Bernard Lyon 1, CNRS, IRCELYON, Villeurbanne, France

¹⁰Meteorological Service Center of Hubei Province, Wuhan, China

1 Introduction

Secondary organic aerosols (SOAs), as an important and complex component of submicron particles (Zhang et al., 2007; Jimenez et al., 2009; Huang et al., 2014), are fully involved in affecting climate (IPCC, 2013) and causing health risks (Nel, 2005; Lim et al., 2012). Volatile organic compounds (VOCs) are ubiquitous in the atmosphere and are recognized as the main precursors of SOAs (Hallquist et al., 2009; Ziemann and Atkinson, 2012). However, the missing intermediate processes from VOCs to SOAs are yet to be elucidated (Hallquist et al., 2009; Ehn et al., 2014).

Benefiting from state-of-the-art measurement technics (Bertram et al., 2011; Jokinen et al., 2012; Lee et al., 2014), many previously unreported oxygenated organic molecules (OOMs), as intermediates from VOCs to SOAs (Ziemann and Atkinson, 2012), have been discovered. Among OOMs, highly oxygenated organic molecules (HOMs), first observed in the gas phase at a boreal forest site (Ehn et al., 2010, 2012) and reviewed by Bianchi et al. (2019), are so functionalized and have such low volatility that they can participate at the beginning of new particle formation (NPF) by stabilizing sulfuric acid (Kulmala et al., 2013; Riccobono et al., 2014) or through clustering alone (Kirkby et al., 2016; Bianchi et al., 2016), and they condense on existing particles and are thus responsible for a large fraction of SOAs (Ehn et al., 2014). In addition to conventional VOC-to-OOM mechanisms summarized in the Master Chemical Mechanism (MCM) (http://mcm.york.ac.uk/, last access: 9 February 2021), recent studies have proposed new pathways, such as autoxidation (Crounse et al., 2013; Jokinen et al., 2014) and multigenerational oxidation (Rollins et al., 2012; Wang et al., 2020b), to form condensable vapors by adding oxygen atoms efficiently. The production of OOMs, especially HOMs, from precursors such as monoterpenes (Ehn et al., 2014; Jokinen et al., 2015; Kirkby et al., 2016; Berndt et al., 2016), sesquiterpenes (Richters et al., 2016), isoprene (Jokinen et al., 2015; Zhao et al., 2021), aromatics (Wang et al., 2017; Molteni et al., 2018; Garmash et al., 2020), and alkanes (Wang et al., 2021) has been investigated in laboratories by using chemical ionization atmospheric pressure interface time-of-flight mass spectrometers with nitrate reagent ions (nitrate CI-APi-TOFs).

New insights and a general understanding about OOMs have been attained, yet many critical details about OOM formation and properties need to be addressed. First, the current kinetic descriptions of OOMs obtained from experiments are still limited, lacking for example individual H-shift rates for autoxidation and reaction rates of multigenerational products with oxidants. Furthermore, the complexity of the real atmosphere makes it more difficult to apply experimental results to ambient environments. The precursors compete for oxidants and vice versa, and their products will interact mechanistically in mixtures of atmospheric vapors (McFiggans et al., 2019; Heinritzi et al., 2020). However, in the labora-

tory we usually study simple systems with a single precursor and a single oxidant. Moreover, most experiments are carried out for environments dominated by biogenic VOCs (BVOCs), while anthropogenic emissions receive less attention. In addition to classic anthropogenic VOCs (AVOCs), large amounts of primary emissions of oxygenated VOCs are also present in urban areas (Karl et al., 2018). The effect of NO_x on OOMs is another key issue. NO_x can terminate peroxy radicals (RO₂), outcompeting autoxidation propagation reactions and other bimolecular reactions ($RO_2 + RO_2$, RO₂ + HO₂), and change the products' distribution and, consequently, size-dependently modulate the growth rates of organic aerosol particles (Yan et al., 2020). Additionally, NO_x contributes non-linearly to atmospheric oxidants, which also influence the production of OOMs (Pye et al., 2019). It is anticipated that NO_x plays a varied role in the formation of OOMs as well as of SOAs in different environments.

Therefore, more extensive OOMs observations are needed to validate the atmospheric implications of experiments, to be coupled with the global or regional model, and finally to comprehensively understand the fate of OOMs in the atmosphere. Until now, only a few ambient observations of OOMs using a nitrate CI-APi-TOF have been reported (Bianchi et al., 2019), and almost all of them focus on rural, forested, or remote atmospheres (Yan et al., 2016; Massoli et al., 2018; Zhang et al., 2020; Beck et al., 2021).

The Yangtze River Delta (YRD) is one of the most developed regions in eastern China. Fine particulate matter, with an aerodynamic diameter smaller than $2.5 \,\mu m$ (PM_{2.5}), has been significantly reduced in eastern China since the implementation of the "Air Pollution Prevention and Control Action Plan" in 2013 (Ding et al., 2019), but (secondary) organic aerosols are still much more abundant than in clean areas (Zhang et al., 2017; Sun et al., 2020). Here we investigate condensable oxygenated organic vapors observed by a nitrate CI-APi-TOF in August-September 2019 at the Station for Observing Regional Processes of the Earth System (SORPES) in the western part of the YRD, an anthropogenicemissions-dominated environment (Fu et al., 2013; Xu et al., 2017) mixed with enhanced biogenic emissions during summer (Wang et al., 2020a; Xu et al., 2021). A variety of oxidants (Liu et al., 2019; Li et al., 2020; Xia et al., 2020) with numerous precursors (VOCs) suggest very complicated atmospheric oxidation processes and thousands of products (OOMs). Thereby, positive matrix factorization (PMF) (Paatero and Tapper, 1994) was applied to timeresolved mass spectra which had been pre-divided into small bins (binPMF; Zhang et al., 2019) to separate various sources or processes of OOMs. Combined with summarizing the ensemble chemical characteristics of OOMs, some interesting findings about the conversion of VOCs to OOMs were obtained.

2 Methodology

2.1 Study site

The SORPES station (32°07′14″ N, 118°57′10″ E; 62 m a.s.l.) is located at Nanjing in the western part of the YRD, one of the most developed regions in eastern China. Due to its unique location, this site can be influenced by air masses from different source regions of anthropogenic emissions, biomass burning, dust, and biogenic emissions (Ding et al., 2013, 2016). Detailed descriptions of the station can be found in previous studies (Nie et al., 2015; Xie et al., 2015; Xu et al., 2018; Wang et al., 2018a; Sun et al., 2018; Shen et al., 2018).

2.2 Instrumentation

The nitrate CI-APi-TOF (Aerodyne Research Inc. and Tofwerk AG), combining a chemical ionization source (CI) and an atmospheric pressure interface time-of-flight mass spectrometer (APi-TOF) equipped with a long time-of-flight model (LTOF) with a mass resolution of 8000–12 000 Th Th⁻¹ (Th denotes thomsons), was deployed to detect ambient sulfuric acid and OOMs. The ambient air was pulled into a laminar flow reactor, where the sample flow (10 L min⁻¹) was surrounded by a purified airflow serving as the sheath flow (25 L min⁻¹), through a stainless-steel tube (100 cm long, 3/4 in. diameter). Nitrate reagent ions were generated in the sheath flow by exposing air-containing nitric acid to a photoionizer X-ray (Model L9491, Hamamatsu, Japan). Detailed description of the instrument has been given elsewhere (Junninen et al., 2010; Jokinen et al., 2012). The data were acquired at a 1 Hz time resolution and analyzed with a tofTools package (version 6.11) based on MATLAB (Math-Works Inc.). Due to the diversity and unknown molecular structures of oxygenated organic compounds, standards for OOMs measurable by the nitrate CI-APi-TOF are still lacking. Like in other studies (Kirkby et al., 2016; Trostl et al., 2016; Stolzenburg et al., 2018), an empirical method was used to quantify the concentrations of OOMs based on the ionization kinetics (pseudo-first-order reaction approximation) in the reaction tube of CI (Eq. 1) (Heinritzi et al., 2016).

$$[OOM_i] = \ln \left(1 + \frac{\sum_{n=0}^{1} \left[OOM_i \cdot (HNO_3)_n \cdot NO_3^- \right]}{+(OOM_i - H)^-} \right) \times C \times T_i$$

$$\left(1 + \frac{\sum_{n=0}^{1} \left[(HNO_3)_n \cdot NO_3^- \right]}{\sum_{n=0}^{2} \left[(HNO_3)_n \cdot NO_3^- \right]} \right) \times C \times T_i$$

Here $[OOM_i]$ is the concentration (molecules cm⁻³) of one OOM. On the right side of the equation, the numerator in the parentheses is the detected total signals (ions s⁻¹) of one OOM charged by nitrate ions in adduct-forming or deprotonated ways, and the denominator is the sum of all reagent ion signals (ions s⁻¹). First, a H₂SO₄-based calibration factor C, with a value of 4.2×10^9 molecules cm⁻³, was obtained

from a calibration using H₂SO₄ (Kuerten et al., 2012) that proceeded taking into account the diffusion loss in the sampling line by assuming that all detected OOMs have the same ionization efficiency as H₂SO₄. The collision frequency of HOMs with nitrate clusters is comparable to that of sulfuric acid with nitrate clusters (Ehn et al., 2014; Hyttinen et al., 2015), yet the collision frequency of some moderately oxygenated molecules with nitrate clusters is relatively slower. Therefore, calibration by this method leads to a lower-limit estimate of OOM concentrations (Ehn et al., 2014; Trostl et al., 2016), but the accurate quantification of OOMs is not the main concern of this study, and the errors in the quantification of OOMs do not change our conclusions. Second, a mass-dependent transmission efficiency T_i of the APi-TOF was inferred in a separate experiment by depleting the reagent ions with several perfluorinated acids (Heinritzi et al., 2016).

VOC precursors were measured by a proton transfer reaction time-of-flight mass spectrometer (PTR-TOF-MS; Ionicon Analytik, Innsbruck, Austria, TOF 1000 ultra). PM_{2.5} was measured with a combined technique of light scattering photometry and beta radiation attenuation (Thermo Scientific SHARP Monitor Model 5030). The chemical compositions of PM_{2.5} were determined on-line using a timeof-flight aerosol chemical speciation monitor (TOF-ACSM, Aerodyne Research Inc.). PMF analysis was further used to separate the organic aerosols (OAs) to primary organic aerosols and secondary organic aerosols (POAs and SOAs). The number concentrations of particles were measured by the scanning mobility particle sizer (SMPS) with a nano differential mobility analyzer (DMA) (4.0 to 63.8 nm) and long DMA (41.4 to 495.8 nm) and the aerodynamic particle sizer (APS) (0.5 to 18.0 µm). NO and NO₂ were measured using a chemiluminescence analyzer equipped with a blue-light converter (TEI, Model 42i-TL); O₃, SO₂, and CO were measured using the ultraviolet photometry, pulsed-UV fluorescence, and IR (infrared) photometry techniques (TEI, Model 49i, 43C, and 48C) respectively. Zero and span calibrations for trace gases were performed weekly during the campaign. Meteorological measurements including relative humidity (RH), wind speed, wind direction, and air temperature were recorded by an automatic weather station (Campbell Scientific, AG1000). $J(O^1D)$ was measured by an ultrafast charge-coupled device detector spectrometer, which is UVB enhanced (Meteorologie Consult GmbH, Germany).

2.3 Hydroxyl radical (OH) estimate

The OH concentration was calculated by applying Eq. (2), based on the assumption that gaseous sulfuric acid is mostly produced from the oxidation of SO₂ by OH and primarily lost by condensing onto particles:

$$[OH] = \frac{[H_2SO_4] \cdot CS}{k_{OH+SO_2} \cdot [SO_2]},$$
(2)

where $k_{\rm OH+SO_2}$ is a termolecular reaction constant for the rate-limiting step of the formation pathway of $\rm H_2SO_4$ in the atmosphere (Finlayson-Pitts and Pitts, 2000) and the condensation sink (CS) is the loss rate of $\rm H_2SO_4$ by condensation to the aerosol surface. The value of $k_{\rm OH+SO_2}$ is inferred from the IUPAC Task Group on Atmospheric Chemical Kinetic Data Evaluation (https://iupac-aeris.ipsl.fr/, last access: 9 August 2021). The value of CS was calculated following Eq. (3) (Kulmala et al., 2012):

$$CS = 2\pi D \sum_{i} \beta_{m_i} d_{p_i} N_i , \qquad (3)$$

where D is the diffusion coefficient of gaseous sulfuric acid, β_m is a transition-regime correction factor dependent on the Knudsen number (Fuchs and Sutugin, 1971), and d_{p_i} and N_i are the diameter and number concentration of particles in size bin i.

It has been proved that $(k_{OH+SO_2} \cdot [SO_2] \cdot [OH])/CS$ is a very reliable proxy for H_2SO_4 during the day (Lu et al., 2019). The ozonolysis of alkenes can form stabilized Criegee intermediates (SCIs) in addition to OH, and SCIs can also oxidize SO_2 to form H_2SO_4 (Mauldin et al., 2012; Guo et al., 2021). A previous study on H_2SO_4 proxies in this site has revealed that the reactions of SO_2 with products from the ozonolysis of alkenes generate a moderate amount of night-time sulfuric acid, with little effect on daytime sulfuric acid (Yang et al., 2021). Thus, OH may be overestimated during the nighttime. In this study, OH was used to calculate the production rates of RO_2 during the daytime (Fig. 4); the error in OH does not change the relative distribution of RO_2 from different precursors.

2.4 The binPMF approach

The binPMF approach has been used to analyze the measured high-resolution (HR) mass spectrometry data. Briefly, the raw spectra were divided into narrow bins with a width of 0.006 Th after mass calibration. The data matrix and error matrix were prepared according to the methods described by Zhang et al. (2019) for the PMF model inputs (Sect. S2) in the Supplement). Differently from the traditional PMF, which uses, for example, unit mass resolution (UMR) or HR data as input, binPMF still retains HR information as much as possible, avoids the uncertainty in HR peak fitting influencing the results of PMF, and separates the complex overlapping peaks for fitting. The PMF analysis in this work uses the Igor-based analyzing interface SoFi (solution finder, version 6.8) and ME-2 as described in Canonaco et al. (2013). After selecting the PMF solution, we fitted the HR peaks in each factor through tofTools.

3 Results and discussions

Figure 1 shows temporal variation in OOMs and related parameters at the SORPES station in the northeastern sub-

urb of Nanjing from 2 August to 6 September 2019. During the observation period, 22 of 35 d had maximum hourly temperatures above 30 °C and 29 d had maximum hourly $J(O^1D)$ values above $2 \times 10^{-5} \,\mathrm{s}^{-1}$. High temperatures and solar radiation indicate strong photochemistry, producing a large amount of ozone, with concentrations often exceeding 80 ppb. Even at night, the concentration of ozone is rarely lower than 10 ppb, resulting from the weak titration of low NO. At the same time, the reaction between ozone and high concentrations of NO₂ can provide sufficient NO₃ radicals, dominating nocturnal degradation of certain VOCs (Wayne et al., 1991). The elevated mixing level of total aromatic hydrocarbons is one of the main characteristics of the atmosphere in densely populated areas, in addition to which there should be many alkanes and alkenes which cannot be observed by the PTR-TOF-MS (Fu et al., 2013; Xu et al., 2017). In the daytime with strong photochemical reactions $(J(O^1D) > 1 \times 10^{-5} \text{ s}^{-1})$, we instead observed concentrations of isoprene higher than those of total aromatics (Fig. S1a in the Supplement). The complex mixtures of anthropogenic and biogenic VOCs can be oxidized through a variety of pathways to produce OOMs, of which some low-volatility components will condense into particles, forming organic aerosols. The concentrations of OOMs with a mass-to-charge ratio (m/z) below 360 Th are usually higher than 10⁶ molecules cm⁻³, and some can even reach up to $10^7 - 10^8$ molecules cm $^{-3}$. Clustered peaks on the spectra of OOMs and their clear daily variations imply a lot of chemical and physical dynamics information (Figs. 1d and S1b), which is the main aspect we want to explore in this work.

The binPMF analysis was performed to characterize the sources or processes of OOMs. A 14-factor solution was selected to interpret the data set, including 3 factors about AVOC daytime chemistry, 3 isoprene-related factors, 3 factors about BVOC nighttime chemistry, 3 factors about nitrated phenols (NPs), and 2 factors excluded from the following discussion. Of these 2 disregarded factors, one is mainly composed of fluorinated contaminations (F contaminations) and the other is mainly a mixture of nitrated phenols and fluorinated contaminations (mixed contaminations). When naming these factors, we prioritize the description of dominated species or their precursors, but if the precursors are complex mixtures, our naming highlights the characteristics of the chemical processes that drive certain factors. Although this may not be the optimal PMF solution, it still separates a lot of useful information. We also stress that the urban OOM mix is unlikely to be a perfect combination of independent, unchanging factors, which is an underlying assumption in the PMF algorithm. As such, there will be no solution which is complete and perfect, but we chose a solution which was able to provide us with interesting insights. Details of the PMF diagnostics are provided in Sect. S2 in the Supplement (Figs. S2–S6). For the convenience of discussions, we have grouped these factors based on shared characteristics of certain factors.

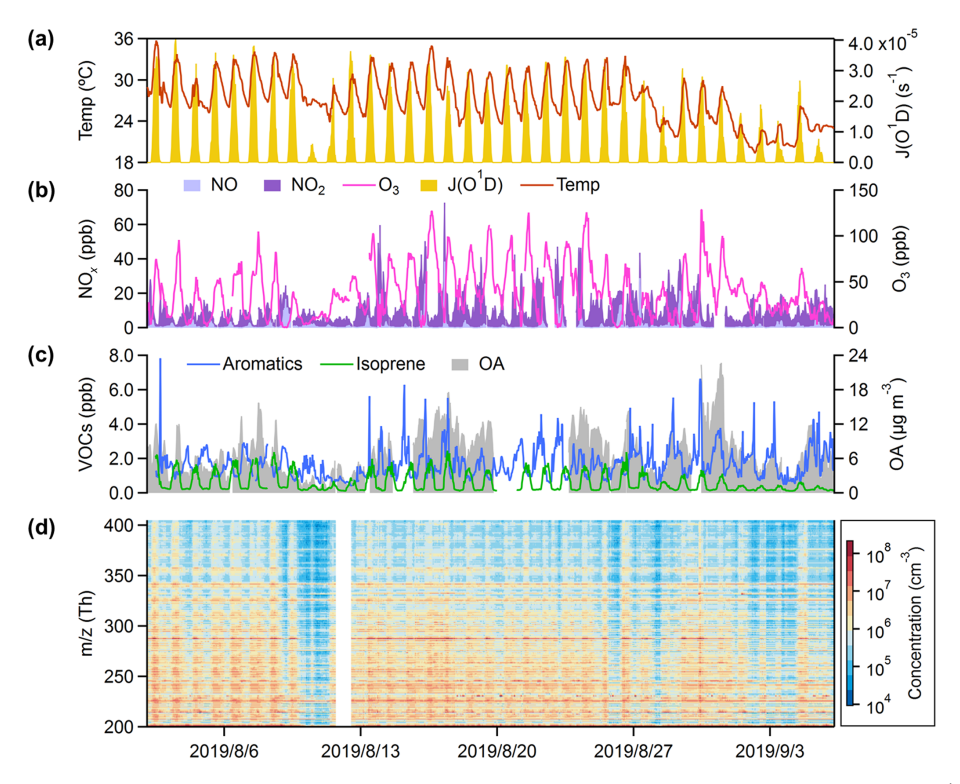


Figure 1. Overview of the observation. Time series of (a) temperature (Temp) and the photolysis frequency of O_3 (JO^1D); (b) O_3 and NO_x ($NO + NO_2$); (c) total aromatics (benzene + toluene + C_8 aromatics + C_9 aromatics + C_{10} aromatics + styrene), isoprene, and OAs; and (d) mass spectra of the nitrate CI-APi-TOF with m/z in the range of 202–404 Th.

3.1 AVOC daytime chemistry

The following daytime factors are characterized by C_6 – C_9 OOMs (Fig. 2a), considered to be derived from the oxidation of anthropogenic VOCs in this urban atmosphere, although we cannot completely exclude the presence of BVOC-derived OOMs, such as C_5 and C_{10} OOMs.

3.1.1 Aro-OOM factor

The averaged double bond equivalent (DBE) of this factor is the largest among all factors (Table 1), with the main signals coming from compounds with DBE > 2 (Fig. 2b) and consistent with the nature of the oxidation products of aromatics (Fig. 3a). Combined with the correlation with the production rates of OH-initiated primary RO₂ from aromatics calculated by Eq. (4) (Fig. 4), this factor is supposedly dominated by aromatic-derived OOMs (the Aro-OOM factor). This factor increases from 05:00 LT with a maximum at 10:00 LT and a sub-peak around 16:00 LT (Fig. 3e), following the diurnal variations in the P_{RO_2} of C_7 – C_{10} aromatics (Fig. 4b–d) but poorly correlated with the P_{RO_2} of benzene (Fig. 4a). Furthermore, OOMs with eight carbon atoms have the highest signal in this factor (Fig. 2a), derived from the most abundant C₈ aromatics + styrene RO₂ (Fig. 4f). Both of these findings can be explained by the fact that substituted aromatics have higher OH reactivity (Bloss et al., 2005) and higher HOM

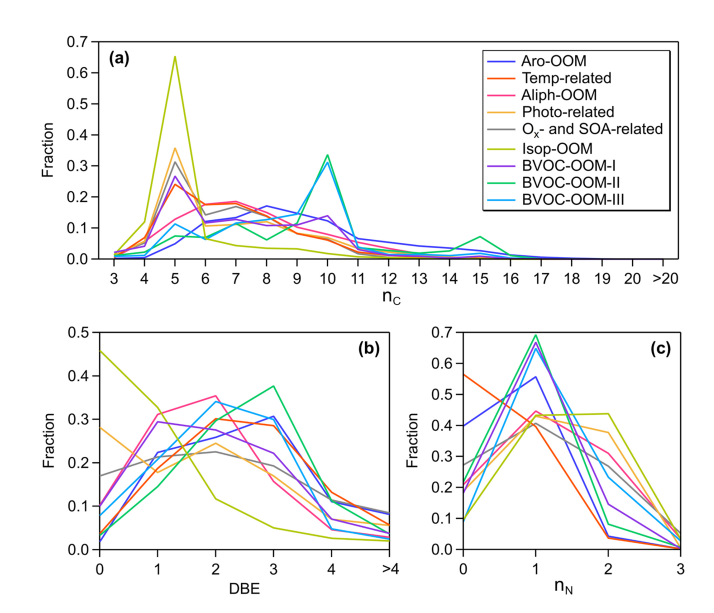


Figure 2. The distributions of observed non-nitro OOMs grouped by (a) the number of carbon atoms (n_C) , (b) DBE, and (c) the number of nitrogen atoms (n_N) in nine factors. Since the signals of RO₂ are very weak, RO₂ from BVOC-OOM-I and BVOC-OOM-II are excluded in (b) to keep the integer value of DBE.

yields (Wang et al., 2017; Molteni et al., 2018) than their homologues with fewer carbon atoms. In terms of molecular formulas, the aromatic-derived OOMs have an overlap with monoterpene-derived OOMs (Mehra et al., 2020). Monoterpenes can contribute more C_{10} OOMs than aromatics ($P_{\text{MT-RO}_2} > P_{C_{10} \text{ Aro-RO}_2}$), but aromatics play a more important role in total in this factor since they provide more RO_2 in the urban atmosphere (Fig. 3f).

$$P_{\text{RO}_2} = k_{\text{OH+VOC}} \cdot [\text{OH}] \cdot [\text{VOC}] \tag{4}$$

The main molecules of the Aro-OOM factor are summarized in Table S2 in the Supplement. The $C_xH_{2x-5}O_6N$ $(x = [6, 12], of which C_8H_{11}O_6N is the most intense) series$ can be produced by Reaction (R1a) of NO with the bicyclic peroxy radicals (HO-Ar- $(O_2)_2$), the key intermediates for aromatic oxidation proposed in the MCM (Bloss et al., 2005; Birdsall and Elrod, 2011). And here dihydroxy nitro-BTEX $(C_x H_{2x-7} O_4 N, x = [6, 8])$ can be treated as an indicator of aromatic oxidation. In addition to the conventional products, $C_9H_{13}O_{7-9}N$ from the $C_xH_{2x-5}O_{7-9}N$ (x = [7, 13]) series is also significant in the OH-initiated and NO_x-influenced oxidation experiments of 1,2,4-trimethylbenzene (Zaytsev et al., 2019) and of 1,3,5-trimethylbenzene (Tsiligiannis et al., 2019). More oxygenated compounds may come from autoxidation and multigenerational OH attacks. However, the effective OSc of this factor (Table 1) is lower than that of oxidation products of aromatics in recent laboratory studies (Zaytsev et al., 2019; Tsiligiannis et al., 2019; Garmash et al., 2020; Wang et al., 2020c). We speculate that the abundances of NO_x relative to oxidants and precursors in these experiments are not sufficient to reproduce the atmospheric conditions during our observation or that HOMs are more concentrated in aerosols due to the large condensation sink at this site (Qi et al., 2015). Although species with DBE < 3 (Fig. 2b) in this factor are most likely produced from multiple OH attacks in aromatic oxidation, we cannot rule out the contribution of alkanes co-emitted with aromatics, such as the series $C_x H_{2x-1} O_6 N$ (x = [5, 14]).

3.1.2 Temp-related factor

This factor is named due to good correlation with temperature (Fig. 5) and shows a maximum intensity in the afternoon at around 15:00 LT (Fig. 3e). The Temp-related factor is the only one dominated by non-nitrogenous organics (Fig. 3b and d) and has the highest effective OSc (Table 1) among all the factors. The $C_xH_{2x-4}O_5$ (x=[5,11], summarized in Table S3 in the Supplement), $C_xH_{2x-2}O_5$ (x=[5,10]), $C_xH_{2x-6}O_5$ (x=[5,11]), and $C_xH_{2x-4}O_6$ (x=[5,10]) series are possibly products from RO_2 terminated by RO_2 (Reaction R2a) or closed-shell products from RO in Reactions (R3a) or (R3b). Temperature starts to rise at 06:00 LT (Fig. 12b), but this factor does not accumulate significantly until after about 10:00 LT (Fig. 3e), when the mixed level of

NO is reduced to 1 ppb (Fig. 4f). This phenomenon suggests a probability of HO₂-driven chemistry of this factor under low-NO conditions since NO can consume HO₂ and compete with HO₂ for RO₂. Such low-NO atmospheric oxidation pathways have been suggested to be non-negligible in the afternoon in central Beijing (Newland et al., 2021).

A factor caused by similar chemical processes called the isoprene afternoon was discovered in the nitrate CI-APi-TOF data collected at a forest site in Centreville, Alabama, USA (Massoli et al., 2018), and correlated well with HO₂, O₃, and temperature. We also observed a number of isoprene oxidation products in the Temp-related factor ($n_C = 4$ and $(n_C = 5 \text{ in Fig. 2a})$. Many of the $C_x H_{2x-1} O_6 N$ (x = [3, 7])and $C_x H_{2x-3} O_6 N$ (x = [4, 9]) series were also present in the light HOM factor which was supposed to be fragments from the oxidation of larger VOCs (e.g., monoterpenes) in Hyytiälä, Finland (Yan et al., 2016), while at the SORPES station, the C₆-C₉ OOMs should mainly come from the oxidation of anthropogenic VOCs. At lower temperatures, the propensity of condensable organic molecules to condense into aerosols makes the concentration measured using the nitrate CI-APi-TOF lower. Thus, the total concentration of the Temp-related factor in the gas and aerosol phases was calculated based on a gas-particle equilibrium (Sect. S5 in the Supplement) and was still found to be temperature dependent (Fig. S7 in the Supplement), illustrating the temperature-influenced chemical process controlling the factor. For instance, unimolecular reaction rates like RO₂ H shifts increase qualitatively with temperature (Bianchi et al., 2019; Frege et al., 2018).

$$RO_2 \cdot + NO \rightarrow RONO_2$$
 (R1a)

$$RO_2 \cdot + NO \rightarrow RO \cdot + NO_2$$
 (R1b)

$$RO_2 \cdot + HO_2 \cdot \rightarrow ROOH + O_2$$
 (R2a)

$$RO_2 \cdot + HO_2 \cdot \rightarrow RO \cdot + \cdot OH + O_2$$
 (R2b)

$$RO \cdot + O_2 \rightarrow RC = O + HO_2 \cdot$$
 (R3a)

$$RO \cdot + O_2 \rightarrow fragments$$
 (R3b)

3.1.3 Aliph-OOM factor

This factor is dominated by organic nitrates (Fig. 3c and d), and contains the bulk of anthropogenic dinitrates and trinitrates. The $C_xH_{2x-2}O_8N_2$ (x=[4,13], summarized in Table S4 in the Supplement) and $C_xH_{2x}O_8N_2$ (x=[4,9]) series have not been reported in aromatic oxidation experiments under high- NO_x conditions (Tsiligiannis et al., 2019; Wang et al., 2020c), and nor have they been reported in the forest or rural environments (Yan et al., 2016; Massoli et al., 2018). A reasonable assumption is that these saturated or nearly saturated compounds are the products of aliphatics (including alkanes, alkenes, aliphatic alcohol, etc.) during their oxidation affected intensively by NO_x in the urban atmosphere. The Aliph-OOM factor has a broad afternoon peak lasting from 14:00 to 19:00 LT (Fig. 3e), suggesting that

Table 1. Summary of molecular characteristics of nine discussed non-nitrated-phenol factors. The calculation of the relevant parameters is given in Sect. S3 in the Supplement. Major peaks of each factor are summarized in Sect. S4 in the Supplement.

Factor	Average concentration (cm ⁻³)	Effective formulas	$\begin{array}{c} MW \\ (g\text{mol}^{-1}) \end{array}$	OSc	O:C	N : C	DBE	$\log_{10}(C^* \; (\mu \mathrm{g m}^{-3}))$ in 300 K
Aro-OOM	1.86×10^{7}	C _{9.1} H _{14.3} O _{6.1} N _{0.6}	230.2	-0.52	0.73	0.08	2.6	-1.7
Temp-related	4.50×10^{7}	$C_{6.8}H_{10.2}O_{6.0}N_{0.5}$	195.8	-0.02	0.95	0.08	2.5	-1.4
Aliph-OOM	2.11×10^{7}	$C_{7.5}H_{12.2}O_{6.7}N_{1.2}$	225.7	-0.55	0.96	0.17	1.9	0.0
Photo-related	4.77×10^{7}	$C_{6.9}H_{11.0}O_{7.4}N_{1.2}$	228.3	-0.28	1.18	0.20	1.8	-1.1
O_x - and SOA-related	2.59×10^{7}	$C_{6.6}H_{9.8}O_{6.8}N_{1.1}$	214.2	-0.24	1.11	0.19	2.2	-0.3
Isop-OOM	2.83×10^{7}	$C_{5.5}H_{9.6}O_{6.9}N_{1.4}$	205.8	-0.51	1.34	0.28	0.9	1.2
BVOC OOM-I	1.68×10^{7}	$C_{7.2}H_{11.5}O_{7.0}N_{1.0}$	224.1	-0.26	1.06	0.16	2.0	-1.4
BVOC OOM-II	9.05×10^{6}	$C_{9.2}H_{14.6}O_{7.1}N_{0.9}$	251.3	-0.45	0.83	0.11	2.5	-2.8
BVOC OOM-III	1.57×10^{7}	$C_{8.6}H_{13.7}O_{6.9}N_{1.2}$	243.3	-0.64	0.87	0.16	2.1	-0.7

Note that MW is the molecular weight, OSc is the carbon oxidation state, O:C is the oxygen-to-carbon ratio, N:C is the nitrogen-to-carbon ratio, DBE is the double bond equivalent, C^* is the saturation concentration, and $\log_{10}(C^*)$ is the volatility.

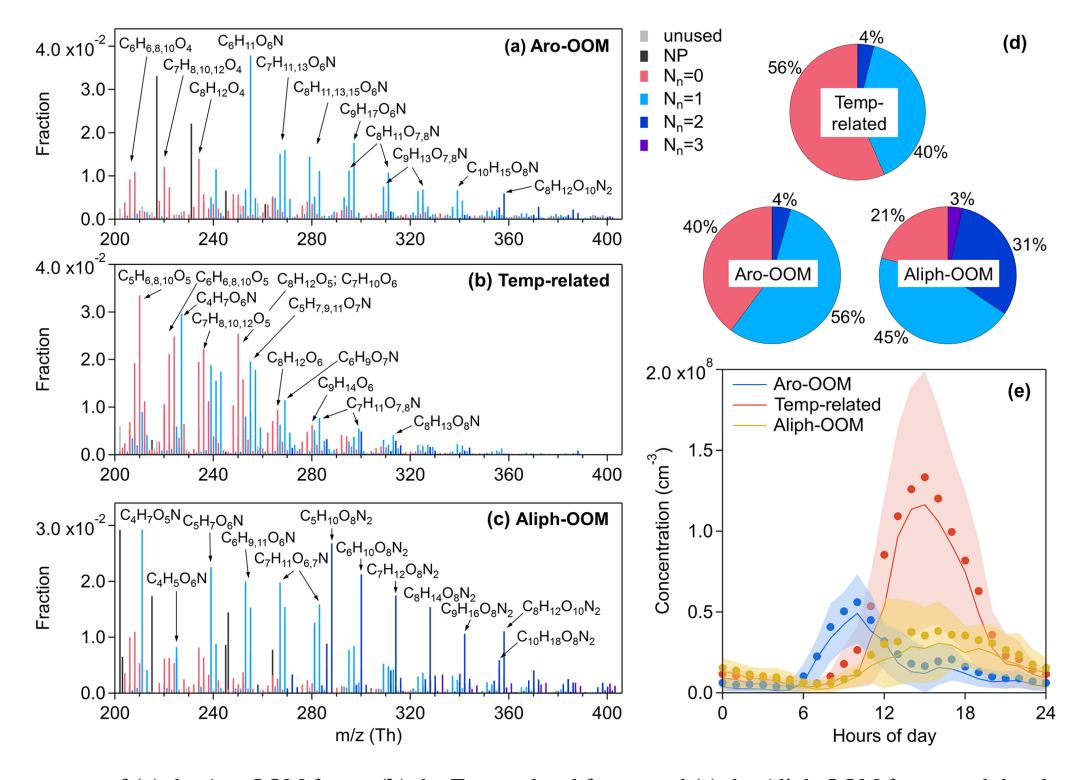


Figure 3. Mass spectra of (a) the Aro-OOM factor, (b) the Temp-related factor, and (c) the Aliph-OOM factor, and the elemental formulas of major peaks are labeled above them. Peaks are color-coded by $n_{\rm N}$ as indicated at the top right of the figure, and the fractions of peaks grouped by $n_{\rm N}$ are reported in (d) the pie charts. The gray bars are fluorinated contaminations or non-identified compounds. The nitrated phenols are drawn separately with black peaks in (a)–(c) and were not included in (d). So $n_{\rm N}$ can more reliably represent the number of nitrate groups in each molecule. Diurnal patterns (Beijing time) of these three factors are shown in (e): the bold solid lines are the median values; shaded areas represent percentiles of 75 % and 25 %; and solid circles represent mean values.

the formation of multi-nitrate requires enough OH exposure time.

Considering a simple scenario of alkane photo-oxidation under high- NO_x conditions, the RO_2 generated from OH attack is completely terminated by NO (Fig. 6a). The chain-

retaining products are $C_nH_{2n}O$ (one more carbonyl group than the precursor) and $C_nH_{2n+1}O_3N$ (one more nitrate group than the precursor), and the re-oxidation of these products is a repetition of the above process which is defined as the basic reaction scheme. The multiple-generation products

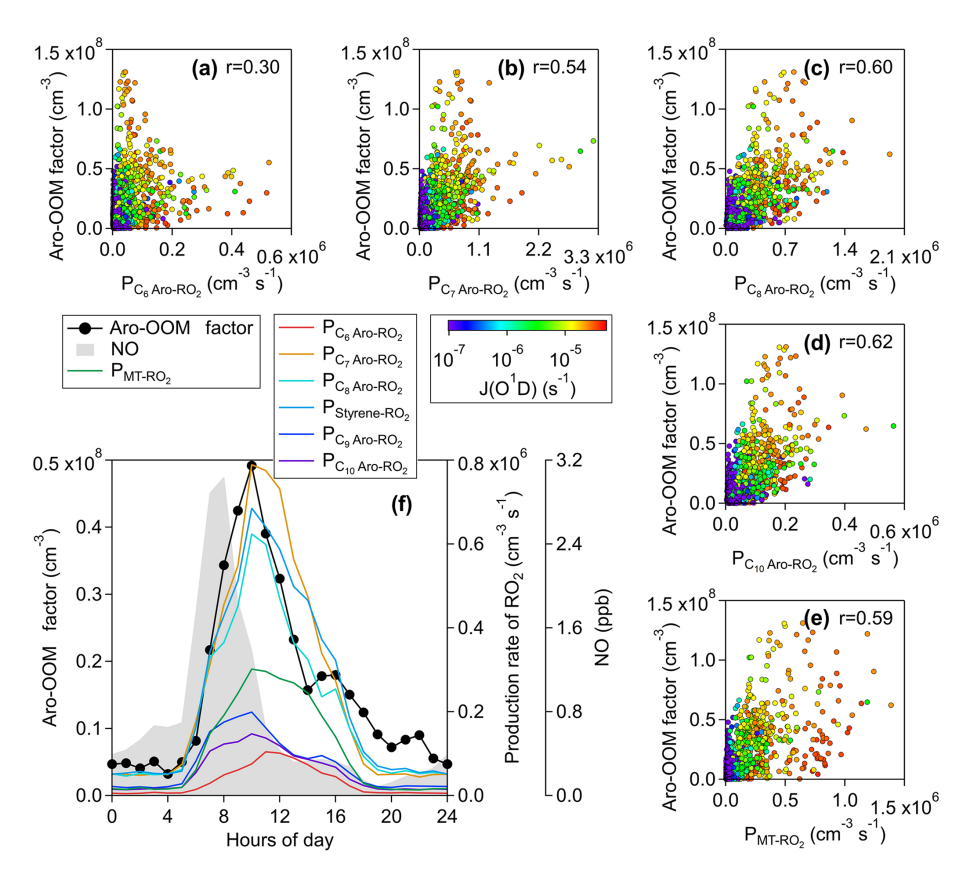


Figure 4. Correlations of the Aro-OOM-dominated factor with the production rate of RO₂ from OH-initiated oxidation of (a) benzene ($P_{C_6 \text{ Aro-RO}_2}$), (b) toluene ($P_{C_7 \text{ Aro-RO}_2}$), (c) C₈ aromatics ($P_{C_8 \text{ Aro-RO}_2}$), (d) C₁₀ aromatics ($P_{C_{10} \text{ Aro-RO}_2}$), and (e) monoterpenes ($P_{\text{MT-RO}_2}$). All the dots are colored by $J(O^1D)$ to show the difference between day and night. The median diurnal patterns of this factor and related parameters are plotted in (f).

of alkanes summarized in Fig. 6b are regarded as reference compounds, which we compare OOMs with to investigate other mechanisms that differ from those shown in Fig. 6a and b. Specifically, this comparison is performed between the reference molecule and OOMs with the same numbers of carbon, hydrogen, and nitrogen atoms but different numbers of oxygen atoms. The number of extra oxygen atoms $(n_{O_{extra}})$ from each aliphatic OOM over its corresponding reference molecule was calculated by Eq. (5), that is, by subtracting carbonyl and nitrate oxygens from the molecule. Thus, $n_{\text{O}_{\text{extra}}}$ can represent the additional oxygenated moieties such as the hydroxyl group (-OH), peroxy group (-OOH), and possibly ether group. These functional groups may come from RO isomerization (Orlando et al., 2003), the addition of OH to alkenes, pre-existing moieties in the precursor, RO₂ autoxidation, or specific RO₂ bimolecular termination reactions $(RO_2 + RO_2, RO_2 + HO_2).$

$$n_{\text{Oextra}} = n_{\text{O}} - \text{DBE} - 3 \times n_{\text{N}} \tag{5}$$

As shown in Fig. 6c, aliphatic OOMs in this factor are mainly the third-generation products followed by the second-generation products, both of which have one or two oxygen-

containing functional groups in addition to the carbonyls and nitrates. It should be noted that the first-generation (Fig. 6a) and basic products (Fig. 6b) here are underestimated due to the low sensitivity of the nitrate CI-APi-TOF to these compounds. The multifunctional products of aliphatics are condensable to form SOAs (correlation coefficients with SOAs shown in Fig. 5). Recent work has showed that autoxidation is more common than previously thought (Wang et al., 2021), and more studies are needed to explore the oxidation mechanisms of anthropogenic aliphatics and to evaluate their contribution to SOAs.

3.2 Isoprene-related chemistry

The following factors are characterized by C_5 OOMs (Fig. 2a), of which an isoprene dihydroxyl dinitrate $C_5H_{10}O_8N_2$ (charged by NO_3^- at m/z 288 Th) is the fingerprint molecule (Fig. 7). Apart from isoprene-derived compounds, OOMs formed from other precursors undergoing similar chemical processes are also allocated to these three factors.

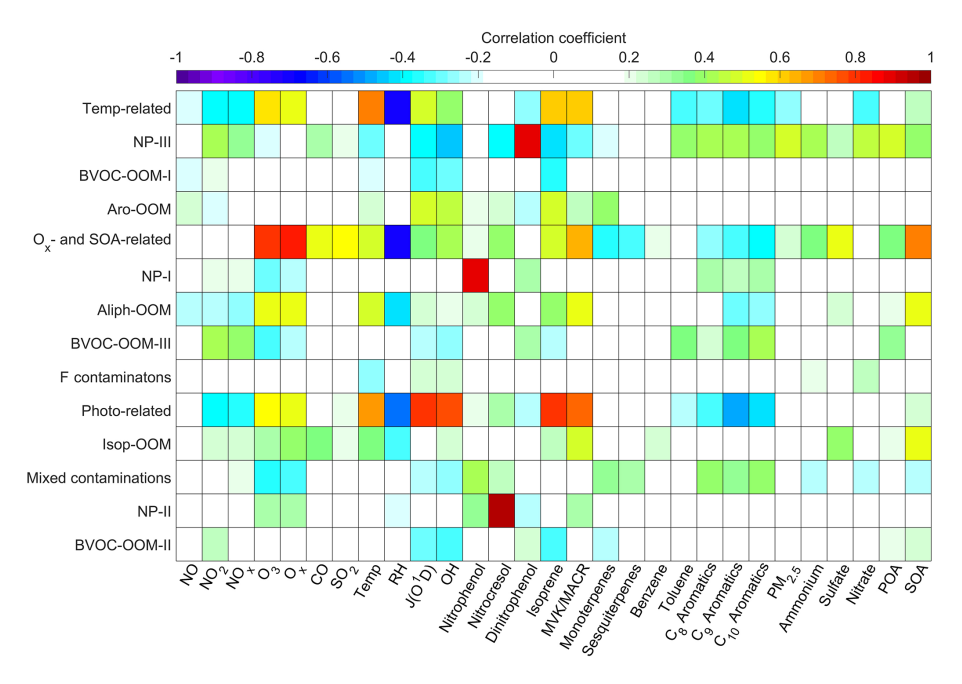


Figure 5. Correlations of PMF factors with external gas-phase and particulate tracers from other instruments deployed at the SORPES station, with the color representing the Pearson correlation coefficients. From left to right, the tracers are gas-phase species (NO, NO₂, NO₃, CO, SO₂), meteorological data (temperature (Temp), relative humidity (RH), photolysis constants ($J(O^1D)$)), nitrate CI-APi-TOF data (OH, nitrophenol, nitrocresol, dinitrophenol), PTR-TOF-MS data (isoprene, methyl vinyl ketone–methacrolein (MVK–MACR)), monoterpenes, sesquiterpenes, benzene, toluene, C₈ aromatics, C₉ aromatics, C₁₀ aromatics), PM_{2.5}, and ACSM data (ammonium, sulfate, nitrate, POAs, SOAs).

3.2.1 Photo-related factor

This factor is defined based on its correlation with $J(O^1D)$ (Fig. 5), having an apparent diurnal cycle with a peak at 12:00 LT (Fig. 7e). The major peak of the Photo-related factor is C₅H₁₀O₈N₂ (Fig. 7a), most probably generated from double OH attack proceeding with double $RO_2 + NO$ termination (Jenkin et al., 2015). C₅H₁₀O₈N₂ can be also produced in an NO₃ + isoprene system (Ng et al., 2008; Zhao et al., 2021), whereas in this study, the nocturnal C₅H₁₀O₈N₂ is principally from the isoprene-derived OOM (Isop-OOM) factor (Fig. 8b) which will be discussed later. Other peaks with $n_C \le 5$, like C₅H₇O₇N, C₄H₇O₆N, and C₅H₉O₆N, are also likely to be the isoprene products. The total signal of compounds with $n_{\rm C} > 5$ is not low, although their respective proportions are not as prominent as those of C₅ species (Fig. 7d), implying the contribution of other precursors together with isoprene. In addition, the relationship of this factor with isoprene and $J(O^1D)$ together (Fig. 5) reveals the effect of light-dependent emission of isoprene on it.

3.2.2 O_x - and SOA-related factor

The atmospheric oxidation of VOCs produces low-volatility compounds, forming SOAs through gas-particle partitioning, and concurrently promotes ozone formation (Atkinson, 2000). Both SOAs and O_x have long lifetimes (> 12 h), and

their correlations have been extensively investigated (Herndon et al., 2008; Wood et al., 2010; Hu et al., 2016). The OOM factor related to ozone and SOAs together (Fig. 5), having slightly elevated concentrations during the daytime (Fig. 7e), is considered to be generated from this photochemical aging process. Apart from C₅H₁₀O₈N₂, other isoprene multi-nitrates are also present in this factor. C₅H₉O₁₀N₃, an isoprene hydroxyl trinitrate requiring at least two steps of oxidation found in the experimental study on isoprene oxidation by NO₃ (Zhao et al., 2021), of course does not appear in the Photo-related factor at all but is mostly apportioned into the O_x- and SOA-related factor and the Isop-OOM factor (Fig. 8c and d). Like the Photo-related factor, isoprene is a significant but not the only precursor of this factor (Figs. 2 and 7). The biggest peak of the O_x - and SOA-related factor is an ion at m/z 264 with the formula $C_6H_5O_3N$ (HNO₃NO₃⁻), identified as an adduct of nitrophenol (C₆H₅O₃N) with nitrate dimmer (HNO₃NO₃ $^{-}$). The time variation in C₆H₅O₃N (HNO₃NO₃⁻) is influenced by the reagent ions in addition to the atmospheric nitrophenol. So far, we do not know why this compound shares the same processes with others, but we performed a test that removed the bins with the unit m/z = 264from the input matrix and still obtained this factor from the PMF model.

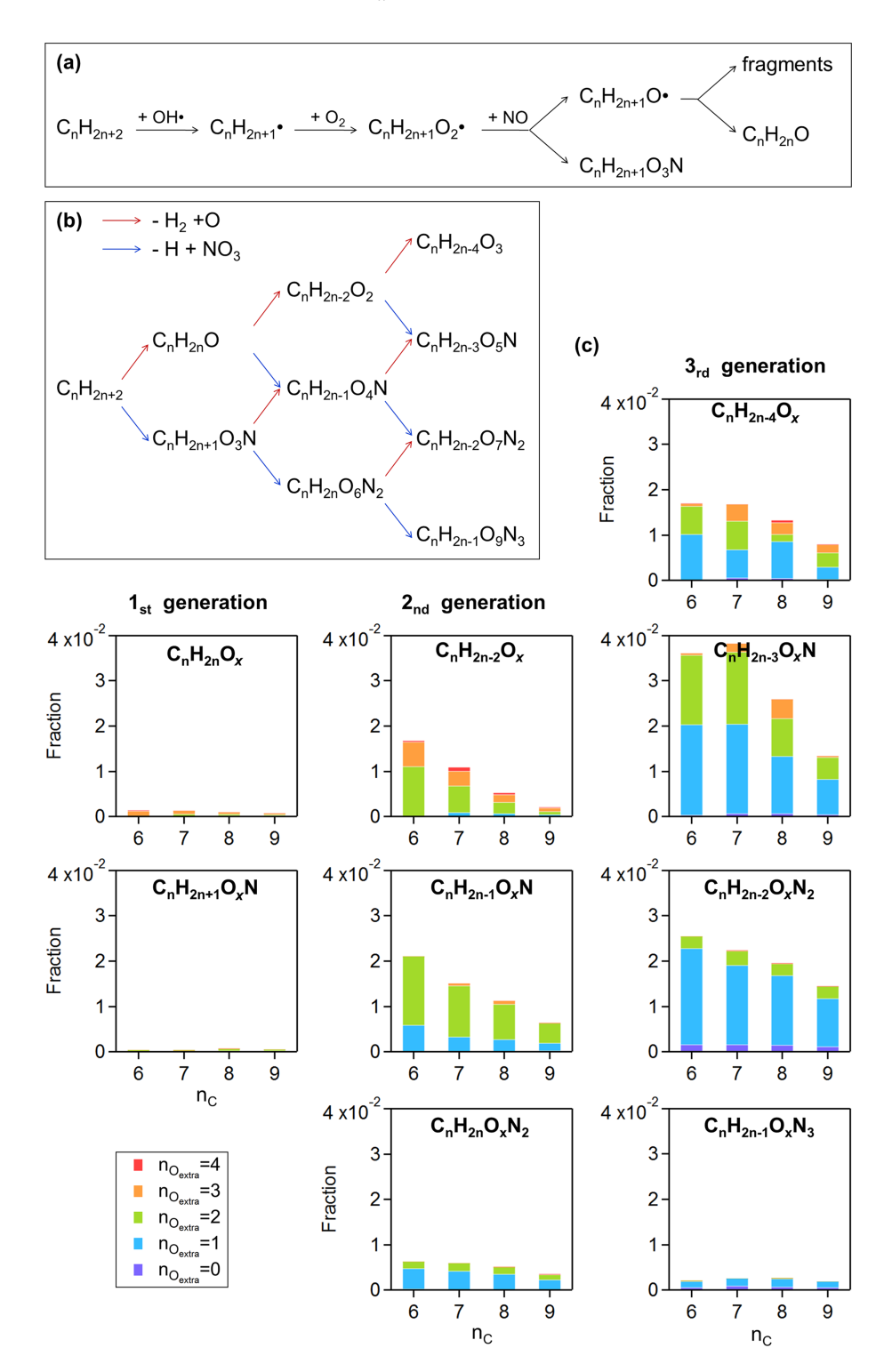


Figure 6. (a) Simplified oxidation mechanism for alkanes attacked by OH once under NO_x -controlled conditions. Panel (b) summarizes the changes in the molecular formula of the first- to third-generation products of alkanes, based on the basic reaction scheme in (a). Panel (c) shows the fraction of potential alkane-derived compounds in the Aliph-OOM factor. The compounds listed in (c) are grouped according to the molecular formulas in (b), i.e., with the same number of carbon, hydrogen, and nitrogen atoms but different numbers of oxygen atoms. The bars in (c) are colored with $n_{O_{extra}}$. Please see text for details about $n_{O_{extra}}$.

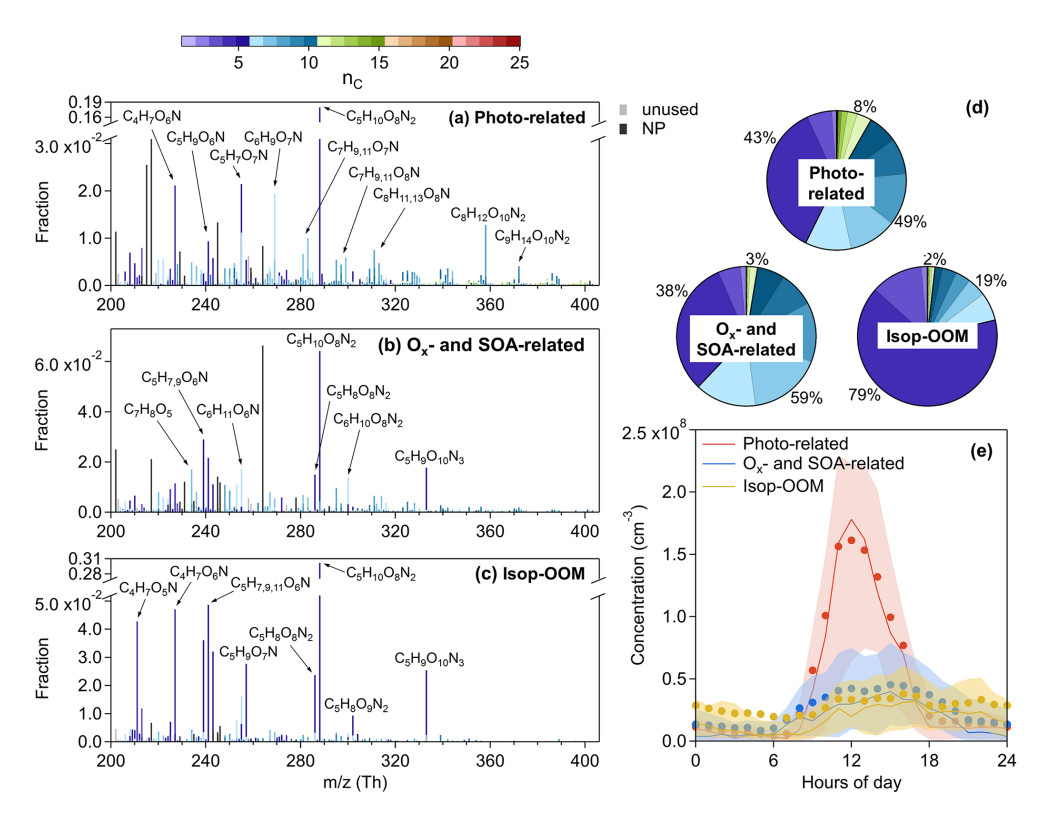


Figure 7. Mass spectra of (a) the Photo-related factor, (b) the O_{x^-} and SOA-related factor, and (c) the Isop-OOM factor, and the elemental formulas of major peaks are labeled above them. Peaks are color-coded by n_C as indicated at the top of the figure, and the fractions of peaks grouped by n_C are reported in (d) the pie charts. The gray bars are fluorinated contaminations or non-identified compounds. The nitrated phenols are drawn separately with black peaks in (a)–(c). The molecules represented by the gray and black bars were not included in (d). Diurnal patterns of the three factors are shown in (e): the bold solid lines are the median values; shaded areas represent percentiles of 75 % and 25 %; and solid circles represent mean values.

3.2.3 Isop-OOM factor

The mass spectra of the Isop-OOM factor, as its name implies, are exclusively contributed by isoprene-derived compounds (Fig. 7c). C₅H₁₀O₈N₂ contributes about 30 % of the intensity of this factor, and the dominance of C₅H₁₀O₈N₂ was also found in the isoprene nitrate type-I factor in Centreville (Massoli et al., 2018). In addition to multi-nitrates $(C_5H_{10}O_{7-8}N_2, C_5H_8O_{6-9}N_2, and C_5H_9O_{10}N_3 summa$ rized in Table S6 in the Supplement), several mononitrate series $(C_4H_7O_{5-7}N, C_5H_9O_{4-9}N, C_5H_7O_{5-8}N, and$ $C_5H_{11}O_{5-6}N$) of this factor are also abundant in the isoprene nitrate type-II factor in Centreville (Massoli et al., 2018). Many of the isoprene nitrates here have been especially investigated in our previous observations in the YRD (Xu et al., 2021) and have been discovered in other field measurements (Lee et al., 2016; Massoli et al., 2018) and in many laboratories (Ng et al., 2008; Lambe et al., 2017). Generally, these compounds are second- and third-generation OH oxidation products of isoprene under high-NO_x conditions (Wennberg et al., 2018).

The diurnal pattern of the Isop-OOM factor is relatively unclear (Fig. 7e), with obvious differences between mean

and median values usually caused by plume events. This indicates that isoprene chemistry, usually varying evidently from day (OH-initiated) to night (NO₃-initiated), is not the driver of this factor. This factor correlates positively with MVK-MACR and SOAs (r > 0.50, shown in Fig. 5) but not with isoprene and OH. It seems that these isoprene OOMs are produced elsewhere and then transported due to their longer lifetime determined by their relatively high volatility (Table 1). The Isop-OOM factors in the continental air masses are more intense than those in the coastal and YRD air masses (Fig. S8 in the Supplement), consistent with the spatial distribution of isoprene emissions (Sindelarova et al., 2014). An archetypal episode affected by continental air masses (13) August to 17 August 2019) is shown in Fig. 8. During this period, C₅H₉O₁₀N₃ was almost entirely transported, while C₅H₁₀O₈N₂ had strong in situ photochemical generation, in addition to the source of transport.

3.3 BVOC nighttime chemistry

The following nighttime factors are characterized by C_{10} OOMs (Fig. 2a), which are identified as the oxidation products of monoterpenes. Except for the BVOC-OOM-I fac-

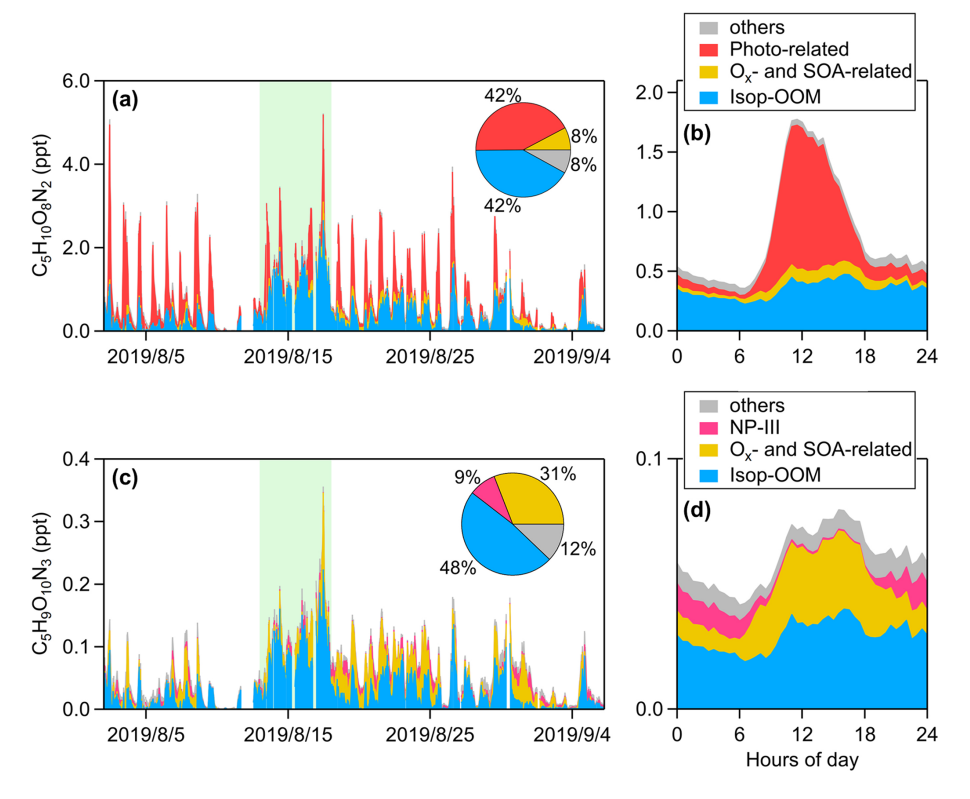


Figure 8. Stacked (a) time series and (b) mean diurnal pattern of isoprene dihydroxyl dinitrate $(C_5H_{10}O_8N_2)$. Stacked (c) time series and (d) mean diurnal pattern of isoprene hydroxyl trinitrate $(C_5H_9O_{10}N_3)$. The contribution ratios of each PMF factor to these two compounds are reported in the respective pie charts. The light-green-shaded area represents a typical episode influenced by transported continental air masses (13 to 17 August 2019).

tor (Fig. 9a), the contribution of isoprene-derived OOMs was much lower in these factors. Compared to the above isoprene-related factors, $C_5H_{10}O_8N_2$ and $C_5H_9O_{10}N_3$ were no longer significantly present in the following factors.

3.3.1 BVOC-OOM-I factor

The first nighttime factor has its maximum concentration at around 20:00 LT and decreases to very low values during the day. It is moderately correlated with the production rate of NO₃ radical (P_{NO_3} derived from Eq. 6) at night and reaches high intensity only under conditions of NO below 1 ppb (Fig. 10a), indicating a chemical process of NO₃ radical. The concentration of this factor is mainly from C₅ peaks, followed by C₆-C₁₀ peaks (Fig. 9d), about 80 % of which are organic nitrates (Fig. 2c), designating the oxidations of isoprene and monoterpenes by NO₃ (BVOC-OOM-I). In the case of isoprene oxidation, the nitrate groups of $C_5H_9O_{4-8}N$, $C_5H_7O_{5-8}N$, and $C_4H_7O_{5-6}N$ series (summarized in Table S8 in the Supplement) are likely to come from the addition of NO₃. Next, the C₅H₁₀O₈₋₉N₂ and C₅H₈O₇₋₁₀N₂ series are probably second-generation products. These compounds derived from an isoprene $+ NO_3$ system have been discussed in previous work with laboratory (Kwan et al., 2012; Zhao et al., 2021) and ambient (Ayres et al., 2015; Xiong et al., 2015) data sets. Additionally, the C_6 – C_{10} species are potentially the products of monoterpenes degraded by NO_3 .

$$P_{\text{NO}_3} = k_{\text{NO}_2 + \text{O}_3} \cdot [\text{NO}_2] \cdot [\text{O}_3]$$
 (6)

3.3.2 BVOC-OOM-II factor

The second nighttime factor is intense at night and over 5 times lower during the day. Like the BVOC-OOM-I factor, this factor has high concentrations when NO is reduced to increase NO₃ availability (Fig. 10b), and about 80% of compounds in this factor are organic nitrates (Fig. 2c). Accordingly, this may also be a factor strongly influenced by NO_3 . It is dominated by $C_6\text{--}C_{10}$ OOMs, among which the highest intensity is at C_{10} (Fig. 9d), coherent with the nature of monoterpene products (BVOC-OOM-II). This factor has weaker signals at C₁₅ which are plausibly the products of sesquiterpenes but could also be dimmers formed from Reaction (R4) (monoterpenes + isoprene or monoterpenes + C₅ monoterpenes fragments). Compared to the BVOC-OOM-I factor (Fig. 9d), this factor has more large mass molecules (C₁₀) and fewer small mass molecules (C₅), resulting in an effective volatility over 1 order of magnitude

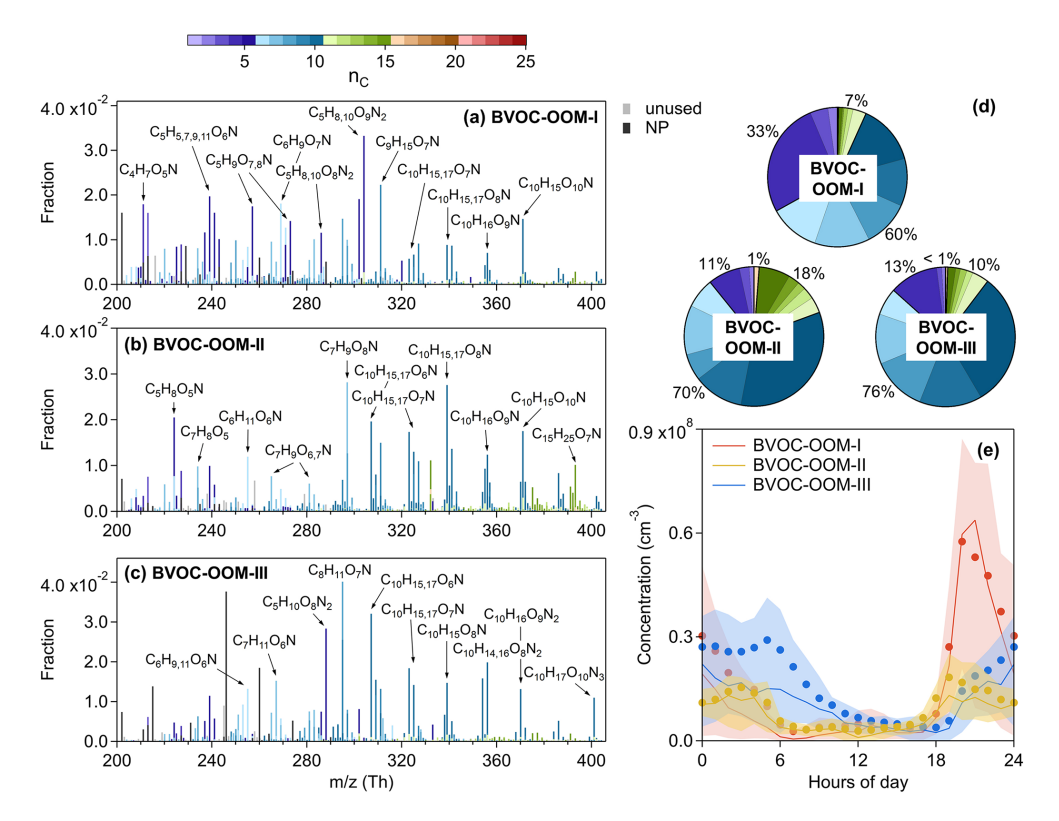


Figure 9. Mass spectra of (a) the BVOC-OOM-I factor, (b) the BVOC-OOM-II factor, and (c) the BVOC-OOM-III factor, and the elemental formulas of major peaks are labeled above them. Peaks are color-coded by n_C as indicated at the top of the figure, and the fractions of peaks grouped by n_C are reported in (d) the pie charts. The gray bars are fluorinated contaminations or non-identified compounds. The nitrated phenols are drawn separately with black peaks in (a)–(c). The molecules represented by the gray and black bars were not included in (d). Diurnal patterns of these three factors are shown in (e): the bold solid lines are the median values; shaded areas represent percentiles of 75 % and 25 %; and solid circles represent mean values.

lower. A NO_3 -initiated factor, called the nighttime type-2 factor, has also been discovered in Hyytiälä, Finland (Yan et al., 2016), but the similar factor we found has a higher proportion of organic nitrates, due to the more abundant NO_x here.

$$\begin{split} &RO_{2} \cdot + R'O_{2} \cdot \rightarrow ROOR' + O_{2} \\ &C_{10}H_{16} + NO_{3} \cdot \stackrel{O_{2}}{\rightarrow} C_{10}H_{16}NO_{5} \cdot \stackrel{H \text{ shift} + O_{2}}{\rightarrow} C_{10}H_{16}NO_{7} \cdot \\ &\stackrel{H \text{ shift} + O_{2}}{\rightarrow} C_{10}H_{16}NO_{9} \cdot \stackrel{H \text{ shift} + O_{2}}{\rightarrow} C_{10}H_{16}NO_{11} \cdot \\ &C_{10}H_{16} + NO_{3} \cdot \stackrel{O_{2}}{\rightarrow} C_{10}H_{16}NO_{5} \cdot \rightarrow C_{10}H_{16}NO_{4} \cdot \text{ (Alkoxy)} \\ &\stackrel{H \text{ shift} + O_{2}}{\rightarrow} C_{10}H_{16}NO_{6} \cdot \stackrel{H \text{ shift} + O_{2}}{\rightarrow} C_{10}H_{16}NO_{8} \cdot \end{aligned} \quad (R5b)$$

In terms of the fingerprint molecules of this factor (summarized in Table S9 in the Supplement), the $C_{10}H_{15}O_{5-12}N$ series are carbonyl products from precursor RO_2 or RO terminations, while the $C_{10}H_{17}O_{5-9}N$ series are alcohol or hydroperoxide products from precursor RO_2 terminations. The $C_7H_9O_{6-8}N$, $C_9H_{15}O_{6-9}N$, $C_9H_{13}O_{7-10}N$, and $C_8H_{13}O_{7-8}N$ series are expected to be fragments. The closed-shell compounds mentioned above have been reported

in the experiments of a monoterpene + NO₃ system (Nah et al., 2016; Faxon et al., 2018; Takeuchi and Ng, 2019).

It is noteworthy that a set of nitrogen-containing radicals, C₁₀H₁₆O₆₋₁₁N (peak fittings are shown in Fig. S9 in the Supplement), is present in the BVOC-OOM-II factor. Starting from a generic monoterpene molecule with the formula $C_{10}H_{16}$, the NO₃ addition with fast O₂ addition results in a peroxy radical with the formula C₁₀H₁₆O₅N. If the initial intermediate RO2 is capable of proceeding via autoxidation by the formal addition of O_2 , we expect radicals, $C_{10}H_{16}O_{5+2x}N$ (x denotes times of autoxidation performed) with an odd oxygen number, to be formed (Reaction R5a). In addition, peroxy radicals with an even oxygen number, $C_{10}H_{16}O_{6+2x}N$, are likely produced via a reaction chain (R5b): (1) RO₂ is propagated to RO through bimolecular reactions, and (2) RO isomerizes to an alcohol by internal H abstraction forming a carbon-centered radical (Orlando et al., 2003; Orlando and Tyndall, 2012); (3) the carbon-centered radical can again take up an oxygen molecule and follow the autoxidation route. The C₁₀H₁₆O₉N radical is also moderately intense in the BVOC-OOM-I factor (Fig. 9a), testifying to the presence of NO₃ chemistry. These C₁₀H₁₆O₆₋₁₁N rad-

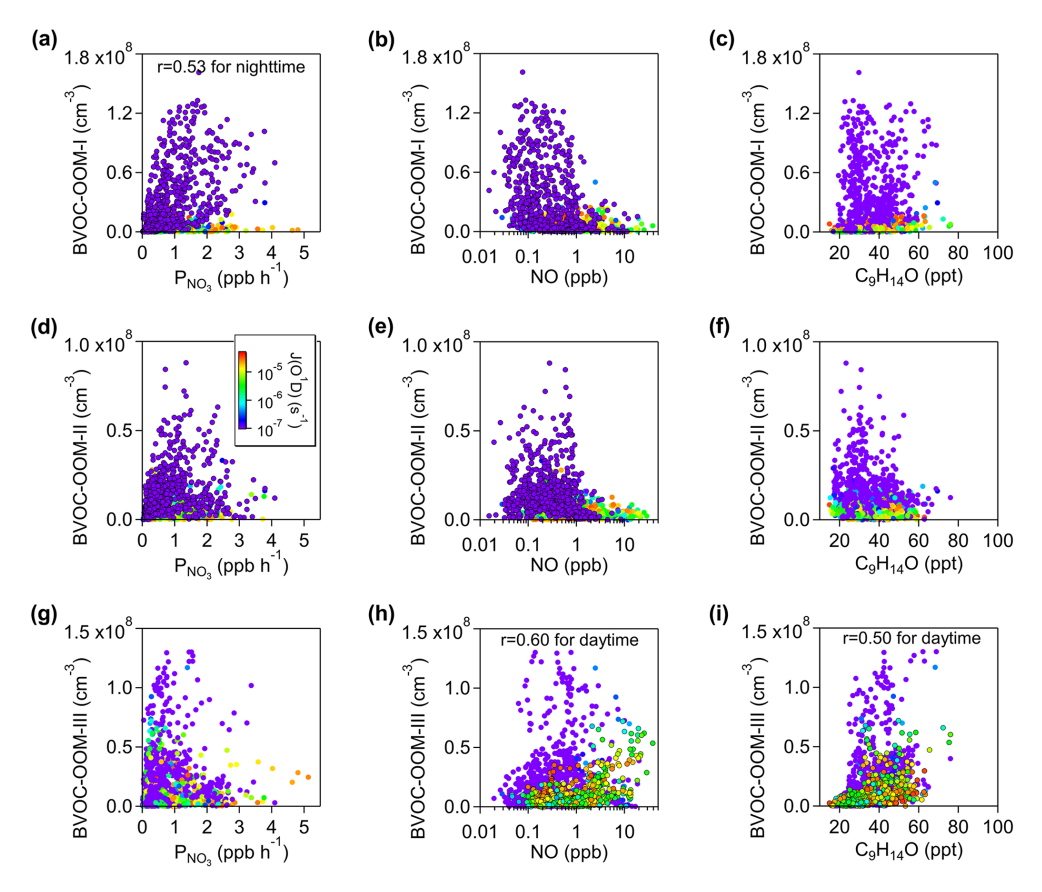


Figure 10. Scatterplots of the BVOC-OOM-I factor with (a) P_{NO_3} , (b) NO, and (c) nopinone ($C_9H_{14}O$). Scatterplots of the BVOC-OOM-II factor with (d) P_{NO_3} , (e) NO, and (f) nopinone ($C_9H_{14}O$). Scatterplots of the BVOC-OOM-III factor with (g) P_{NO_3} , (h) NO, and (i) nopinone ($C_9H_{14}O$). All the dots are colored by $J(O^1D)$ to show the difference between day and night. The Pearson correlation coefficient shown in (a) is calculated for the nighttime, but the correlation coefficients in (h) and (i) are only for the daytime.

icals are also reported in the CLOUD chamber (Yan et al., 2020). In addition to C_{10} radicals, a C_5 radical, $C_5H_8O_5N$ (peak fittings are shown in Fig. S9), is also found in the BVOC-OOM-II factor. $C_5H_8O_5N$ is possibly derived from the oxidation of isoprene initiated by NO_3 , as observed in the laboratory (Zhao et al., 2021). Another hypothesis is that $C_5H_8O_5N$ is formed from the fragmentation process of monoterpenes.

3.3.3 BVOC-OOM-III factor

The third nighttime factor (BVOC-OOM-III) is dominated by nitrogen-containing species with a contribution ratio of about 90%, among which dinitrates account for more than 20% (Fig. 2c). When grouped by carbon numbers, C_{10} OOMs have the strongest signal. Unlike the above two NO₃-related factors, this factor shows no correlation with P_{NO_3} but has positive correlation with NO, especially during the daytime (Fig. 10h). $C_9H_{14}O$, a typical product of NO-affected monoterpene oxidation (Calogirou et al., 1999), is found to be correlated with this factor (Fig. 10i). It is reasonable to infer that these organic nitrates may come from termina-

tions of monoterpene RO₂ by NO. In addition to the elevated intensity during the nighttime, this factor still remains at a relatively high concentration in the morning, a concentration which is much higher than those of the two NO₃related factors (Fig. 9e). Owing to the suppression of RO₂ autoxidation by NO and the relatively insufficient oxidant in dark environments, the effective OSc of the BVOC-OOM-III factor is lower than those of other factors. Apart from the mononitrates summarized in Table S10 in the Supplement, the $C_{10}H_{16}O_{7-10}N_2$ (dinitrates) and $C_{10}H_{17}O_{10}N_3$ (a trinitrate charged by NO_3^- at m/z 401) are most likely the result of multiple-generation processes involving OH or NO₃ oxidation of monoterpenes and $RO_2 + NO$ terminations. A similar factor, called terpene nitrates, has also been reported in Centreville, USA (Massoli et al., 2018), while in Hyytiälä, Finland (Yan et al., 2016), the daytime type-1 factor is related to NO.

3.4 Nitrated-phenol factors

Nitrated phenols are of concern because of their phytotoxicity (Rippen et al., 1987) and as important chromophores of

brown carbon in aerosols (Desyaterik et al., 2013; Mohr et al., 2013). The sources of these highly volatile compounds are attributed to biomass burning, vehicle exhausts, and secondary gas-phase or aqueous-phase production (Harrison et al., 2005). Here we identified three factors about NPs, including the NP-I factor dominated by nitrophenol, the NP-II factor dominated by substituted nitrophenols, and the NP-III factor dominated by dinitrophenols. Although the mass spectrum of the NP-III factor is less pure than those of the NP-I and NP-II factors (Fig. 11), its time series follows well with C₆H₄O₅N₂ (Fig. 11f), implying that this factor is driven by dinitrated-phenol chemistry. Since nitrated phenols have been broadly investigated and relatively clearly recognized (Harrison et al., 2005; Yuan et al., 2016; Wang et al., 2018b; Cheng et al., 2021), they are not discussed too much here. It seems that the chemistry of nitrated phenols is distinctive from that of other OOMs.

3.5 Ensemble chemical properties

After performing PMF analysis, over 1000 non-nitro molecules have been identified through HR peak fitting for each factor. The mean concentration of total non-nitro OOMs reconstructed from the selected PMF solution is about $2.1 \times$ 10⁸ molecules cm⁻³. Ensemble chemical properties of these non-nitro OOMs are summarized in Fig. 12. The number of carbon atoms implies the precursor information of OOMs. C₅ OOMs, which principally consist of isoprene products benefiting from the high reactivity and intensive emissions of isoprene in summer, are the most abundant (Fig. 12c), while C₆-C₉ OOMs are mostly likely formed from the oxidation of AVOCs such as aromatic and aliphatic series in the urban and suburban atmosphere, and as we expected, these AVOCderived OOMs account for about 50% of the total signal (Fig. 12c). The intensity of OOMs decreases from C₇ to C₉ determined by the concentration distribution of precursors but becomes a plateau at C₁₀ (Fig. 12c), indicating another source of C₁₀ OOMs, such as monoterpene oxidation. These results underscore the formation of SOA precursors from a mixture of anthropogenic and biogenic emissions, under ongoing forest cover increases (Wang et al., 2020a) in highly urbanized eastern China.

In addition to the anthropogenic VOCs, another humaninduced perturbation on the formation of OOMs is the NO_x affected chemistry of VOCs, i.e., $RO_2 + NO$ terminations or NO_3 -initiated oxidations. As shown in Fig. 12c, about 72 % of OOMs are nitrogen-bearing compounds, regarded as organic nitrates within the allowed range of uncertainty. If isoprene nitrates are not included, organic nitrates peak at C_7 as do the nitrogen-free species, showing the significant production of organic nitrates through the AVOCs $+ NO_x$ pathways. The NO_x effect on AVOC-derived OOMs, typified by the Aro-OOM factor and the Aliph-OOM factor, is not shown in previous ambient measurements (Yan et al., 2016; Lee et al., 2016; Massoli et al., 2018). OOMs grouped by carbon numbers or nitrogen numbers consistently have high absolute concentrations in the daytime (Fig. 12a and b), revealing the crucial role of photochemical progress, involving $RO_2 + NO$ termination reactions, in OOMs. In addition, The $C_5 - C_{10}$ OOMs are enhanced again during 19:00–22:00 LT, and the nighttime peak of C_{10} OOMs is even higher than their daytime peak (Fig. 12a). The nocturnal C_{10} OOMs are more intense than C_9 OOMs (Fig. 12a), and there are more C_{10} nitrates than C_9 nitrates (Fig. 12c). These results show the fate of VOCs degraded by NO_3 during the nighttime, and it is more important to monoterpenes. In contrast to nitrogen-free OOMs, organic nitrates are enriched through the reactions of BVOCs with NO_3 in the early evening (Fig. 12b), as indicated by three BVOC nighttime chemistry factors.

Apart from reflecting the influence of NO_x , multi-nitrates also imply the multiple generations of VOC oxidation, and multiple generations are evident in the products of isoprene (e.g., $C_5H_{10}O_8N_2$ and $C_5H_9O_{10}N_3$) due to its two carbon–carbon double bonds. As products of mononitrates, multi-nitrates follow mononitrates in their diurnal variation, with double peaks initiated by OH and NO_3 respectively (Fig. 12b). Considering that the formation of organic nitrate is only a small branch of RO_2+NO termination, the contribution of multi-step oxidation should be larger than that shown in Fig. 12c.

4 Conclusions

We have investigated the sources and characteristics of gasphase OOMs observed using a nitrate CI-APi-TOF at the SORPES station in the YRD of eastern China, an environment dominated by anthropogenic emissions with enhanced biogenic emissions during summer.

The binPMF analysis, which avoids the uncertainty introduced by high-resolution peak fitting to the input data matrix, was applied to deconvolve the complexity of the data set, and it resolved 14 factors, among which 12 factors have been discussed in detail. A morning factor (Aro-OOM), correlated with the production rates of RO₂ from aromatics, is characterized by unsaturated products of aromatics such as $C_xH_{2x-5}O_{6-9}N$ (x = [6, 12]). An afternoon factor (Aliph-OOM), containing the bulk of C₆-C₉ dinitrates and trinitrates such as $C_x H_{2x-2} O_8 N_2$ (x = [4, 13]) and $C_x H_{2x} O_8 N_2$ (x = [4, 8]), is assumed to be derived from aliphatic oxidation. A transported factor (Isop-OOM) correlates with MVK-MACR and SOAs and is exclusively dominated by isoprene nitrates (e.g., C₅H₁₀O₈N₂ and C₅H₉O₁₀N₃). A nighttime factor (BVOC-OOM-III), related to NO, is dominated by terpenes nitrates such as C₁₀H₁₅O₆N, $C_{10}H_{16}O_{7-10}N_2$, and $C_{10}H_{17}O_{10}N_3$. In addition to the factors distinguished by precursors, several factors are driven by chemistry. A factor following $J(O^1D)$ (Photo-related), consisting of isoprene products mixed with others, is thought

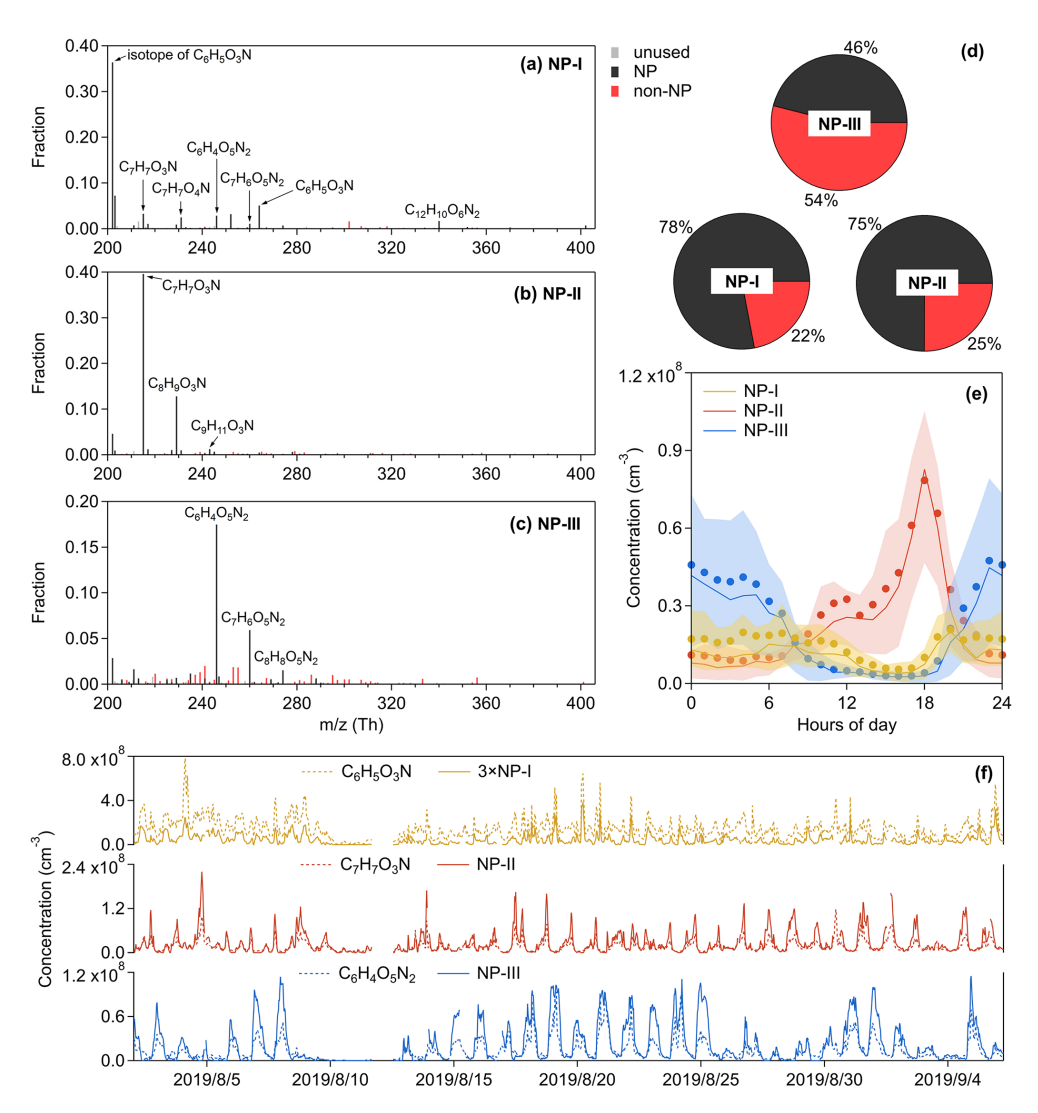


Figure 11. Mass spectra of (a) the NP-I factor, (b) the NP-II factor, and (c) the NP-III factor, and the elemental formulas of major peaks are labeled above them. The gray bars are fluorinated contaminations or non-identified compounds. The nitrated phenols are drawn separately with black peaks in (a–c), while other OOMs are plotted as red peaks. The proportions of these two types of OOMs are shown in (d) the pie chart. The molecules represented by the gray were not included in (d). Diurnal patterns of these three factors are shown in (e): the bold solid lines are the median values; shaded areas represent percentiles of 75 % and 25 %; and solid circles represent mean values. (f) Time series of PMF factors and tracers.

to be produced by in situ photochemistry. An afternoon factor (Temp-related), having the most abundant nitrogen-free OOMs such as $C_xH_{2x-4}O_{5-6}$ (x=[5,10]), $C_xH_{2x-2}O_5$ (x=[5,10]), and $C_xH_{2x-6}O_4$ (x=[5,10]), is generated involving temperature-influenced chemistry. A daytime factor (O_x - and SOA-related), correlated well with O_x and SOAs, indicates the photochemical aging process. Two nighttime factors (BVOC-OOM-I and BVOC-OOM-II), benefiting from NO_3 and suppressed by NO, are considered to be produced from the NO_3 -initiated oxidation of BVOCs, and both of them have the fingerprint molecule, $C_{10}H_{16}O_9N$. The remaining three factors are governed by nitrated phenols.

All of these factors from various precursors are influenced in different ways by NO_x . Over 1000 non-nitro molecules have been identified and then reconstructed from the selected solution of binPMF, and about 72% of the total signal is contributed by nitrogen-containing OOMs, almost regarded as organic nitrates formed through $RO_2 + NO$ terminations or NO_3 -initiated oxidations. Moreover, multi-nitrates have a contribution ratio of about 24% to total concentration, indicating the significant presence of multiple oxidation generations, especially for isoprene (e.g., $C_5H_{10}O_8N_2$ and $C_5H_9O_{10}N_3$). The nitrate CI-APi-TOF data set presented here highlights the decisive role of NO_x chemistry on OOM formation in densely populated areas.

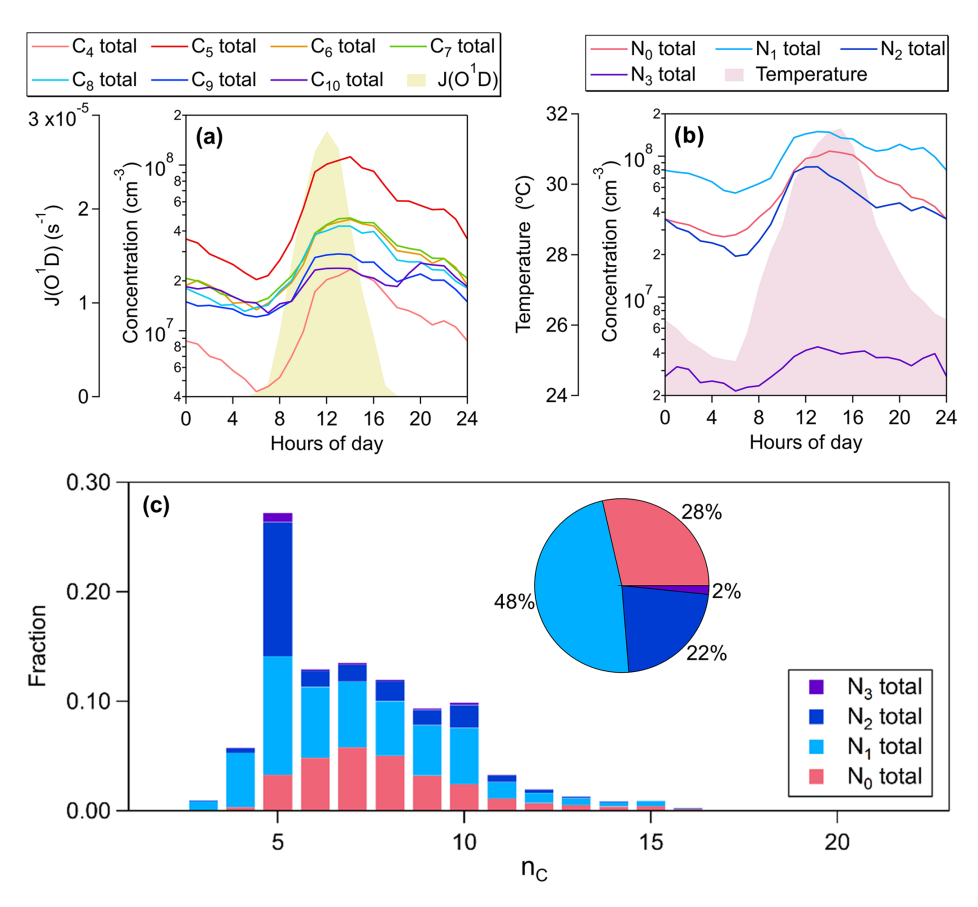


Figure 12. Ensemble chemical properties of non-nitro OOMs reconstructed from the selected PMF solution. (a) Median diurnal cycles of total compounds with a carbon number of 5–10. (b) Median diurnal cycles of total compounds with $n_{\rm N}$ of 0–3. (c) The distributions of total observed OOMs at different $n_{\rm C}$ values. OOMs on each carbon number are grouped by nitrogen number, and the total concentration fractions of each groups are reported in the pie chart. Since we selected peaks in the m/z range of 202–404 Th, OOMs with $n_{\rm C} < 5$ or $n_{\rm C} > 10$ detected by the nitrate CI-APi-TOF are underestimated.

The differences in OOMs observed in different environments are so clear, and the underlying causes for this are well worth considering. The precursors, oxidants, and formation pathways of OOMs change when moving from urbanized areas to pristine regions, as AVOC and NO_x concentrations decrease and BVOC concentrations increase. This process can also occur under the trend of global warming and anthropogenic emissions mitigation, but we still know very little about it. Clarifying the variations in compositions, properties, and the formation efficiency of OOMs will help us to understand the evolution of SOA production during this process. In summary, our findings highlight the dramatic interactions between anthropogenic and biogenic emissions and encourage more investigations from a mechanistic point of view.

Appendix A: The selected solution for binPMF analysis of nitrate CI-APi-TOF data

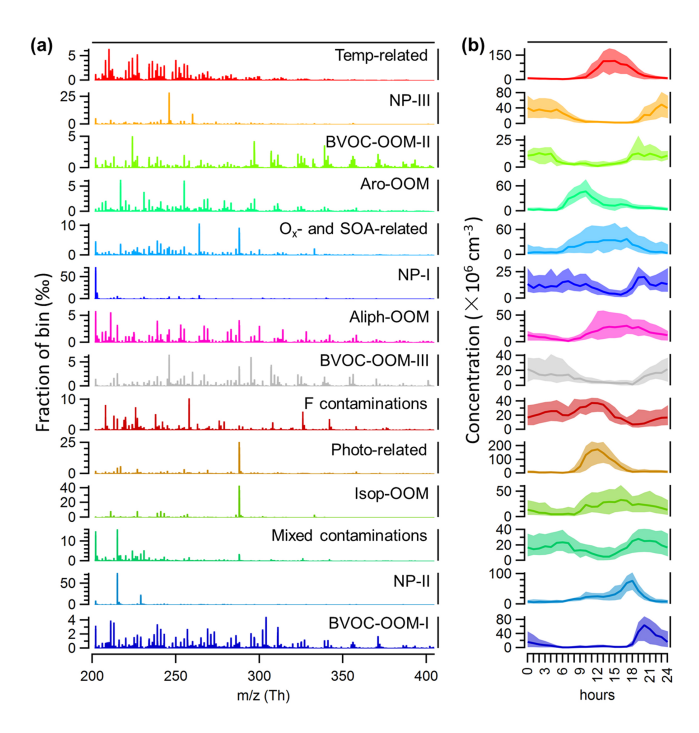


Figure A1. The selected solution for binPMF analysis of nitrate CI-APi-TOF data, showing the **(a)** mass profile and **(b)** diurnal cycle of different factors.

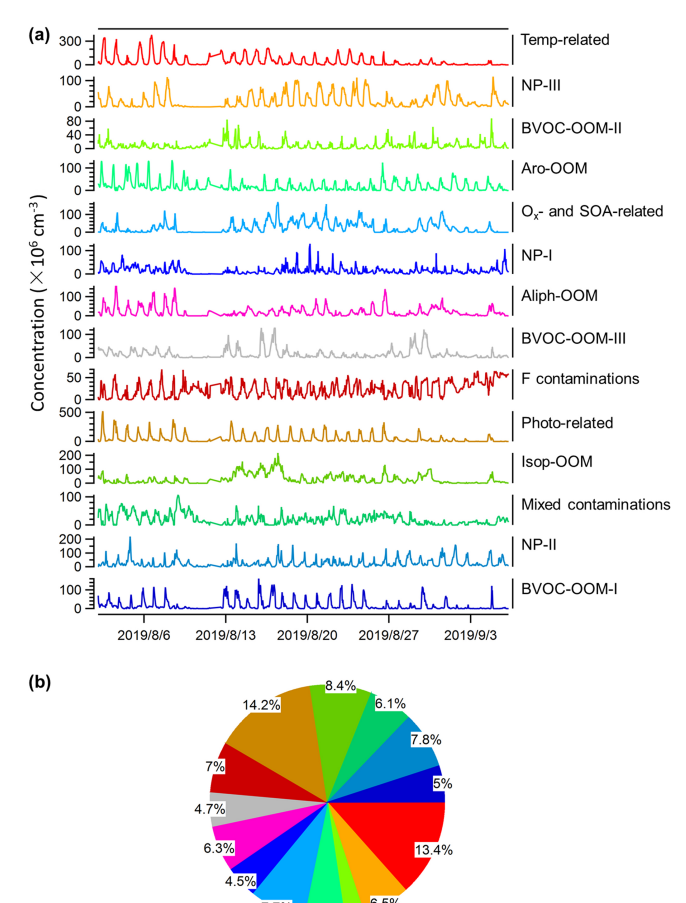


Figure A2. The selected solution for binPMF analysis of the nitrate CI-APi-TOF, showing the (a) time series of and (b) contribution to the total signal reconstructed by PMF of each factor.

Data availability. Measurement data at the SORPES station, including OOM data and relevant trace gas and aerosol data as well as meteorological data, are available upon request from the corresponding author before the SORPES database is open to the public.

Supplement. The supplement related to this article is available online at: https://doi.org/10.5194/acp-21-14789-2021-supplement.

Author contributions. WN and AD designed this research. YL, YL, DG, CL, ZX, LC, TW, LW, PS, XQ, JW, and XC conducted the measurements. YL, WN, CY, YZ, DH, ZW, and DW analyzed the data. YL, WN, ND, ME, and AD wrote the paper.

Competing interests. Some authors are members of the editorial board of Atmospheric Chemistry and Physics. The peer-review process was guided by an independent editor, and the authors have also no other competing interests to declare.

Disclaimer. Publisher's note: Copernicus Publications remains neutral with regard to jurisdictional claims in published maps and institutional affiliations.

Acknowledgements. We thank colleagues and students at the School of Atmospheric Sciences at Nanjing University for their contributions to the maintenance of the measurements. We thank the tofTools team for providing tools for mass spectrometry analysis.

Financial support. This work was mainly funded by the National Key R&D Program of China (2016YFC0202000), the National Natural Science Foundation of China (NSFC) (41875175 and 42075101), the Shanghai Rising-Star Program (19QB1402900), the Jiangsu Province Key R&D Program Major Technology Demonstration (BE 2019704), and the US National Science Foundation grant CHE-1807530.

Review statement. This paper was edited by Thomas Karl and reviewed by two anonymous referees.

References

- Atkinson, R.: Atmospheric chemistry of VOCs and NOx, Atmos. Environ., 34, 2063–2101, https://doi.org/10.1016/s1352-2310(99)00460-4, 2000.
- Ayres, B. R., Allen, H. M., Draper, D. C., Brown, S. S., Wild, R. J., Jimenez, J. L., Day, D. A., Campuzano-Jost, P., Hu, W., de Gouw, J., Koss, A., Cohen, R. C., Duffey, K. C., Romer, P., Baumann, K., Edgerton, E., Takahama, S., Thornton, J. A., Lee, B. H., Lopez-Hilfiker, F. D., Mohr, C., Wennberg, P. O., Nguyen, T. B., Teng, A., Goldstein, A. H., Olson, K., and Fry, J. L.:

- Organic nitrate aerosol formation via NO₃ + biogenic volatile organic compounds in the southeastern United States, Atmos. Chem. Phys., 15, 13377–13392, https://doi.org/10.5194/acp-15-13377-2015, 2015.
- Beck, L. J., Sarnela, N., Junninen, H., Hoppe, C. J. M., Garmash, O., Bianchi, F., Riva, M., Rose, C., Peräkylä, O., Wimmer, D., Kausiala, O., Jokinen, T., Ahonen, L., Mikkilä, J., Hakala, J., He, X.-C., Kontkanen, J., Wolf, K. K. E., Cappelletti, D., Mazzola, M., Traversi, R., Petroselli, C., Viola, A. P., Vitale, V., Lange, R., Massling, A., Nøjgaard, J. K., Krejci, R., Karlsson, L., Zieger, P., Jang, S., Lee, K., Vakkari, V., Lampilahti, J., Thakur, R. C., Leino, K., Kangasluoma, J., Duplissy, E.-M., Siivola, E., Marbouti, M., Tham, Y. J., Saiz-Lopez, A., Petäjä, T., Ehn, M., Worsnop, D. R., Skov, H., Kulmala, M., Kerminen, V.-M., and Sipilä, M.: Differing mechanisms of new particle formation at two Arctic sites, Geophys. Res. Lett., 48, e2020GL091334, https://doi.org/10.1029/2020GL091334, 2021.
- Berndt, T., Richters, S., Jokinen, T., Hyttinen, N., Kurten, T., Otkjaer, R. V., Kjaergaard, H. G., Stratmann, F., Herrmann, H., Sipila, M., Kulmala, M., and Ehn, M.: Hydroxyl radical-induced formation of highly oxidized organic compounds, Nat. Commun., 7, 13677, https://doi.org/10.1038/ncomms13677, 2016.
- Bertram, T. H., Kimmel, J. R., Crisp, T. A., Ryder, O. S., Yatavelli, R. L. N., Thornton, J. A., Cubison, M. J., Gonin, M., and Worsnop, D. R.: A field-deployable, chemical ionization time-of-flight mass spectrometer, Atmos. Meas. Tech., 4, 1471–1479, https://doi.org/10.5194/amt-4-1471-2011, 2011.
- Bianchi, F., Tröstl, J., Junninen, H., Frege, C., Henne, S., Hoyle, C. R., Molteni, U., Herrmann, E., Adamov, A., Bukowiecki, N., Chen, X., Duplissy, J., Gysel, M., Hutterli, M., Kangasluoma, J., Kontkanen, J., Kürten, A., Manninen, H. E., Münch, S., Peräkylä, O., Petäjä, T., Rondo, L., Williamson, C., Weingartner, E., Curtius, J., Worsnop, D. R., Kulmala, M., Dommen, J., and Baltensperger, U.: New particle formation in the free troposphere: A question of chemistry and timing, Science, 352, 1109, https://doi.org/10.1126/science.aad5456, 2016.
- Bianchi, F., Kurten, T., Riva, M., Mohr, C., Rissanen, M. P., Roldin, P., Berndt, T., Crounse, J. D., Wennberg, P. O., Mentel, T. F., Wildt, J., Junninen, H., Jokinen, T., Kulmala, M., Worsnop, D. R., Thornton, J. A., Donahue, N., Kjaergaard, H. G., and Ehn, M.: Highly oxygenated organic molecules (HOM) from gas-phase autoxidation involving peroxy radicals: a key contributor to atmospheric aerosol, Chem. Rev., 119, 3472–3509, https://doi.org/10.1021/acs.chemrev.8b00395, 2019.
- Birdsall, A. W. and Elrod, M. J.: Comprehensive NO-dependent study of the products of the oxidation of atmospherically relevant aromatic compounds, J. Phys. Chem. A, 115, 5397–5407, https://doi.org/10.1021/jp2010327, 2011.
- Bloss, C., Wagner, V., Jenkin, M. E., Volkamer, R., Bloss, W. J., Lee, J. D., Heard, D. E., Wirtz, K., Martin-Reviejo, M., Rea, G., Wenger, J. C., and Pilling, M. J.: Development of a detailed chemical mechanism (MCMv3.1) for the atmospheric oxidation of aromatic hydrocarbons, Atmos. Chem. Phys., 5, 641–664, https://doi.org/10.5194/acp-5-641-2005, 2005.
- Calogirou, A., Larsen, B. R., and Kotzias, D.: Gas-phase terpene oxidation products: a review, Atmos. Environ., 33, 1423–1439, https://doi.org/10.1016/S1352-2310(98)00277-5, 1999.
- Canonaco, F., Crippa, M., Slowik, J. G., Baltensperger, U., and Prévôt, A. S. H.: SoFi, an IGOR-based interface for

- the efficient use of the generalized multilinear engine (ME-2) for the source apportionment: ME-2 application to aerosol mass spectrometer data, Atmos. Meas. Tech., 6, 3649–3661, https://doi.org/10.5194/amt-6-3649-2013, 2013.
- Cheng, X., Chen, Q., Li, Y., Huang, G., Liu, Y., Lu, S., Zheng, Y., Qiu, W., Lu, K., Qiu, X., Bianchi, F., Yan, C., Yuan, B., Shao, M., Wang, Z., Canagaratna, M. R., Zhu, T., Wu, Y., and Zeng, L.: Secondary production of gaseous nitrated phenols in polluted urban environments, Environ. Sci. Technol., 55, 4410–4419, https://doi.org/10.1021/acs.est.0c07988, 2021.
- Crounse, J. D., Nielsen, L. B., Jørgensen, S., Kjaergaard, H. G., and Wennberg, P. O.: Autoxidation of organic compounds in the atmosphere, J. Phys. Chem. Lett., 4, 3513–3520, https://doi.org/10.1021/jz4019207, 2013.
- Desyaterik, Y., Sun, Y., Shen, X., Lee, T., Wang, X., Wang, T., and Collett, J. L.: Speciation of "brown" carbon in cloud water impacted by agricultural biomass burning in eastern China, J. Geophys. Res.-Atmos., 118, 7389–7399, https://doi.org/10.1002/jgrd.50561, 2013.
- Ding, A., Nie, W., Huang, X., Chi, X., Sun, J., Kerminen, V.-M., Xu, Z., Guo, W., Petäjä, T., Yang, X., Kulmala, M., and Fu, C.: Long-term observation of air pollution-weather/climate interactions at the SORPES station: a review and outlook, Front. Env. Sci. Eng., 10, 15, https://doi.org/10.1007/s11783-016-0877-3, 2016.
- Ding, A., Huang, X., Nie, W., Chi, X., Xu, Z., Zheng, L., Xu, Z., Xie, Y., Qi, X., Shen, Y., Sun, P., Wang, J., Wang, L., Sun, J., Yang, X.-Q., Qin, W., Zhang, X., Cheng, W., Liu, W., Pan, L., and Fu, C.: Significant reduction of PM_{2.5} in eastern China due to regional-scale emission control: evidence from SORPES in 2011–2018, Atmos. Chem. Phys., 19, 11791–11801, https://doi.org/10.5194/acp-19-11791-2019, 2019.
- Ding, A. J., Fu, C. B., Yang, X. Q., Sun, J. N., Zheng, L. F., Xie, Y. N., Herrmann, E., Nie, W., Petäjä, T., Kerminen, V.-M., and Kulmala, M.: Ozone and fine particle in the western Yangtze River Delta: an overview of 1 yr data at the SORPES station, Atmos. Chem. Phys., 13, 5813–5830, https://doi.org/10.5194/acp-13-5813-2013, 2013.
- Ehn, M., Junninen, H., Petäjä, T., Kurtén, T., Kerminen, V.-M., Schobesberger, S., Manninen, H. E., Ortega, I. K., Vehkamäki, H., Kulmala, M., and Worsnop, D. R.: Composition and temporal behavior of ambient ions in the boreal forest, Atmos. Chem. Phys., 10, 8513–8530, https://doi.org/10.5194/acp-10-8513-2010, 2010.
- Ehn, M., Kleist, E., Junninen, H., Petäjä, T., Lönn, G., Schobesberger, S., Dal Maso, M., Trimborn, A., Kulmala, M., Worsnop, D. R., Wahner, A., Wildt, J., and Mentel, Th. F.: Gas phase formation of extremely oxidized pinene reaction products in chamber and ambient air, Atmos. Chem. Phys., 12, 5113–5127, https://doi.org/10.5194/acp-12-5113-2012, 2012.
- Ehn, M., Thornton, J. A., Kleist, E., Sipila, M., Junninen, H., Pullinen, I., Springer, M., Rubach, F., Tillmann, R., Lee, B., Lopez-Hilfiker, F., Andres, S., Acir, I. H., Rissanen, M., Jokinen, T., Schobesberger, S., Kangasluoma, J., Kontkanen, J., Nieminen, T., Kurten, T., Nielsen, L. B., Jorgensen, S., Kjaergaard, H. G., Canagaratna, M., Maso, M. D., Berndt, T., Petaja, T., Wahner, A., Kerminen, V. M., Kulmala, M., Worsnop, D. R., Wildt, J., and Mentel, T. F.: A large source of low-volatility secondary organic aerosol, Nature, 506, 476–479, https://doi.org/10.1038/nature13032, 2014.

- Faxon, C., Hammes, J., Le Breton, M., Pathak, R. K., and Hallquist, M.: Characterization of organic nitrate constituents of secondary organic aerosol (SOA) from nitrate-radical-initiated oxidation of limonene using high-resolution chemical ionization mass spectrometry, Atmos. Chem. Phys., 18, 5467–5481, https://doi.org/10.5194/acp-18-5467-2018, 2018.
- Finlayson-Pitts, B. J. and Pitts, J. N.: CHAPTER 8 Acid Deposition: Formation and Fates of Inorganic and Organic Acids in the Troposphere, in: Chemistry of the Upper and Lower Atmosphere, edited by: Finlayson-Pitts, B. J. and Pitts, J. N., Academic Press, San Diego, 294–348, 2000.
- Frege, C., Ortega, I. K., Rissanen, M. P., Praplan, A. P., Steiner, G., Heinritzi, M., Ahonen, L., Amorim, A., Bernhammer, A.-K., Bianchi, F., Brilke, S., Breitenlechner, M., Dada, L., Dias, A., Duplissy, J., Ehrhart, S., El-Haddad, I., Fischer, L., Fuchs, C., Garmash, O., Gonin, M., Hansel, A., Hoyle, C. R., Jokinen, T., Junninen, H., Kirkby, J., Kürten, A., Lehtipalo, K., Leiminger, M., Mauldin, R. L., Molteni, U., Nichman, L., Petäjä, T., Sarnela, N., Schobesberger, S., Simon, M., Sipilä, M., Stolzenburg, D., Tomé, A., Vogel, A. L., Wagner, A. C., Wagner, R., Xiao, M., Yan, C., Ye, P., Curtius, J., Donahue, N. M., Flagan, R. C., Kulmala, M., Worsnop, D. R., Winkler, P. M., Dommen, J., and Baltensperger, U.: Influence of temperature on the molecular composition of ions and charged clusters during pure biogenic nucleation, Atmos. Chem. Phys., 18, 65–79, https://doi.org/10.5194/acp-18-65-2018, 2018.
- Fu, X., Wang, S. X., Zhao, B., Xing, J., Cheng, Z., Liu, H., and Hao, J. M.: Emission inventory of primary pollutants and chemical speciation in 2010 for the Yangtze River Delta region, China, Atmos. Environ., 70, 39–50, https://doi.org/10.1016/j.atmosenv.2012.12.034, 2013.
- Fuchs, N. A. and Sutugin, A. G.: High-Dispersed Aerosols, in: Topics in Current Aerosol Research, edited by: Hidy, G. M. and Brock, J. R., Pergamon, 1, 1971.
- Garmash, O., Rissanen, M. P., Pullinen, I., Schmitt, S., Kausiala, O., Tillmann, R., Zhao, D., Percival, C., Bannan, T. J., Priestley, M., Hallquist, Å. M., Kleist, E., Kiendler-Scharr, A., Hallquist, M., Berndt, T., McFiggans, G., Wildt, J., Mentel, T. F., and Ehn, M.: Multi-generation OH oxidation as a source for highly oxygenated organic molecules from aromatics, Atmos. Chem. Phys., 20, 515–537, https://doi.org/10.5194/acp-20-515-2020, 2020.
- Guo, Y., Yan, C., Li, C., Ma, W., Feng, Z., Zhou, Y., Lin, Z., Dada, L., Stolzenburg, D., Yin, R., Kontkanen, J., Daellenbach, K. R., Kangasluoma, J., Yao, L., Chu, B., Wang, Y., Cai, R., Bianchi, F., Liu, Y., and Kulmala, M.: Formation of nighttime sulfuric acid from the ozonolysis of alkenes in Beijing, Atmos. Chem. Phys., 21, 5499–5511, https://doi.org/10.5194/acp-21-5499-2021, 2021.
- Hallquist, M., Wenger, J. C., Baltensperger, U., Rudich, Y., Simpson, D., Claeys, M., Dommen, J., Donahue, N. M., George, C., Goldstein, A. H., Hamilton, J. F., Herrmann, H., Hoffmann, T., Iinuma, Y., Jang, M., Jenkin, M. E., Jimenez, J. L., Kiendler-Scharr, A., Maenhaut, W., McFiggans, G., Mentel, Th. F., Monod, A., Prévôt, A. S. H., Seinfeld, J. H., Surratt, J. D., Szmigielski, R., and Wildt, J.: The formation, properties and impact of secondary organic aerosol: current and emerging issues, Atmos. Chem. Phys., 9, 5155–5236, https://doi.org/10.5194/acp-9-5155-2009, 2009.

- Harrison, M. A. J., Barra, S., Borghesi, D., Vione, D., Arsene, C., and Iulian Olariu, R.: Nitrated phenols in the atmosphere: a review, Atmos. Environ., 39, 231–248, https://doi.org/10.1016/j.atmosenv.2004.09.044, 2005.
- Heinritzi, M., Simon, M., Steiner, G., Wagner, A. C., Kürten, A., Hansel, A., and Curtius, J.: Characterization of the massdependent transmission efficiency of a CIMS, Atmos. Meas. Tech., 9, 1449–1460, https://doi.org/10.5194/amt-9-1449-2016, 2016.
- Heinritzi, M., Dada, L., Simon, M., Stolzenburg, D., Wagner, A. C., Fischer, L., Ahonen, L. R., Amanatidis, S., Baalbaki, R., Baccarini, A., Bauer, P. S., Baumgartner, B., Bianchi, F., Brilke, S., Chen, D., Chiu, R., Dias, A., Dommen, J., Duplissy, J., Finkenzeller, H., Frege, C., Fuchs, C., Garmash, O., Gordon, H., Granzin, M., El Haddad, I., He, X., Helm, J., Hofbauer, V., Hoyle, C. R., Kangasluoma, J., Keber, T., Kim, C., Kürten, A., Lamkaddam, H., Laurila, T. M., Lampilahti, J., Lee, C. P., Lehtipalo, K., Leiminger, M., Mai, H., Makhmutov, V., Manninen, H. E., Marten, R., Mathot, S., Mauldin, R. L., Mentler, B., Molteni, U., Müller, T., Nie, W., Nieminen, T., Onnela, A., Partoll, E., Passananti, M., Petäjä, T., Pfeifer, J., Pospisilova, V., Quéléver, L. L. J., Rissanen, M. P., Rose, C., Schobesberger, S., Scholz, W., Scholze, K., Sipilä, M., Steiner, G., Stozhkov, Y., Tauber, C., Tham, Y. J., Vazquez-Pufleau, M., Virtanen, A., Vogel, A. L., Volkamer, R., Wagner, R., Wang, M., Weitz, L., Wimmer, D., Xiao, M., Yan, C., Ye, P., Zha, Q., Zhou, X., Amorim, A., Baltensperger, U., Hansel, A., Kulmala, M., Tomé, A., Winkler, P. M., Worsnop, D. R., Donahue, N. M., Kirkby, J., and Curtius, J.: Molecular understanding of the suppression of new-particle formation by isoprene, Atmos. Chem. Phys., 20, 11809–11821, https://doi.org/10.5194/acp-20-11809-2020, 2020.
- Herndon, S. C., Onasch, T. B., Wood, E. C., Kroll, J. H., Canagaratna, M. R., Jayne, J. T., Zavala, M. A., Knighton, W. B., Mazzoleni, C., Dubey, M. K., Ulbrich, I. M., Jimenez, J. L., Seila, R., de Gouw, J. A., de Foy, B., Fast, J., Molina, L. T., Kolb, C. E., and Worsnop, D. R.: Correlation of secondary organic aerosol with odd oxygen in Mexico City, Geophys. Res. Lett., 35, L15804, https://doi.org/10.1029/2008gl034058, 2008.
- Hu, W., Hu, M., Hu, W., Jimenez, J. L., Yuan, B., Chen, W., Wang, M., Wu, Y., Chen, C., Wang, Z., Peng, J., Zeng, L., and Shao, M.: Chemical composition, sources, and aging process of submicron aerosols in Beijing: Contrast between summer and winter, J. Geophys. Res.-Atmos., 121, 1955–1977, https://doi.org/10.1002/2015jd024020, 2016.
- Huang, R. J., Zhang, Y. L., Bozzetti, C., Ho, K. F., Cao, J. J.,
 Han, Y. M., Daellenbach, K. R., Slowik, J. G., Platt, S. M.,
 Canonaco, F., Zotter, P., Wolf, R., Pieber, S. M., Bruns, E.
 A., Crippa, M., Ciarelli, G., Piazzalunga, A., Schwikowski,
 M., Abbaszade, G., Schnelle-Kreis, J., Zimmermann, R., An,
 Z. S., Szidat, S., Baltensperger, U., El Haddad, I., and Prevot, A. S. H.: High secondary aerosol contribution to particulate pollution during haze events in China, Nature, 514, 218–222, https://doi.org/10.1038/nature13774, 2014.
- Hyttinen, N., Kupiainen-Määttä, O., Rissanen, M. P., Muuronen, M., Ehn, M., and Kurtén, T.: Modeling the Charging of Highly Oxidized Cyclohexene Ozonolysis Products Using Nitrate-Based Chemical Ionization, J. Phys. Chem. A, 119, 6339–6345, https://doi.org/10.1021/acs.jpca.5b01818, 2015.

- IPCC: Climate Change 2013 The physical science basis: working group I contribution to the fifth assessment report of the Intergovernmental Panel on Climate Change, Cambridge University Press, Cambridge, 2013.
- Jenkin, M. E., Young, J. C., and Rickard, A. R.: The MCM v3.3.1 degradation scheme for isoprene, Atmos. Chem. Phys., 15, 11433–11459, https://doi.org/10.5194/acp-15-11433-2015, 2015
- Jimenez, J. L., Canagaratna, M. R., Donahue, N. M., Prevot, A. S. H., Zhang, Q., Kroll, J. H., DeCarlo, P. F., Allan, J. D., Coe, H., Ng, N. L., Aiken, A. C., Docherty, K. S., Ulbrich, I. M., Grieshop, A. P., Robinson, A. L., Duplissy, J., Smith, J. D., Wilson, K. R., Lanz, V. A., Hueglin, C., Sun, Y. L., Tian, J., Laaksonen, A., Raatikainen, T., Rautiainen, J., Vaattovaara, P., Ehn, M., Kulmala, M., Tomlinson, J. M., Collins, D. R., Cubison, M. J., Dunlea, E. J., Huffman, J. A., Onasch, T. B., Alfarra, M. R., Williams, P. I., Bower, K., Kondo, Y., Schneider, J., Drewnick, F., Borrmann, S., Weimer, S., Demerjian, K., Salcedo, D., Cottrell, L., Griffin, R., Takami, A., Miyoshi, T., Hatakeyama, S., Shimono, A., Sun, J. Y., Zhang, Y. M., Dzepina, K., Kimmel, J. R., Sueper, D., Jayne, J. T., Herndon, S. C., Trimborn, A. M., Williams, L. R., Wood, E. C., Middlebrook, A. M., Kolb, C. E., Baltensperger, U., and Worsnop, D. R.: Evolution of organic aerosols in the atmosphere, Science, 326, 1525–1529, https://doi.org/10.1126/science.1180353, 2009.
- Jokinen, T., Sipilä, M., Junninen, H., Ehn, M., Lönn, G., Hakala, J., Petäjä, T., Mauldin III, R. L., Kulmala, M., and Worsnop, D. R.: Atmospheric sulphuric acid and neutral cluster measurements using CI-APi-TOF, Atmos. Chem. Phys., 12, 4117–4125, https://doi.org/10.5194/acp-12-4117-2012, 2012.
- Jokinen, T., Sipila, M., Richters, S., Kerminen, V. M., Paasonen, P., Stratmann, F., Worsnop, D., Kulmala, M., Ehn, M., Herrmann, H., and Berndt, T.: Rapid autoxidation forms highly oxidized RO₂ radicals in the atmosphere, Angew. Chem. Int. Edit., 53, 14596–14600, https://doi.org/10.1002/anie.201408566, 2014.
- Jokinen, T., Berndt, T., Makkonen, R., Kerminen, V. M., Junninen, H., Paasonen, P., Stratmann, F., Herrmann, H., Guenther, A. B., Worsnop, D. R., Kulmala, M., Ehn, M., and Sipila, M.: Production of extremely low volatile organic compounds from biogenic emissions: Measured yields and atmospheric implications, P. Natl. Acad. Sci. USA, 112, 7123–7128, https://doi.org/10.1073/pnas.1423977112, 2015.
- Junninen, H., Ehn, M., Petäjä, T., Luosujärvi, L., Kotiaho, T., Kostiainen, R., Rohner, U., Gonin, M., Fuhrer, K., Kulmala, M., and Worsnop, D. R.: A high-resolution mass spectrometer to measure atmospheric ion composition, Atmos. Meas. Tech., 3, 1039–1053, https://doi.org/10.5194/amt-3-1039-2010, 2010.
- Karl, T., Striednig, M., Graus, M., Hammerle, A., and Wohlfahrt, G.: Urban flux measurements reveal a large pool of oxygenated volatile organic compound emissions, P. Natl. Acad. Sci. USA, 115, 1186, https://doi.org/10.1073/pnas.1714715115, 2018.
- Kirkby, J., Duplissy, J., Sengupta, K., Frege, C., Gordon, H.,
 Williamson, C., Heinritzi, M., Simon, M., Yan, C., Almeida, J.,
 Trostl, J., Nieminen, T., Ortega, I. K., Wagner, R., Adamov, A.,
 Amorim, A., Bernhammer, A. K., Bianchi, F., Breitenlechner,
 M., Brilke, S., Chen, X. M., Craven, J., Dias, A., Ehrhart, S., Flagan, R. C., Franchin, A., Fuchs, C., Guida, R., Hakala, J., Hoyle,
 C. R., Jokinen, T., Junninen, H., Kangasluoma, J., Kim, J., Krapf,
 M., Kurten, A., Laaksonen, A., Lehtipalo, K., Makhmutov, V.,

- Mathot, S., Molteni, U., Onnela, A., Perakyla, O., Piel, F., Petaja, T., Praplan, A. P., Pringle, K., Rap, A., Richards, N. A. D., Riipinen, I., Rissanen, M. P., Rondo, L., Sarnela, N., Schobesberger, S., Scott, C. E., Seinfeld, J. H., Sipila, M., Steiner, G., Stozhkov, Y., Stratmann, F., Tome, A., Virtanen, A., Vogel, A. L., Wagner, A. C., Wagner, P. E., Weingartner, E., Wimmer, D., Winkler, P. M., Ye, P. L., Zhang, X., Hansel, A., Dommen, J., Donahue, N. M., Worsnop, D. R., Baltensperger, U., Kulmala, M., Carslaw, K. S., and Curtius, J.: Ion-induced nucleation of pure biogenic particles, Nature, 533, p. 521, https://doi.org/10.1038/nature17953, 2016.
- Kuerten, A., Rondo, L., Ehrhart, S., and Curtius, J.: Calibration of a chemical ionization mass spectrometer for the measurement of gaseous sulfuric acid, J. Phys. Chem. A, 116, 6375–6386, https://doi.org/10.1021/jp212123n, 2012.
- Kulmala, M., Petaja, T., Nieminen, T., Sipila, M., Manninen, H. E., Lehtipalo, K., Dal Maso, M., Aalto, P. P., Junninen, H., Paasonen, P., Riipinen, I., Lehtinen, K. E., Laaksonen, A., and Kerminen, V. M.: Measurement of the nucleation of atmospheric aerosol particles, Nat. Protoc., 7, 1651–1667, https://doi.org/10.1038/nprot.2012.091, 2012.
- Kulmala, M., Kontkanen, J., Junninen, H., Lehtipalo, K., Manninen, H. E., Nieminen, T., Petaja, T., Sipila, M., Schobesberger, S., Rantala, P., Franchin, A., Jokinen, T., Jarvinen, E., Aijala, M., Kangasluoma, J., Hakala, J., Aalto, P. P., Paasonen, P., Mikkila, J., Vanhanen, J., Aalto, J., Hakola, H., Makkonen, U., Ruuskanen, T., Mauldin III, R. L., Duplissy, J., Vehkamaki, H., Back, J., Kortelainen, A., Riipinen, I., Kurten, T., Johnston, M. V., Smith, J. N., Ehn, M., Mentel, T. F., Lehtinen, K. E. J., Laaksonen, A., Kerminen, V.-M., and Worsnop, D. R.: Direct observations of atmospheric aerosol nucleation, Science, 339, 943–946, https://doi.org/10.1126/science.1227385, 2013.
- Kwan, A. J., Chan, A. W. H., Ng, N. L., Kjaergaard, H. G., Seinfeld, J. H., and Wennberg, P. O.: Peroxy radical chemistry and OH radical production during the NO₃-initiated oxidation of isoprene, Atmos. Chem. Phys., 12, 7499–7515, https://doi.org/10.5194/acp-12-7499-2012, 2012.
- Lambe, A., Massoli, P., Zhang, X., Canagaratna, M., Nowak, J., Daube, C., Yan, C., Nie, W., Onasch, T., Jayne, J., Kolb, C., Davidovits, P., Worsnop, D., and Brune, W.: Controlled nitric oxide production via O(¹D) + N₂O reactions for use in oxidation flow reactor studies, Atmos. Meas. Tech., 10, 2283–2298, https://doi.org/10.5194/amt-10-2283-2017, 2017.
- Lee, B. H., Lopez-Hilfiker, F. D., Mohr, C., Kurtén, T., Worsnop, D. R., and Thornton, J. A.: An iodide-adduct high-resolution time-of-flight chemical-ionization mass spectrometer: application to atmospheric inorganic and organic compounds, Environ. Sci. Technol., 48, 6309–6317, https://doi.org/10.1021/es500362a, 2014.
- Lee, B. H., Mohr, C., Lopez-Hilfiker, F. D., Lutz, A., Hallquist, M.,
 Lee, L., Romer, P., Cohen, R. C., Iyer, S., Kurtén, T., Hu, W., Day,
 D. A., Campuzano-Jost, P., Jimenez, J. L., Xu, L., Ng, N. L., Guo,
 H., Weber, R. J., Wild, R. J., Brown, S. S., Koss, A., de Gouw,
 J., Olson, K., Goldstein, A. H., Seco, R., Kim, S., McAvey, K.,
 Shepson, P. B., Starn, T., Baumann, K., Edgerton, E. S., Liu, J.,
 Shilling, J. E., Miller, D. O., Brune, W., Schobesberger, S., Ambro, E. L., and Thornton, J. A.: Highly functionalized organic
 nitrates in the southeast United States: Contribution to secondary
 organic aerosol and reactive nitrogen budgets, P. Natl. Acad.

- Sci. USA, 113, 1516, https://doi.org/10.1073/pnas.1508108113, 2016.
- Li, Y., Nie, W., Liu, Y., Huang, D., Xu, Z., Peng, X., George, C., Yan, C., Tham, Y. J., Yu, C., Xia, M., Fu, X., Wang, X., Xue, L., Wang, Z., Xu, Z., Chi, X., Wang, T., and Ding, A.: Photoinduced production of chlorine molecules from titanium dioxide surfaces containing chloride, Environ. Sci. Tech. Let., 7, 70–75, https://doi.org/10.1021/acs.estlett.9b00704, 2020.
- Lim, S. S., Vos, T., Flaxman, A. D., Danaei, G., Shibuya, K., Adair-Rohani, H., Amann, M., Anderson, H. R., Andrews, K. G., Aryee, M., Atkinson, C., Bacchus, L. J., Bahalim, A. N., Balakrishnan, K., Balmes, J., Barker-Collo, S., Baxter, A., Bell, M. L., Blore, J. D., Blyth, F., Bonner, C., Borges, G., Bourne, R., Boussinesq, M., Brauer, M., Brooks, P., Bruce, N. G., Brunekreef, B., Bryan-Hancock, C., Bucello, C., Buchbinder, R., Bull, F., Burnett, R. T., Byers, T. E., Calabria, B., Carapetis, J., Carnahan, E., Chafe, Z., Charlson, F., Chen, H. L., Chen, J. S., Cheng, A. T. A., Child, J. C., Cohen, A., Colson, K. E., Cowie, B. C., Darby, S., Darling, S., Davis, A., Degenhardt, L., Dentener, F., Des Jarlais, D. C., Devries, K., Dherani, M., Ding, E. L., Dorsey, E. R., Driscoll, T., Edmond, K., Ali, S. E., Engell, R. E., Erwin, P. J., Fahimi, S., Falder, G., Farzadfar, F., Ferrari, A., Finucane, M. M., Flaxman, S., Fowkes, F. G. R., Freedman, G., Freeman, M. K., Gakidou, E., Ghosh, S., Giovannucci, E., Gmel, G., Graham, K., Grainger, R., Grant, B., Gunnell, D., Gutierrez, H. R., Hall, W., Hoek, H. W., Hogan, A., Hosgood, H. D., Hoy, D., Hu, H., Hubbell, B. J., Hutchings, S. J., Ibeanusi, S. E., Jacklyn, G. L., Jasrasaria, R., Jonas, J. B., Kan, H. D., Kanis, J. A., Kassebaum, N., Kawakami, N., Khang, Y. H., Khatibzadeh, S., Khoo, J. P., Kok, C., Laden, F., Lalloo, R., Lan, Q., Lathlean, T., Leasher, J. L., Leigh, J., Li, Y., Lin, J. K., Lipshultz, S. E., London, S., Lozano, R., Lu, Y., Mak, J., Malekzadeh, R., Mallinger, L., Marcenes, W., March, L., Marks, R., Martin, R., McGale, P., McGrath, J., Mehta, S., Mensah, G. A., Merriman, T. R., Micha, R., Michaud, C., Mishra, V., Hanafiah, K. M., Mokdad, A. A., Morawska, L., Mozaffarian, D., Murphy, T., Naghavi, M., Neal, B., Nelson, P. K., Nolla, J. M., Norman, R., Olives, C., Omer, S. B., Orchard, J., Osborne, R., Ostro, B., Page, A., Pandey, K. D., Parry, C. D. H., Passmore, E., Patra, J., Pearce, N., Pelizzari, P. M., Petzold, M., Phillips, M. R., Pope, D., Pope, C. A., Powles, J., Rao, M., Razavi, H., Rehfuess, E. A., Rehm, J. T., Ritz, B., Rivara, F. P., Roberts, T., Robinson, C., Rodriguez-Portales, J. A., Romieu, I., Room, R., Rosenfeld, L. C., Roy, A., Rushton, L., Salomon, J. A., Sampson, U., Sanchez-Riera, L., Sanman, E., Sapkota, A., Seedat, S., Shi, P. L., Shield, K., Shivakoti, R., Singh, G. M., Sleet, D. A., Smith, E., Smith, K. R., Stapelberg, N. J. C., Steenland, K., Stockl, H., Stovner, L. J., Straif, K., Straney, L., Thurston, G. D., Tran, J. H., Van Dingenen, R., van Donkelaar, A., Veerman, J. L., Vijayakumar, L., Weintraub, R., Weissman, M. M., White, R. A., Whiteford, H., Wiersma, S. T., Wilkinson, J. D., Williams, H. C., Williams, W., Wilson, N., Woolf, A. D., Yip, P., Zielinski, J. M., Lopez, A. D., Murray, C. J. L., and Ezzati, M.: A comparative risk assessment of burden of disease and injury attributable to 67 risk factors and risk factor clusters in 21 regions, 1990-2010: a systematic analysis for the Global Burden of Disease Study 2010, Lancet, 380, 2224-2260, https://doi.org/10.1016/s0140-6736(12)61766-8, 2012.
- Liu, Y., Nie, W., Xu, Z., Wang, T., Wang, R., Li, Y., Wang, L., Chi, X., and Ding, A.: Semi-quantitative understanding of source con-

- tribution to nitrous acid (HONO) based on 1 year of continuous observation at the SORPES station in eastern China, Atmos. Chem. Phys., 19, 13289–13308, https://doi.org/10.5194/acp-19-13289-2019, 2019.
- Lu, Y., Yan, C., Fu, Y., Chen, Y., Liu, Y., Yang, G., Wang, Y., Bianchi, F., Chu, B., Zhou, Y., Yin, R., Baalbaki, R., Garmash, O., Deng, C., Wang, W., Liu, Y., Petäjä, T., Kerminen, V.-M., Jiang, J., Kulmala, M., and Wang, L.: A proxy for atmospheric daytime gaseous sulfuric acid concentration in urban Beijing, Atmos. Chem. Phys., 19, 1971–1983, https://doi.org/10.5194/acp-19-1971-2019, 2019.
- Massoli, P., Stark, H., Canagaratna, M. R., Krechmer, J. E., Xu, L., Ng, N. L., Mauldin III, R. L., Yan, C., Kimmel, J., Misztal, P. K., Jimenez, J. L., Jayne, J. T., and Worsnop, D. R.: Ambient Measurements of Highly Oxidized Gas-Phase Molecules during the Southern Oxidant and Aerosol Study (SOAS) 2013, ACS Earth Space Chem., 2, 653–672, https://doi.org/10.1021/acsearthspacechem.8b00028, 2018.
- Mauldin III, R. L., Berndt, T., Sipilä, M., Paasonen, P., Petäjä, T., Kim, S., Kurtén, T., Stratmann, F., Kerminen, V. M., and Kulmala, M.: A new atmospherically relevant oxidant of sulphur dioxide, Nature, 488, 193–196, https://doi.org/10.1038/nature11278, 2012.
- McFiggans, G., Mentel, T. F., Wildt, J., Pullinen, I., Kang, S., Kleist, E., Schmitt, S., Springer, M., Tillmann, R., Wu, C., Zhao, D., Hallquist, M., Faxon, C., Le Breton, M., Hallquist, A. M., Simpson, D., Bergstrom, R., Jenkin, M. E., Ehn, M., Thornton, J. A., Alfarra, M. R., Bannan, T. J., Percival, C. J., Priestley, M., Topping, D., and Kiendler-Scharr, A.: Secondary organic aerosol reduced by mixture of atmospheric vapours, Nature, 565, 587–593, https://doi.org/10.1038/s41586-018-0871-y, 2019.
- Mehra, A., Wang, Y., Krechmer, J. E., Lambe, A., Majluf, F., Morris, M. A., Priestley, M., Bannan, T. J., Bryant, D. J., Pereira, K. L., Hamilton, J. F., Rickard, A. R., Newland, M. J., Stark, H., Croteau, P., Jayne, J. T., Worsnop, D. R., Canagaratna, M. R., Wang, L., and Coe, H.: Evaluation of the chemical composition of gas- and particle-phase products of aromatic oxidation, Atmos. Chem. Phys., 20, 9783–9803, https://doi.org/10.5194/acp-20-9783-2020, 2020.
- Mohr, C., Lopez-Hilfiker, F. D., Zotter, P., Prevot, A. S., Xu, L., Ng, N. L., Herndon, S. C., Williams, L. R., Franklin, J. P., Zahniser, M. S., Worsnop, D. R., Knighton, W. B., Aiken, A. C., Gorkowski, K. J., Dubey, M. K., Allan, J. D., and Thornton, J. A.: Contribution of nitrated phenols to wood burning brown carbon light absorption in Detling, United Kingdom during winter time, Environ. Sci. Technol., 47, 6316–6324, https://doi.org/10.1021/es400683v, 2013.
- Molteni, U., Bianchi, F., Klein, F., El Haddad, I., Frege, C., Rossi, M. J., Dommen, J., and Baltensperger, U.: Formation of highly oxygenated organic molecules from aromatic compounds, Atmos. Chem. Phys., 18, 1909–1921, https://doi.org/10.5194/acp-18-1909-2018, 2018.
- Nah, T., Sanchez, J., Boyd, C. M., and Ng, N. L.: Photochemical aging of α -pinene and β -pinene secondary organic aerosol formed from nitrate radical oxidation, Environ. Sci. Technol., 50, 222–231, https://doi.org/10.1021/acs.est.5b04594, 2016.
- Nel, A.: Air pollution-related illness: Effects of particles, Science, 308, 804–806, https://doi.org/10.1126/science.1108752, 2005.

- Newland, M. J., Bryant, D. J., Dunmore, R. E., Bannan, T. J., Acton, W. J. F., Langford, B., Hopkins, J. R., Squires, F. A., Dixon, W., Drysdale, W. S., Ivatt, P. D., Evans, M. J., Edwards, P. M., Whalley, L. K., Heard, D. E., Slater, E. J., Woodward-Massey, R., Ye, C., Mehra, A., Worrall, S. D., Bacak, A., Coe, H., Percival, C. J., Hewitt, C. N., Lee, J. D., Cui, T., Surratt, J. D., Wang, X., Lewis, A. C., Rickard, A. R., and Hamilton, J. F.: Low-NO atmospheric oxidation pathways in a polluted megacity, Atmos. Chem. Phys., 21, 1613–1625, https://doi.org/10.5194/acp-21-1613-2021, 2021.
- Ng, N. L., Kwan, A. J., Surratt, J. D., Chan, A. W. H., Chhabra, P. S., Sorooshian, A., Pye, H. O. T., Crounse, J. D., Wennberg, P. O., Flagan, R. C., and Seinfeld, J. H.: Secondary organic aerosol (SOA) formation from reaction of isoprene with nitrate radicals (NO₃), Atmos. Chem. Phys., 8, 4117–4140, https://doi.org/10.5194/acp-8-4117-2008, 2008.
- Nie, W., Ding, A. J., Xie, Y. N., Xu, Z., Mao, H., Kerminen, V.-M., Zheng, L. F., Qi, X. M., Huang, X., Yang, X.-Q., Sun, J. N., Herrmann, E., Petäjä, T., Kulmala, M., and Fu, C. B.: Influence of biomass burning plumes on HONO chemistry in eastern China, Atmos. Chem. Phys., 15, 1147–1159, https://doi.org/10.5194/acp-15-1147-2015, 2015.
- Orlando, J. J. and Tyndall, G. S.: Laboratory studies of organic peroxy radical chemistry: an overview with emphasis on recent issues of atmospheric significance, Chem. Soc. Rev., 41, 6294– 6317, https://doi.org/10.1039/c2cs35166h, 2012.
- Orlando, J. J., Tyndall, G. S., and Wallington, T. J.: The atmospheric chemistry of alkoxy radicals, Chem. Rev., 103, 4657–4689, https://doi.org/10.1021/cr020527p, 2003.
- Paatero, P. and Tapper, U.: Positve matrix factorization a nonnegative factor model with optimal utilization of error-estimates of data values, Environmetrics, 5, 111–126, https://doi.org/10.1002/env.3170050203, 1994.
- Pye, H. O. T., D'Ambro, E. L., Lee, B., Schobesberger, S., Takeuchi, M., Zhao, Y., Lopez-Hilfiker, F., Liu, J. M., Shilling, J. E., Xing, J., Mathur, R., Middlebrook, A. M., Liao, J., Welti, A., Graus, M., Warneke, C., de Gouw, J. A., Holloway, J. S., Ryerson, T. B., Pollack, I. B., and Thornton, J. A.: Anthropogenic enhancements to production of highly oxygenated molecules from autoxidation, P. Natl. Acad. Sci. USA, 116, 6641–6646, https://doi.org/10.1073/pnas.1810774116, 2019.
- Qi, X. M., Ding, A. J., Nie, W., Petäjä, T., Kerminen, V.-M., Herrmann, E., Xie, Y. N., Zheng, L. F., Manninen, H., Aalto, P., Sun, J. N., Xu, Z. N., Chi, X. G., Huang, X., Boy, M., Virkkula, A., Yang, X.-Q., Fu, C. B., and Kulmala, M.: Aerosol size distribution and new particle formation in the western Yangtze River Delta of China: 2 years of measurements at the SORPES station, Atmos. Chem. Phys., 15, 12445–12464, https://doi.org/10.5194/acp-15-12445-2015, 2015.
- Riccobono, F., Schobesberger, S., Scott, C. E., Dommen, J., Ortega,
 I. K., Rondo, L., Almeida, J., Amorim, A., Bianchi, F., Breitenlechner, M., David, A., Downard, A., Dunne, E. M., Duplissy,
 J., Ehrhart, S., Flagan, R. C., Franchin, A., Hansel, A., Junninen,
 H., Kajos, M., Keskinen, H., Kupc, A., Kuerten, A., Kvashin,
 A. N., Laaksonen, A., Lehtipalo, K., Makhmutov, V., Mathot,
 S., Nieminen, T., Onnela, A., Petaja, T., Praplan, A. P., Santos,
 F. D., Schallhart, S., Seinfeld, J. H., Sipila, M., Spracklen, D.
 V., Stozhkov, Y., Stratmann, F., Tome, A., Tsagkogeorgas, G.,
 Vaattovaara, P., Viisanen, Y., Vrtala, A., Wagner, P. E., Weingart-

- ner, E., Wex, H., Wimmer, D., Carslaw, K. S., Curtius, J., Donahue, N. M., Kirkby, J., Kulmala, M., Worsnop, D. R., and Baltensperger, U.: Oxidation products of biogenic emissions contribute to nucleation of atmospheric particles, Science, 344, 717–721, https://doi.org/10.1126/science.1243527, 2014.
- Richters, S., Herrmann, H., and Berndt, T.: Highly oxidized RO₂ radicals and consecutive products from the ozonolysis of three sesquiterpenes, Environ. Sci. Technol., 50, 2354–2362, https://doi.org/10.1021/acs.est.5b05321, 2016.
- Rippen, G., Zietz, E., Frank, R., Knacker, T., and Klöpffer, W.: Do airborne nitrophenols contribute to forest decline?, Environ. Technol. Lett., 8, 475–482, https://doi.org/10.1080/09593338709384508, 1987.
- Rollins, A. W., Browne, E. C., Min, K. E., Pusede, S. E., Wooldridge, P. J., Gentner, D. R., Goldstein, A. H., Liu, S., Day, D. A., Russell, L. M., and Cohen, R. C.: Evidence for NO_x control over nighttime SOA formation, Science, 337, 1210, https://doi.org/10.1126/science.1221520, 2012.
- Shen, Y., Virkkula, A., Ding, A., Wang, J., Chi, X., Nie, W., Qi, X., Huang, X., Liu, Q., Zheng, L., Xu, Z., Petäjä, T., Aalto, P. P., Fu, C., and Kulmala, M.: Aerosol optical properties at SORPES in Nanjing, east China, Atmos. Chem. Phys., 18, 5265–5292, https://doi.org/10.5194/acp-18-5265-2018, 2018.
- Sindelarova, K., Granier, C., Bouarar, I., Guenther, A., Tilmes, S., Stavrakou, T., Müller, J.-F., Kuhn, U., Stefani, P., and Knorr, W.: Global data set of biogenic VOC emissions calculated by the MEGAN model over the last 30 years, Atmos. Chem. Phys., 14, 9317–9341, https://doi.org/10.5194/acp-14-9317-2014, 2014.
- Stolzenburg, D., Fischer, L., Vogel, A. L., Heinritzi, M., Schervish, M., Simon, M., Wagner, A. C., Dada, L., Ahonen, L. R., Amorim, A., Baccarini, A., Bauer, P. S., Baumgartner, B., Bergen, A., Bianchi, F., Breitenlechner, M., Brilke, S., Mazon, S. B., Chen, D., Dias, A., Draper, D. C., Duplissy, J., El Haddad, I., Finkenzeller, H., Frege, C., Fuchs, C., Garmash, O., Gordon, H., He, X., Helm, J., Hofbauer, V., Hoyle, C. R., Kim, C., Kirkby, J., Kontkanen, J., Kuerten, A., Lampilahti, J., Lawler, M., Lehtipalo, K., Leiminger, M., Mai, H., Mathot, S., Mentler, B., Molteni, U., Nie, W., Nieminen, T., Nowak, J. B., Ojdanic, A., Onnela, A., Passananti, M., Petaja, T., Quelever, L. L. J., Rissanen, M. P., Sarnela, N., Schallhart, S., Tauber, C., Tome, A., Wagner, R., Wang, M., Weitz, L., Wimmer, D., Xiao, M., Yan, C., Ye, P., Zha, Q., Baltensperger, U., Curtius, J., Dommen, J., Flagan, R. C., Kulmala, M., Smith, J. N., Worsnop, D. R., Hansel, A., Donahue, N. M., and Winkler, P. M.: Rapid growth of organic aerosol nanoparticles over a wide tropospheric temperature range, P. Natl. Acad. Sci. USA, 115, 9122-9127, https://doi.org/10.1073/pnas.1807604115, 2018.
- Sun, P., Nie, W., Chi, X., Xie, Y., Huang, X., Xu, Z., Qi, X., Xu, Z., Wang, L., Wang, T., Zhang, Q., and Ding, A.: Two years of online measurement of fine particulate nitrate in the western Yangtze River Delta: influences of thermodynamics and N₂O₅ hydrolysis, Atmos. Chem. Phys., 18, 17177–17190, https://doi.org/10.5194/acp-18-17177-2018, 2018.
- Sun, P., Nie, W., Wang, T., Chi, X., Huang, X., Xu, Z., Zhu, C., Wang, L., Qi, X., Zhang, Q., and Ding, A.: Impact of air transport and secondary formation on haze pollution in the Yangtze River Delta: In situ online observations in Shanghai and Nanjing, Atmos. Environ., 225, 117350, https://doi.org/10.1016/j.atmosenv.2020.117350, 2020.

- Takeuchi, M. and Ng, N. L.: Chemical composition and hydrolysis of organic nitrate aerosol formed from hydroxyl and nitrate radical oxidation of α -pinene and β -pinene, Atmos. Chem. Phys., 19, 12749–12766, https://doi.org/10.5194/acp-19-12749-2019, 2019.
- Trostl, J., Chuang, W. K., Gordon, H., Heinritzi, M., Yan, C., Molteni, U., Ahlm, L., Frege, C., Bianchi, F., Wagner, R., Simon, M., Lehtipalo, K., Williamson, C., Craven, J. S., Duplissy, J., Adamov, A., Almeida, J., Bernhammer, A. K., Breitenlechner, M., Brilke, S., Dias, A., Ehrhart, S., Flagan, R. C., Franchin, A., Fuchs, C., Guida, R., Gysel, M., Hansel, A., Hoyle, C. R., Jokinen, T., Junninen, H., Kangasluoma, J., Keskinen, H., Kim, J., Krapf, M., Kurten, A., Laaksonen, A., Lawler, M., Leiminger, M., Mathot, S., Mohler, O., Nieminen, T., Onnela, A., Petaja, T., Piel, F. M., Miettinen, P., Rissanen, M. P., Rondo, L., Sarnela, N., Schobesberger, S., Sengupta, K., Sipila, M., Smith, J. N., Steiner, G., Tome, A., Virtanen, A., Wagner, A. C., Weingartner, E., Wimmer, D., Winkler, P. M., Ye, P., Carslaw, K. S., Curtius, J., Dommen, J., Kirkby, J., Kulmala, M., Riipinen, I., Worsnop, D. R., Donahue, N. M., and Baltensperger, U.: The role of low-volatility organic compounds in initial particle growth in the atmosphere, Nature, 533, 527–531, https://doi.org/10.1038/nature18271, 2016.
- Tsiligiannis, E., Hammes, J., Salvador, C. M., Mentel, T. F., and Hallquist, M.: Effect of NO_x on 1,3,5-trimethylbenzene (TMB) oxidation product distribution and particle formation, Atmos. Chem. Phys., 19, 15073–15086, https://doi.org/10.5194/acp-19-15073-2019, 2019.
- Wang, J., Nie, W., Cheng, Y., Shen, Y., Chi, X., Wang, J., Huang, X., Xie, Y., Sun, P., Xu, Z., Qi, X., Su, H., and Ding, A.: Light absorption of brown carbon in eastern China based on 3 year multi-wavelength aerosol optical property observations and an improved absorption Ångström exponent segregation method, Atmos. Chem. Phys., 18, 9061–9074, https://doi.org/10.5194/acp-18-9061-2018, 2018a.
- Wang, J., Feng, L., Palmer, P. I., Liu, Y., Fang, S., Bosch, H., O'Dell, C. W., Tang, X., Yang, D., Liu, L., and Xia, C.: Large Chinese land carbon sink estimated from atmospheric carbon dioxide data, Nature, 586, 720–723, https://doi.org/10.1038/s41586-020-2849-9, 2020a.
- Wang, L., Wang, X., Gu, R., Wang, H., Yao, L., Wen, L., Zhu, F., Wang, W., Xue, L., Yang, L., Lu, K., Chen, J., Wang, T., Zhang, Y., and Wang, W.: Observations of fine particulate nitrated phenols in four sites in northern China: concentrations, source apportionment, and secondary formation, Atmos. Chem. Phys., 18, 4349–4359, https://doi.org/10.5194/acp-18-4349-2018, 2018b.
- Wang, M., Chen, D., Xiao, M., Ye, Q., Stolzenburg, D., Hofbauer, V., Ye, P., Vogel, A. L., Mauldin, R. L., Amorim, A., Baccarini, A., Baumgartner, B., Brilke, S., Dada, L., Dias, A., Duplissy, J., Finkenzeller, H., Garmash, O., He, X.-C., Hoyle, C. R., Kim, C., Kvashnin, A., Lehtipalo, K., Fischer, L., Molteni, U., Petäjä, T., Pospisilova, V., Quéléver, L. L. J., Rissanen, M., Simon, M., Tauber, C., Tomé, A., Wagner, A. C., Weitz, L., Volkamer, R., Winkler, P. M., Kirkby, J., Worsnop, D. R., Kulmala, M., Baltensperger, U., Dommen, J., El-Haddad, I., and Donahue, N. M.: Photo-oxidation of aromatic hydrocarbons produces low-volatility organic compounds, Environ. Sci. Technol., 54, 7911–7921, https://doi.org/10.1021/acs.est.0c02100, 2020b.

- Wang, S., Wu, R., Berndt, T., Ehn, M., and Wang, L.: Formation of Highly Oxidized Radicals and Multifunctional Products from the Atmospheric Oxidation of Alkylbenzenes, Environ. Sci. Technol., 51, 8442–8449, https://doi.org/10.1021/acs.est.7b02374, 2017.
- Wang, Y., Mehra, A., Krechmer, J. E., Yang, G., Hu, X., Lu, Y., Lambe, A., Canagaratna, M., Chen, J., Worsnop, D., Coe, H., and Wang, L.: Oxygenated products formed from OH-initiated reactions of trimethylbenzene: autoxidation and accretion, Atmos. Chem. Phys., 20, 9563–9579, https://doi.org/10.5194/acp-20-9563-2020, 2020c.
- Wang, Z., Ehn, M., Rissanen, M. P., Garmash, O., Quéléver, L., Xing, L., Monge-Palacios, M., Rantala, P., Donahue, N. M., Berndt, T., and Sarathy, S. M.: Efficient alkane oxidation under combustion engine and atmospheric conditions, Communications Chemistry, 4, 18, https://doi.org/10.1038/s42004-020-00445-3, 2021.
- Wayne, R. P., Barnes, I., Biggs, P., Burrows, J. P., Canosamas, C. E., Hjorth, J., Lebras, G., Moortgat, G. K., Perner, D., Poulet, G., Restelli, G., and Sidebottom, H.: The nitrated radical physics, chemistry, and the atmosphere, Atmos. Environ. A-Gen., 25, 1–203, https://doi.org/10.1016/0960-1686(91)90192-a, 1991.
- Wennberg, P. O., Bates, K. H., Crounse, J. D., Dodson, L. G., McVay, R. C., Mertens, L. A., Nguyen, T. B., Praske, E., Schwantes, R. H., Smarte, M. D., St Clair, J. M., Teng, A. P., Zhang, X., and Seinfeld, J. H.: Gas-phase reactions of isoprene and its major oxidation products, Chem. Rev., 118, 3337–3390, https://doi.org/10.1021/acs.chemrev.7b00439, 2018.
- Wood, E. C., Canagaratna, M. R., Herndon, S. C., Onasch, T. B., Kolb, C. E., Worsnop, D. R., Kroll, J. H., Knighton, W. B., Seila, R., Zavala, M., Molina, L. T., DeCarlo, P. F., Jimenez, J. L., Weinheimer, A. J., Knapp, D. J., Jobson, B. T., Stutz, J., Kuster, W. C., and Williams, E. J.: Investigation of the correlation between odd oxygen and secondary organic aerosol in Mexico City and Houston, Atmos. Chem. Phys., 10, 8947–8968, https://doi.org/10.5194/acp-10-8947-2010, 2010.
- Xia, M., Peng, X., Wang, W., Yu, C., Sun, P., Li, Y., Liu, Y., Xu, Z., Wang, Z., Xu, Z., Nie, W., Ding, A., and Wang, T.: Significant production of ClNO₂ and possible source of Cl₂ from N₂O₅ uptake at a suburban site in eastern China, Atmos. Chem. Phys., 20, 6147–6158, https://doi.org/10.5194/acp-20-6147-2020, 2020.
- Xie, Y., Ding, A., Nie, W., Mao, H., Qi, X., Huang, X., Xu, Z., Kerminen, V.-M., Petäjä, T., Chi, X., Virkkula, A., Boy, M., Xue, L., Guo, J., Sun, J., Yang, X., Kulmala, M., and Fu, C.: Enhanced sulfate formation by nitrogen dioxide: Implications from in situ observations at the SOR-PES station, J. Geophys. Res.-Atmos., 120, 12679–12694, https://doi.org/10.1002/2015jd023607, 2015.
- Xiong, F., McAvey, K. M., Pratt, K. A., Groff, C. J., Hostetler, M. A., Lipton, M. A., Starn, T. K., Seeley, J. V., Bertman, S. B., Teng, A. P., Crounse, J. D., Nguyen, T. B., Wennberg, P. O., Misztal, P. K., Goldstein, A. H., Guenther, A. B., Koss, A. R., Olson, K. F., de Gouw, J. A., Baumann, K., Edgerton, E. S., Feiner, P. A., Zhang, L., Miller, D. O., Brune, W. H., and Shepson, P. B.: Observation of isoprene hydroxynitrates in the southeastern United States and implications for the fate of NO_x, Atmos. Chem. Phys., 15, 11257–11272, https://doi.org/10.5194/acp-15-11257-2015, 2015.

- Xu, Z., Huang, X., Nie, W., Chi, X., Xu, Z., Zheng, L., Sun, P., and Ding, A.: Influence of synoptic condition and holiday effects on VOCs and ozone production in the Yangtze River Delta region, China, Atmos. Environ., 168, 112–124, https://doi.org/10.1016/j.atmosenv.2017.08.035, 2017.
- Xu, Z., Huang, X., Nie, W., Shen, Y., Zheng, L., Xie, Y., Wang, T., Ding, K., Liu, L., Zhou, D., Qi, X., and Ding, A.: Impact of biomass burning and vertical mixing of residual-layer aged plumes on ozone in the Yangtze River Delta, China: a tethered-balloon measurement and modeling study of a multiday ozone opisode, J. Geophys. Res.-Atmos., 123, 11786–11803, https://doi.org/10.1029/2018jd028994, 2018.
- Xu, Z. N., Nie, W., Liu, Y. L., Sun, P., Huang, D. D., Yan, C., Krechmer, J., Ye, P. L., Xu, Z., Qi, X. M., Zhu, C. J., Li, Y. Y., Wang, T. Y., Wang, L., Huang, X., Tang, R. Z., Guo, S., Xiu, G. L., Fu, Q. Y., Worsnop, D., Chi, X. G., and Ding, A. J.: Multifunctional products of isoprene oxidation in polluted atmosphere and their contribution to SOA, Geophys. Res. Lett., 48, e2020GL089276, https://doi.org/10.1029/2020gl089276, 2021.
- Yan, C., Nie, W., Äijälä, M., Rissanen, M. P., Canagaratna, M. R., Massoli, P., Junninen, H., Jokinen, T., Sarnela, N., Häme, S. A. K., Schobesberger, S., Canonaco, F., Yao, L., Prévôt, A. S. H., Petäjä, T., Kulmala, M., Sipilä, M., Worsnop, D. R., and Ehn, M.: Source characterization of highly oxidized multifunctional compounds in a boreal forest environment using positive matrix factorization, Atmos. Chem. Phys., 16, 12715–12731, https://doi.org/10.5194/acp-16-12715-2016, 2016.
- Yan, C., Nie, W., Vogel, A. L., Dada, L., Lehtipalo, K., Stolzenburg, D., Wagner, R., Rissanen, M. P., Xiao, M., Ahonen, L., Fischer, L., Rose, C., Bianchi, F., Gordon, H., Simon, M., Heinritzi, M., Garmash, O., Roldin, P., Dias, A., Ye, P., Hofbauer, V., Amorim, A., Bauer, P. S., Bergen, A., Bernhammer, A. K., Breitenlechner, M., Brilke, S., Buchholz, A., Mazon, S. B., Canagaratna, M. R., Chen, X., Ding, A., Dommen, J., Draper, D. C., Duplissy, J., Frege, C., Heyn, C., Guida, R., Hakala, J., Heikkinen, L., Hoyle, C. R., Jokinen, T., Kangasluoma, J., Kirkby, J., Kontkanen, J., Kürten, A., Lawler, M. J., Mai, H., Mathot, S., Mauldin, R. L., Molteni, U., Nichman, L., Nieminen, T., Nowak, J., Ojdanic, A., Onnela, A., Pajunoja, A., Petäjä, T., Piel, F., Quéléver, L. L. J., Sarnela, N., Schallhart, S., Sengupta, K., Sipilä, M., Tomé, A., Tröstl, J., Väisänen, O., Wagner, A. C., Ylisirniö, A., Zha, Q., Baltensperger, U., Carslaw, K. S., Curtius, J., Flagan, R. C., Hansel, A., Riipinen, I., Smith, J. N., Virtanen, A., Winkler, P. M., Donahue, N. M., Kerminen, V. M., Kulmala, M., Ehn, M., and Worsnop, D. R.: Size-dependent influence of NO_x on the growth rates of organic aerosol particles, Science Advances, 6, eaay4945, https://doi.org/10.1126/sciadv.aay4945, 2020.
- Yang, L., Nie, W., Liu, Y., Xu, Z., Xiao, M., Qi, X., Li, Y., Wang, R., Zou, J., Paasonen, P., Yan, C., Xu, Z., Wang, J., Zhou, C., Yuan, J., Sun, J., Chi, X., Kerminen, V.-M., Kulmala, M., and Ding, A.: Towards building a physical proxy for gas-phase sulfuric acid concentration based on its budget analysis in polluted Yangtze River Delta, east China, Environ. Sci. Technol., https://doi.org/10.1021/acs.est.1c00738, 2021.
- Yuan, B., Liggio, J., Wentzell, J., Li, S.-M., Stark, H., Roberts, J. M.,
 Gilman, J., Lerner, B., Warneke, C., Li, R., Leithead, A., Osthoff,
 H. D., Wild, R., Brown, S. S., and de Gouw, J. A.: Secondary formation of nitrated phenols: insights from observations during the Uintah Basin Winter Ozone Study (UBWOS) 2014, At-

- mos. Chem. Phys., 16, 2139–2153, https://doi.org/10.5194/acp-16-2139-2016, 2016.
- Zaytsev, A., Koss, A. R., Breitenlechner, M., Krechmer, J. E., Nihill, K. J., Lim, C. Y., Rowe, J. C., Cox, J. L., Moss, J., Roscioli, J. R., Canagaratna, M. R., Worsnop, D. R., Kroll, J. H., and Keutsch, F. N.: Mechanistic study of the formation of ringretaining and ring-opening products from the oxidation of aromatic compounds under urban atmospheric conditions, Atmos. Chem. Phys., 19, 15117–15129, https://doi.org/10.5194/acp-19-15117-2019, 2019.
- Zhang, Q., Jimenez, J. L., Canagaratna, M. R., Allan, J. D., Coe, H., Ulbrich, I., Alfarra, M. R., Takami, A., Middlebrook, A. M., Sun, Y. L., Dzepina, K., Dunlea, E., Docherty, K., De-Carlo, P. F., Salcedo, D., Onasch, T., Jayne, J. T., Miyoshi, T., Shimono, A., Hatakeyama, S., Takegawa, N., Kondo, Y., Schneider, J., Drewnick, F., Borrmann, S., Weimer, S., Demerjian, K., Williams, P., Bower, K., Bahreini, R., Cottrell, L., Griffin, R. J., Rautiainen, J., Sun, J. Y., Zhang, Y. M., and Worsnop, D. R.: Ubiquity and dominance of oxygenated species in organic aerosols in anthropogenically-influenced Northern Hemisphere midlatitudes, Geophys. Res. Lett., 34, 6, https://doi.org/10.1029/2007gl029979, 2007.
- Zhang, Y., Tang, L., Croteau, P. L., Favez, O., Sun, Y., Canagaratna, M. R., Wang, Z., Couvidat, F., Albinet, A., Zhang, H., Sciare, J., Prévôt, A. S. H., Jayne, J. T., and Worsnop, D. R.: Field characterization of the PM_{2.5} Aerosol Chemical Speciation Monitor: insights into the composition, sources, and processes of fine particles in eastern China, Atmos. Chem. Phys., 17, 14501–14517, https://doi.org/10.5194/acp-17-14501-2017, 2017.

- Zhang, Y., Peräkylä, O., Yan, C., Heikkinen, L., Äijälä, M., Daellenbach, K. R., Zha, Q., Riva, M., Garmash, O., Junninen, H., Paatero, P., Worsnop, D., and Ehn, M.: A novel approach for simple statistical analysis of high-resolution mass spectra, Atmos. Meas. Tech., 12, 3761–3776, https://doi.org/10.5194/amt-12-3761-2019, 2019.
- Zhang, Y., Peräkylä, O., Yan, C., Heikkinen, L., Äijälä, M., Daellenbach, K. R., Zha, Q., Riva, M., Garmash, O., Junninen, H., Paatero, P., Worsnop, D., and Ehn, M.: Insights into atmospheric oxidation processes by performing factor analyses on subranges of mass spectra, Atmos. Chem. Phys., 20, 5945–5961, https://doi.org/10.5194/acp-20-5945-2020, 2020.
- Zhao, D., Pullinen, I., Fuchs, H., Schrade, S., Wu, R., Acir, I.-H., Tillmann, R., Rohrer, F., Wildt, J., Guo, Y., Kiendler-Scharr, A., Wahner, A., Kang, S., Vereecken, L., and Mentel, T. F.: Highly oxygenated organic molecule (HOM) formation in the isoprene oxidation by NO₃ radical, Atmos. Chem. Phys., 21, 9681–9704, https://doi.org/10.5194/acp-21-9681-2021, 2021.
- Ziemann, P. J. and Atkinson, R.: Kinetics, products, and mechanisms of secondary organic aerosol formation, Chem. Soc. Rev., 41, 6582–6605, https://doi.org/10.1039/c2cs35122f, 2012.

Supplement of Atmos. Chem. Phys., 21, 14789–14814, 2021 https://doi.org/10.5194/acp-21-14789-2021-supplement © Author(s) 2021. CC BY 4.0 License.





Supplement of

Formation of condensable organic vapors from anthropogenic and biogenic volatile organic compounds (VOCs) is strongly perturbed by \mathbf{NO}_x in eastern China

Yuliang Liu et al.

Correspondence to: Wei Nie (niewei@nju.edu.cn)

The copyright of individual parts of the supplement might differ from the article licence.

Table of contents

S1 Diurnal pattern of mass spectra of nitrate CI-APi-TOF and related parameters	1
S2 PMF inputs and diagnostics	1
S3 Calculation of molecular properties of OOMs	
S4 Main peaks of 9 discussed non-nitrated-phenols factors	
S5 The dependence of Temp-related factor on temperature	
S6 Air masses reaching the SORPES station	
S7 High resolution peak fitting	
57 High resolution peak fitting	+ 0

S1 Diurnal pattern of mass spectra of nitrate CI-APi-TOF and related parameters

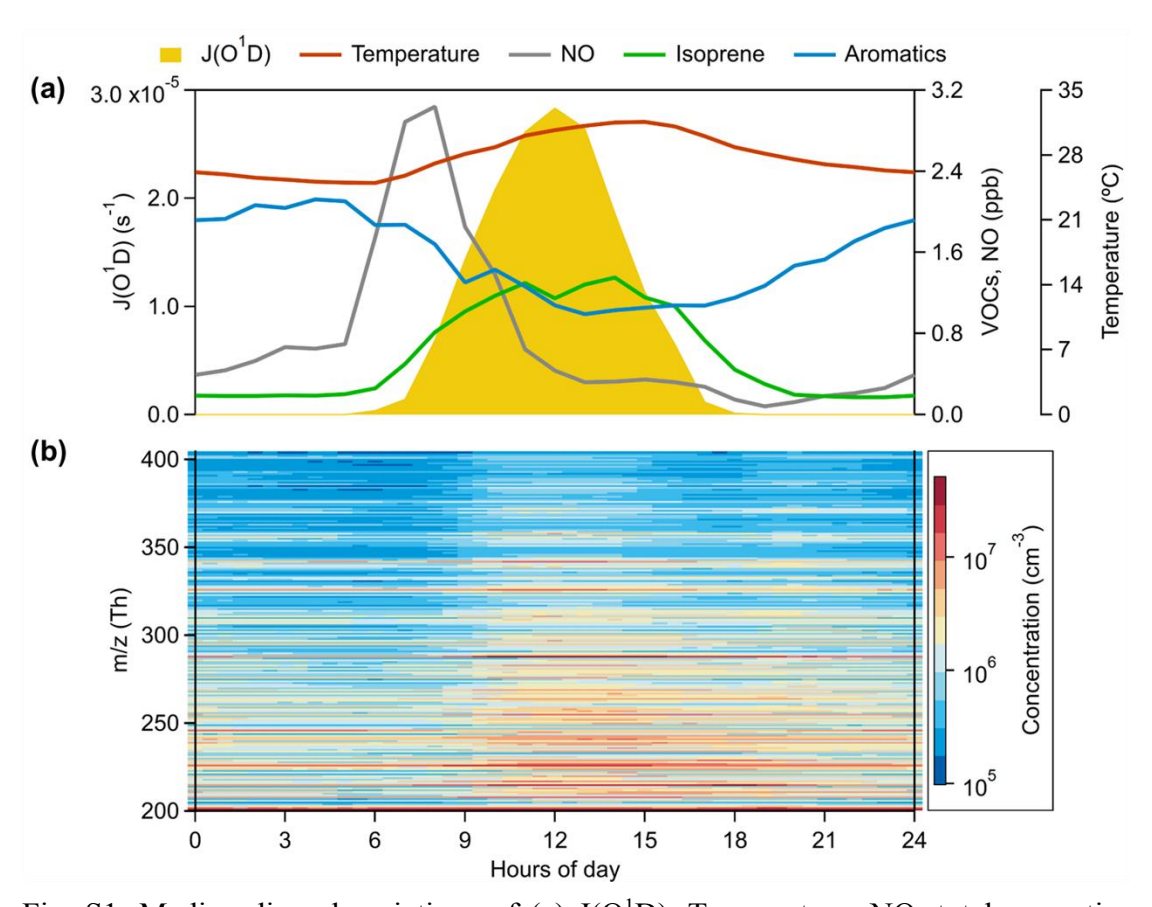


Fig. S1. Median diurnal variations of (a) $J(O^1D)$, Temperature, NO, total aromatics (benzene + toluene + C_8 aromatics + C_9 aromatics + C_{10} aromatics + styrene), and isoprene, and (b) mass spectra of nitrate CI-APi-TOF with m/z in the range of 201-404 Th.

S2 PMF inputs and diagnostics

S2.1 binPMF inputs

Data matrix

In binPMF, as described in Zhang et al. (2019), the mass spectra are divided into small bins of 0.006 Th width after baseline subtraction and mass axis calibration. Figure S1 (b) shows the averaged binned spectrum measured by nitrate CI-APi-TOF. We deleted bins of nitrophenol and some fluorinated contaminations (Table S1) from the raw spectra. The concentration of nitrophenol (C₆H₅NO₃(NO₃-)) is about one order of magnitude higher than other compounds, but it is not our main concern. Fluorinated contaminations come from Teflon tube volatiles and perfluoric acid for mass dependent transmission efficiency calibrations, so these artificially introduced compounds with high signals should also not be taken into the PMF model. To avoid unnecessary computation, for each nominal m/z in the range of 202-404 Th, only signal regions with signal-to-noise ratio >1 were adopted as data matrix for PMF inputs.

Table S1. Peak list of deleted bins

Mass-to-charge (Th)	Formulas
201.0153	C ₆ H ₅ NO ₃ (NO ₃ ⁻)
207.9875	$C_2F_4HCOOH(NO_3^-)$
225.9780	$C_2F_5COOH(NO_3^-)$
241.9730	$C_3F_5OCOOH(NO_3^-)$
262.9760	$C_4F_9COO^-$
275.9748	$C_3F_7COOH(NO_3^-)$
307.9811	$C_4F_8HCOOH(NO_3^-)$
325.9716	$C_4F_9COOH(NO_3^-)$
341.9666	$C_4F_9OCOOH(NO_3^-)$
362.9696	$C_6F_{13}COO^{-}$
375.9685	$C_5F_{11}COOH(NO_3^-)$

Error matrix

The error matrix was calculated based on Eq. (1) (Polissar et al., 1998)

$$S_{ij} = \sigma_{ij} + \sigma_{noise} \tag{1}$$

where S_{ij} represents the uncertainty of m/z j at time i and σ_{ij} stands for counting statistics uncertainty and is estimated as follows:

$$\sigma_{ij} = a \times \frac{\sqrt{I_{ij}}}{\sqrt{t}} \tag{2}$$

where I is the signal intensity term, in unit of ions per second; ts stands for length of averaging in seconds, and a is an empirical coefficient to compensate for unaccounted

uncertainties (Allan et al., 2003; Yan et al., 2016) and is 1.28 in this study as previously estimated from laboratory experiments (Yan et al., 2016). The σ_{noise} term was estimated as the median of the standard deviations from signals in the bins in the region between nominal masses, where no physically meaningful signals are expected.

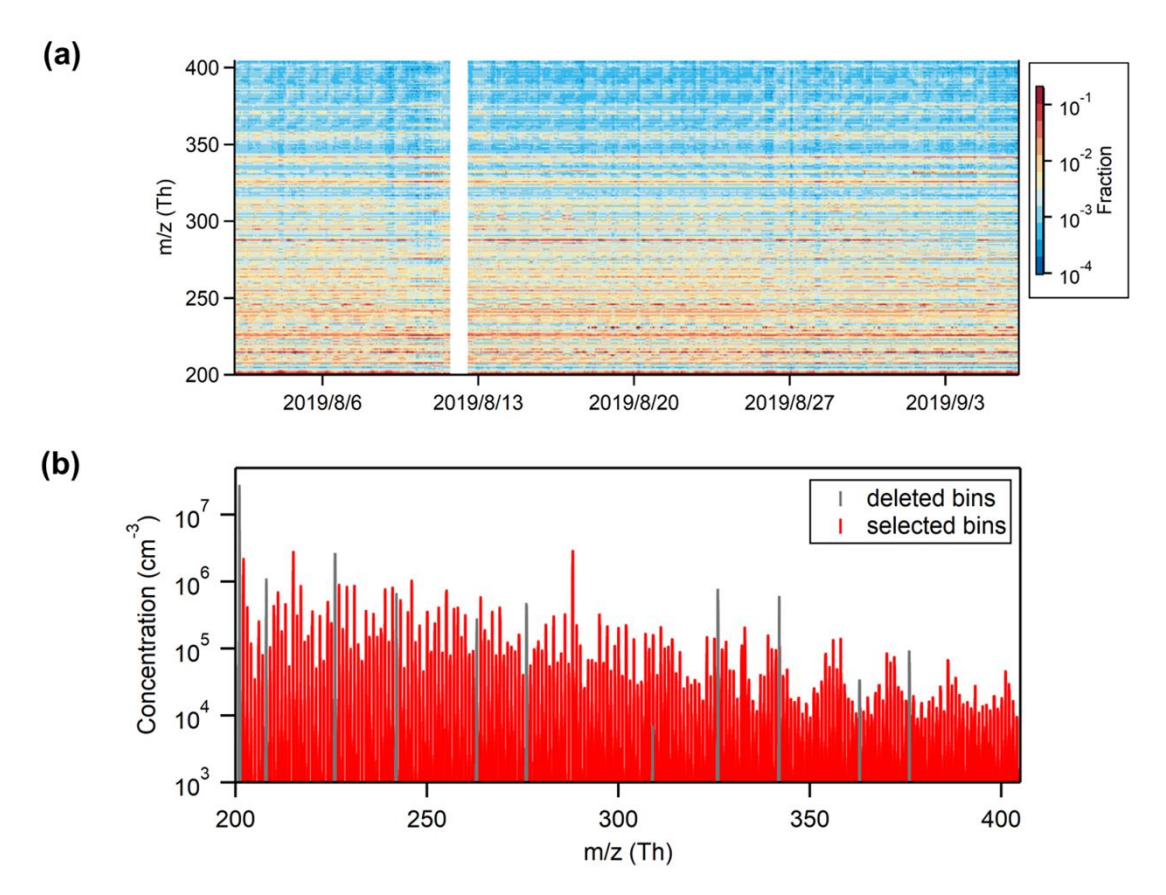


Fig. S2. (a) Normalized mass spectra of nitrate CI-APi-TOF with m/z in the range of 202-404 Th. (b) Averaged binned spectrum measured by nitrate CI-APi-TOF. After delete some bins (gray) affected by compounds listed in Table S1, remaining bins (red) with unit m/z in the range of 202-404 Th were adopted as data matrix for PMF inputs.

S2.2 Evolution

As mentioned in previous classic works applying PMF (Zhang et al., 2011; Yan et al., 2016), the choice of the proper number of factors is the most critical decision towards interpreting the PMF results. When the number of factors solved exceeds 8, the rates of decrease in Q/Q_{exp} (Fig. S2 (a)) and of increase in absolute values (Fig. S2(c)) slow down. A variable should be regarded as explained only if the UEV for that variable is less than 25 % (Fig. S2 (b). These mathematical diagnostics give us solutions with 9-20 factors to choose from. Solution of more factors can explain more subtle variations in the data, but too many factors can split a physically meaningful factor into unrealistic ones. The evolution of PMF solutions has been carefully viewed, and the first occurrences of main factors are denoted in the corresponding solutions (Fig. S2 (a)). For example, the 'F contaminations' factor, mainly comprising fluorinated

contaminations from perfluorinated acids and Teflon tubing volatiles, first appears purely in the solution of three factors, while the Aliph-OOM factor did not appear until the solution of the 14 factors. Due to the non-uniqueness of the PMF solution, the order of first occurrence of different factors may vary slightly. To some extent, the selection of PMF solutions depends on the interpretability of the factors. From our analysis, solutions with more than 14 factors did not provide new process-specific information and made the interpretability of the results more difficult because of factor splitting and fewer unique correlations with external tracers.

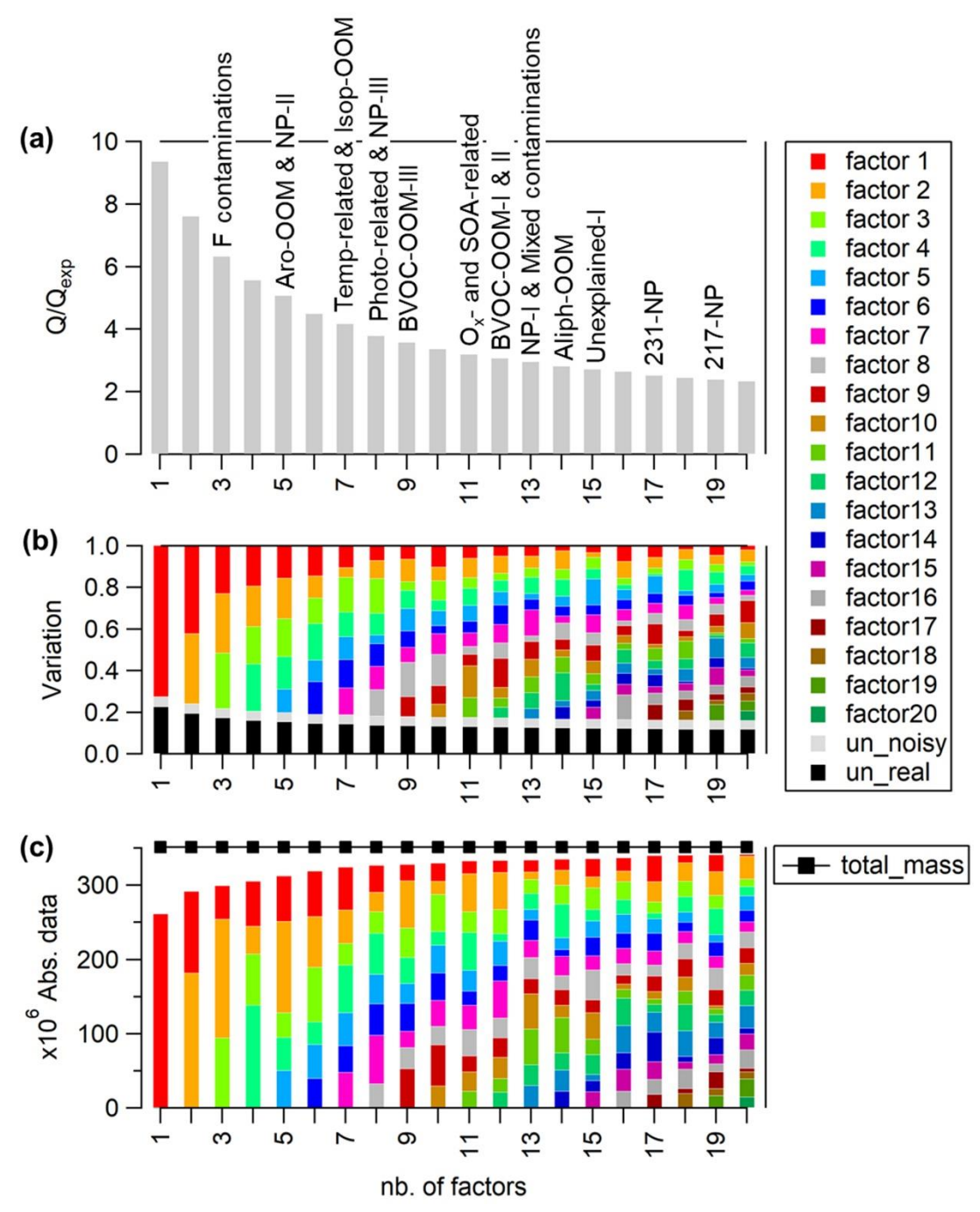


Fig. S3. Diagnostics of PMF solutions, including the evolutions of (a) Q/Q_{exp}, (b) the explained variation (EV) and unexplained variation (UEV), and (c) absolute values

resolved by PMF. In (b) UEV is further separated into the real UEV for data possessing a high signal-to-noise value (un real) and UEV for noisy data (un noisy).

S2.3 Rotation

Rotational ambiguity of PMF solution with 14 factors has been checked here (Fig. S3). We set the fpeak to increase from -4.0 to 4.0 with a difference of 0.2, for the global control of such rotations. All solutions are divided into two types, one containing 13 + 'Mixed contaminations' factors and the other containing 13 + 'Unexplained I' factors, with the former occurring more frequently. The 'Mixed contaminations' factor consists of mainly by nitrated phenols and fluorinated contaminations, and is negatively correlated with the 'F contaminations' factor (Fig. S5), meaning these two factors are somewhat over split. The 'Unexplained I' factor has no correlation with external tracer data, and seems to abstract some signal from the Temp-related factor, but peaks at around 17:30 in its diurnal pattern. Finally, the solution with a fpeak value of -0.2 is selected to analysis data.

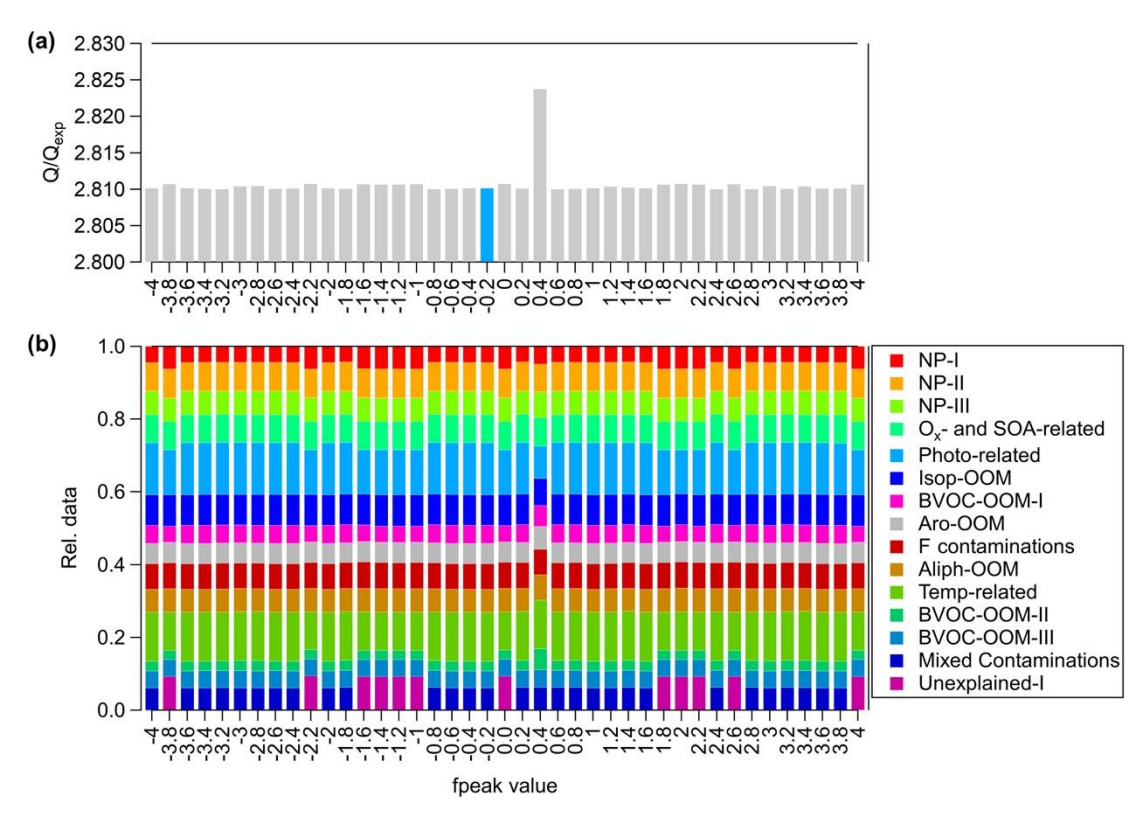


Fig. S4. (a) Q/Q_{exp} distribution on rotation of 14-factors solutions, the one with an fpeak value of -0.2 is the selected solution. (b) The relative contribution ratio of factors in each solution with different values of fpeak.

S2.4 Residual

The residual histograms are an easy and fast method for investigating whether the PMF result contains some systematic under- or overestimation. As showed in Fig. S4, the

time series of residuals looks full of noise, and dihydroxy nitro-benzene (C₆H₅NO₄, charged by NO₃⁻ at unit m/z 217 Th) and dihydroxy nitro-toluene (C₇H₇NO₄, charged by NO₃⁻ at unit m/z 231 Th) are the largest peaks in mass spectra of residuals. But these two compounds will be distributed to two different factors about nitrated phenols, in the solutions of 17-20 factors (denoted as '217-NP' and '231-NP' factors in Fig. S2 (a)). In order to separate out these two factors, the other physically meaningful factors will be over-split. Since the factors about nitrated phenols are not our main concern, it's reasonable to choose the 14-factors solution.

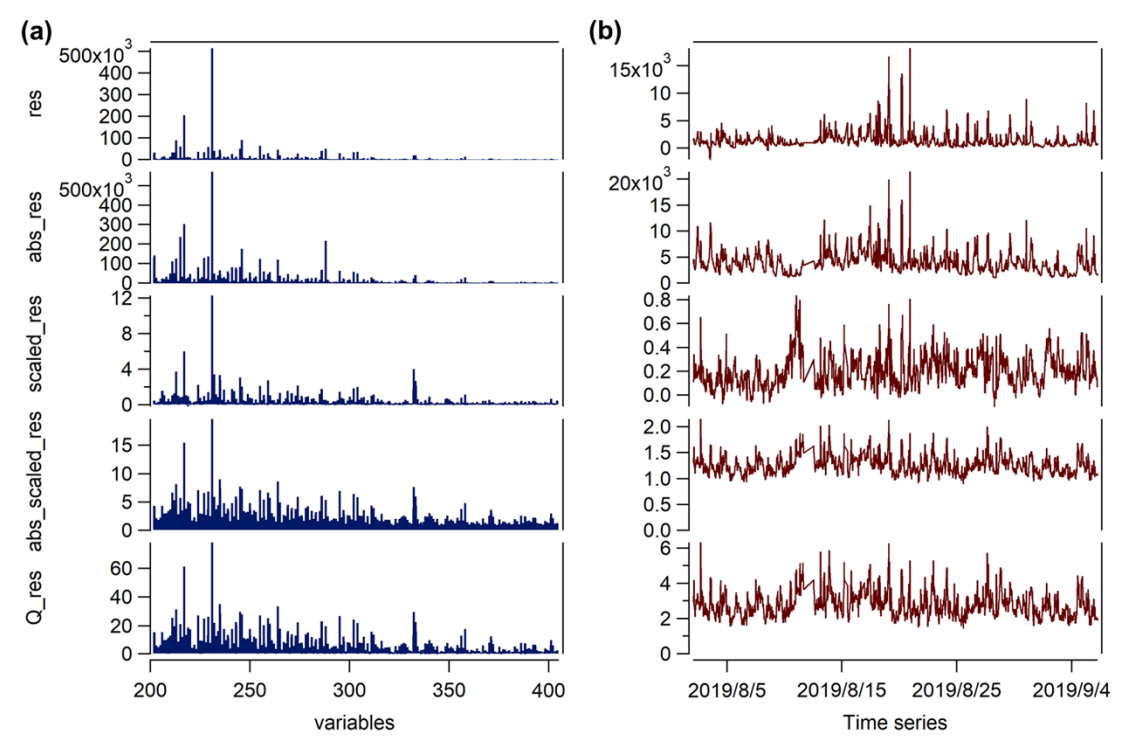


Fig. S5. (a) Mass spectra and (b) time series plots showing the residual histograms of the solution selected.

S2.5 Comparison between the factors

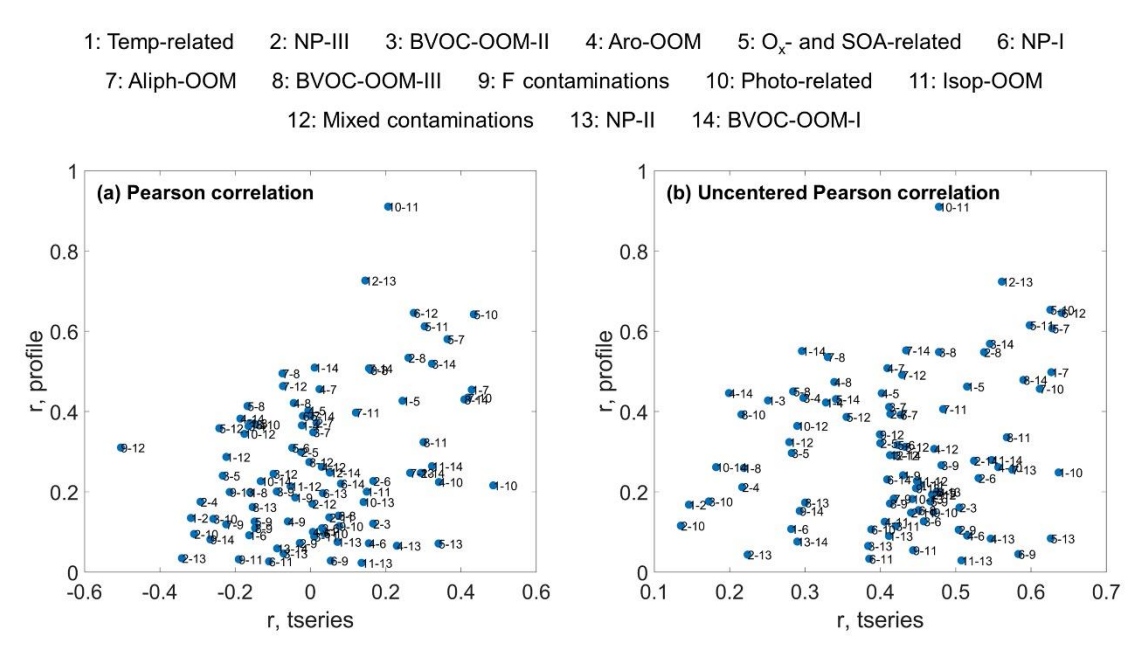


Fig. S6. Comparison among the factors through (a) Pearson correlation and (b) Uncentered Pearson correlation. The x-axis shows the correlation of the time series between the factors, and the y-axis shows the correlation of the spectra between the factors.

S3 Calculation of molecular properties of OOMs

Carbon oxidation state (OSc)

The OS_c of each **non-nitro** OOM was calculated based on Eq. (3) modified from that in Kroll et al. (2011) include organic nitrate contributions, by assuming that all nitrogen come from the nitrate group (-ONO₂), which are more likely to be detected by the nitrate CI-APi-TOF. A group oxidation state of -1 was applied to -ONO₂ functionality:

$$OS_c = 2(n_O - 3n_N)/n_C - n_H/n_C + n_N/n_C$$
(3)

Where n_C , n_H , n_O , and n_N denote the number of carbons, hydrogen, oxygen, and nitrogen in the molecule, respectively. The formula is only valid when $n_O \ge 3 \times n_N$, meaning that there is enough oxygen to account for the -ONO₂ group. Almost all of fitted HR peaks satisfy this condition, further indicating that the detected nitrogen is likely to occur entirely in the -ONO₂ group. However, it is worth mentioning that polyfunctional nitrogenous species with reduced N functionalities (i.e., heterocyclic, amine or nitrite) can still be detected by the nitrate CI-APi-TOF if they contain sufficient oxygenated functional groups (e.g., -OH, -OOH).

Double bond equivalent (DBE)

The DBE of each OOM was calculated using Eq. (4), by assuming that all nitrogen come from the nitrate group (-ONO₂) or nitro group (-NO₂). Here DBE represents the combined effect of double or triple bonds, as well as the ring structure, in the molecule.

$$DBE = n_C + 1 - (n_H + n_N)/2$$
 (4)

Volatility Basis Set (VBS)

The saturation concentration (volatility) of selected OOMs was estimated based on the group-contribution method proposed by Donahue et al. (2011):

$$\log_{10}C^*(300K) = (25 - n_C) \cdot b_C - (n_O - 2n_N) \cdot b_O - 2\left[\frac{(n_O - 2n_N) \cdot n_C}{n_C + n_O - 2n_N}\right] \cdot b_{CO}$$
 (5)

Where $b_C = 0.475$, $b_O = 2.3$, $b_{CO} = -0.3$. The effect of nitrate group (-ONO₂) on volatility is similar to hydroxyl group (-OH).

The temperature dependence of volatilities is described by Eq. (6), according to Stolzenburg et al. (2018):

$$log_{10}C_i^*(T) = log_{10}C_i^*(300K) + \frac{\Delta H_{vap}}{R \cdot ln(10)} \left(\frac{1}{300} - \frac{1}{T}\right)$$
 (6)

The evaporation enthalpy (ΔH_{vap}) can be linked to the saturation mass concentration at 300 K, $\log_{10} C^*(300K)$, according to Donahue et al. (2011) and combined with Epstein et al. (2010):

$$\Delta H_{vap}[kJ \ mol^{-1}] = 129 - 5.7 \cdot log_{10}(C^*(300K))$$
 (7)

S4 Main peaks of 9 discussed non-nitrated-phenols factors

S4.1 Aro-OOM factor

Table S2. Molecular characteristics of the Aro-OOM factor. Presented as several sets of compounds, and the members of each sets differ in the addition of a -CH₂ moiety. Only the signals that account for more than one thousandth of the factor are selected to reduce uncertainties. The clustering reagent ion NO₃⁻ or HNO₃NO₃⁻ has been omitted from the formulas.

No.	Formulas	Contribution to the factor (%)	DBE	no	n _N	
1	$C_xH_{2x-1}O_6N$, $x=[3, 14]$	11.0	1	6	1	
2	$C_xH_{2x-7}O_4N, x=[6, 8]$	6.2	4	4	1 ^a	
3	$C_xH_{2x-3}O_6N$, $x=[5, 15]$	5.3	2	6	1	
4	$C_xH_{2x-4}O_4$, $x=[6, 11]$	4.6	3	4	0	
5	$C_xH_{2x-3}O_7N$, $x=[6, 13]$	3.5	2	7	1	
6	$C_xH_{2x-5}O_7N$, $x=[7, 14]$	3.5	3	7	1	
7	$C_xH_{2x-5}O_8N$, $x=[8, 13]$	2.9	3	8	1	
8	$C_xH_{2x-4}O_5$, $x=[5, 12]$	2.9	3	5	0	
9	$C_xH_{2x-5}O_6N$, $x=[6, 12]$	2.8	3	6	1	
10	$C_xH_{2x-2}O_4$, $x=[6, 10]$	2.7	2	6	0	

a. The nitrogen atom comes from the nitro functional group.

S4.2 Temp-related factor

Table S3. Molecular characteristics of the Temp-related factor. Presented as several sets of compounds, and the members of each sets differ in the addition of a -CH₂ moiety. Only the signals that account for more than one thousandth of the factor are selected to reduce uncertainties. The clustering reagent ion NO₃⁻ or HNO₃NO₃⁻ has been omitted from the formulas.

No.	Formulas	Contribution to the factor (%)	DBE	no	$n_{\rm N}$
1	$C_xH_{2x-4}O_5$, $x=[5, 11]$	10.0	3	5	0
2	$C_xH_{2x-2}O_5$, $x=[5, 10]$	7.8	2	5	0
3	$C_xH_{2x-1}O_6N$, $x=[3, 7]$	6.0	1	6	1
4	$C_xH_{2x-6}O_5$, $x=[5, 11]$	5.4	4	5	0
5	$C_xH_{2x-4}O_6$, $x=[5, 10]$	5.3	3	6	0
6	$C_xH_{2x-3}O_7N$, $x=[4, 10]$	5.0	2	7	1
7	$C_xH_{2x-3}O_6N$, $x=[4, 9]$	4.3	2	6	1
8	$C_xH_{2x-1}O_7N$, $x=[4, 9]$	2.9	1	7	1
9	$C_xH_{2x-4}O_4$, $x=[6, 9]$	2.3	4	4	0
10	$C_xH_{2x-6}O_6$, $x=[7, 11]$	2.1	4	6	0

S4.3 Aliph-OOM factor

Table S4. Molecular characteristics of the Aliph-OOM factor. Presented as several sets of compounds, and the members of each sets differ in the addition of a -CH₂ moiety. Only the signals that account for more than one thousandth of the factor are selected to reduce uncertainties. The clustering reagent ion NO₃⁻ or HNO₃NO₃⁻ has been omitted

from the formulas.

No.	Formulas	Contribution to the factor (%)	DBE	no	nn
1	$C_xH_{2x-3}O_6N$, $x=[4, 12]$	10.0	2	6	1
2	$C_xH_{2x-2}O_8N_2$, $x=[4, 13]$	9.0	1	8	2
3	$C_xH_{2x-3}O_7N$, $x=[5, 12]$	5.9	2	7	1
4	$C_xH_{2x-1}O_6N$, $x=[3, 11]$	5.7	1	6	1
5	$C_xH_{2x-1}O_5N$, $x=[4, 9]$	4.9	1	5	1
6	$C_xH_{2x}O_8N_2$, $x=[4, 9]$	3.4	0	8	2
7	$C_xH_{2x-5}O_7N$, $x=[6, 13]$	2.8	3	7	1
8	$C_xH_{2x-4}O_4$, $x=[6, 10]$	2.8	3	4	0
9	$C_xH_{2x}O_7N_2$, $x=[4, 11]$	2.2	0	7	2
10	$C_xH_{2x-4}O_5, x=[5, 11]$	2.2	3	5	0

S4.4 Photo-related factor

Table S5. Molecular characteristics of the Photo-related factor. Presented as several sets of compounds, and the members of each sets differ in the addition of a -CH₂ moiety. Only the signals that account for more than one thousandth of the factor are selected to reduce uncertainties. The clustering reagent ion NO₃⁻ or HNO₃NO₃⁻ has been omitted from the formulas.

No.	Formulas	Contribution to the factor (%)	DBE	no	$n_{ m N}$
1	$C_xH_{2x}O_8N_2, x=[5]$	18.0	0	8	2
2	$C_xH_{2x-3}O_7N$, $x=[4, 11]$	6.5	2	7	1
3	$C_xH_{2x-1}O_6N$, $x=[3, 10]$	6.3	1	6	1
4	$C_xH_{2x-7}O_4N$, $x=[6, 8]$	3.6	4	4	1 ^b
5	$C_xH_{2x-7}O_3N$, $x=[7, 8]^a$	3.3	4	3	1 ^b
6	$C_xH_{2x-5}O_7N$, $x=[5, 11]$	2.5	3	7	1
7	$C_xH_{2x-4}O_{10}N_2$, $x=[7, 10]$	2.2	2	10	2
8	$C_xH_{2x-3}O_8N$, $x=[5, 10]$	2.1	2	8	1
9	$C_xH_{2x-5}O_8N$, $x=[6, 11]$	2.1	3	8	1
10	$C_xH_{2x-4}O_5, x=[5, 8]$	2.0	3	5	0

a. Do not contain nitro phenol with a carbon number of 6, because we removed it before binPMF. b. The nitrogen atom comes from the nitro functional group.

S4.5 O_x- and SOA-related factor

Table S6. Molecular characteristics of the O_x- and SOA-related factor. Presented as several sets of compounds, and the members of each sets differ in the addition of a -

CH₂ moiety. Only the signals that account for more than one thousandth of the factor are selected to reduce uncertainties. The clustering reagent ion NO₃⁻ or HNO₃NO₃⁻ has been omitted from the formulas.

No.	Formulas	Contribution to the factor (%)	DBE	no	nn
1	$C_xH_{2x-7}O_3N$, $x=[6, 8]$	7.5	4	3	1ª
2	$C_xH_{2x}O_8N_2, x=[5]$	6.4	0	8	2
3	$C_xH_{2x-1}O_6N$, $x=[3, 9]$	6.3	1	6	1
4	$C_xH_{2x-3}O_6N$, $x=[4, 9]$	6.2	2	6	1
5	$C_xH_{2x-2}O_8N_2$, $x=[4, 10]$	4.7	1	8	2
6	$C_xH_{2x-6}O_5$, $x=[6, 10]$	3.5	4	5	0
7	$C_xH_{2x-7}O_4N$, $x=[6, 8]$	3.5	4	4	1 ^a
8	$C_xH_{2x-4}O_5, x=[5, 9]$	2.9	3	5	0
9	$C_xH_{2x-5}O_7N$, $x=[5, 10]$	2.5	3	7	1
10	$C_xH_{2x-1}O_{10}N_3, x=[5]$	1.7	0	10	3

a. The nitrogen atom comes from the nitro functional group.

S4.6 Isop-OOM factor

Table S7. Molecular characteristics of the Isop-OOM factor. Presented as several sets of compounds, and the members of each sets differ in the addition of a '-O' moiety. Only the signals that account for more than one thousandth of the factor are selected to reduce uncertainties. The clustering reagent ion NO₃⁻ or HNO₃NO₃⁻ has been omitted from the formulas.

No.	Formulas	Contribution to the factor (%)	DBE	nc	nn
1	$C_5H_{10}O_xN_2$, $x=[7, 8]$	30.7	0	5	2
2	$C_4H_7O_xN, x=[5, 6]$	9.0	1	4	1
3	$C_5H_9O_xN, x=[4, 7]$	8.8	1	5	1
4	$C_5H_7O_xN, x=[5, 8]$	4.6	2	5	1
5	$C_5H_8O_xN_2, x=[6, 9]$	3.6	1	5	2
6	$C_5H_{11}O_xN$, $x=[5, 6]$	3.5	0	5	1
7	$C_5H_9O_xN_3$, $x=[10]$	2.5	0	5	3

S4.7 BVOC-OOM-I factor

Table S8. Molecular characteristics of the BVOC-OOM-I factor. Presented as several sets of compounds, and the members of each sets differ in the addition of a '-O' moiety. Only the signals that account for more than one thousandth of the factor are selected to reduce uncertainties. The clustering reagent ion NO₃⁻ or HNO₃NO₃⁻ has been omitted from the formulas.

No.	Formulas	Contribution to the factor (%)	DBE	nc	nn
1	$C_5H_9O_xN, x=[4, 8]$	6.0	1	5	1
2	$C_5H_{10}O_xN_2$, $x=[7, 10]$	4.1	0	5	2
3	$C_9H_{15}O_xN$, $x=[6, 9]$	3.6	2	9	1
4	$C_{10}H_{15}O_xN$, $x=[6, 11]$	3.6	3	10	1
5	$C_5H_7O_xN, x=[5, 8]$	3.4	2	5	1
6	$C_5H_8O_xN_2$, $x=[7, 10]$	3.3	1	5	2
7	$C_6H_{11}O_xN$, $x=[5, 9]$	2.9	1	6	1
8	$C_6H_9O_xN, x=[5, 8]$	2.7	2	6	1
9	$C_4H_7O_xN, x=[5, 6]$	2.7	1	4	1
10	$C_7H_9O_xN, x=[6, 8]$	2.5	3	7	1

S4.8 BVOC-OOM-II factor

Table S9. Molecular characteristics of the BVOC-OOM-II factor. Presented as several sets of compounds, and the members of each sets differ in the addition of a '-O' moiety. Only the signals that account for more than one thousandth of the factor are selected to reduce uncertainties. The clustering reagent ion NO₃⁻ or HNO₃NO₃⁻ has been omitted from the formulas.

No.	Formulas	Contribution to the factor (%)	DBE	nc	n _N
1	$C_{10}H_{15}O_xN$, $x=[5, 12]$	9.8	3	10	1
2	$C_{10}H_{17}O_xN$, $x=[5, 10]$	4.4	2	10	1
2	$C_7H_9O_xN, x=[6, 8]$	4.2	3	7	1
4	$C_9H_{15}O_xN$, $x=[6, 9]$	3.7	2	9	1
5	$C_{10}H_{16}O_xN$, $x=[6, 11]$	3.3	2.5	10	1
6	$C_{10}H_{16}O_xN_2$, $x=[7, ,11]$	2.5	2	10	2
7	$C_9H_{13}O_xN$, $x=[6, 10]$	2.2	3	9	1
8	$C_5H_8O_xN, x=[5]$	2.1	1.5	5	1
9	$C_8H_{13}O_xN$, $x=[6, 8]$	1.7	2	8	1
10	$C_6H_{11}O_xN$, $x=[6, 8]$	1.6	1	6	1

S4.9 BVOC-OOM-III factor

Table S10. Molecular characteristics of the BVOC-OOM-III factor. Presented as several sets of compounds, and the members of each sets differ in the addition of a '-O' moiety. Only the signals that account for more than one thousandth of the factor are selected to reduce uncertainties. The clustering reagent ion NO₃⁻ or HNO₃NO₃⁻ has been omitted from the formulas.

No.	Formulas	Contribution to the factor (%)	DBE	nc	nn
1	$C_{10}H_{15}O_xN$, $x=[5, 9]$	7.1	3	10	1
2	$C_8H_{11}O_xN$, $x=[6, 8]$	4.5	3	8	1
3	$C_9H_{15}O_xN$, $x=[5, 8]$	4.4	2	9	1
4	$C_{10}H_{16}O_xN_2$, $x=[7, 10]$	4.1	2	10	2
5	$C_{10}H_{17}O_xN$, $x=[5, 8]$	3.9	2	10	1
6	$C_6H_4O_xN_2, x=[5]$	3.8	4	6	2 ^a
7	$C_7H_{11}O_xN$, $x=[5, 7]$	3.0	2	7	1
8	$C_5H_{10}O_xN_2$, $x=[8]$	2.8	0	5	2
9	$C_{10}H_{18}O_xN_2$, $x=[7, 10]$	2.6	1	10	2
10	$C_9H_{13}O_xN, x=[5, 8]$	2.4	3	9	1

a. The nitrogen atom comes from the nitro functional group.

S5 The dependence of Temp-related factor on temperature

The total concentration of this factor in the gas and aerosol phases was calculated considering the effect of temperature on gas-particle partitioning (Eq. 8), so that we can investigate the possible formation mechanisms from the correlation analysis of Fig. S6 (c) and (d).

$$\zeta_{i} = \left(1 + \frac{C_{i}^{*}}{C_{OA}}\right)^{-1} \tag{8}$$

In equation 1, ζ_i represents the partitioning coefficient (the ratio of the concentration of compound i in the condensed phase to its total concentration in the atmosphere), COA is the total mass concentration of organic aerosol, and C_i *represents the saturation concentration of compound i.

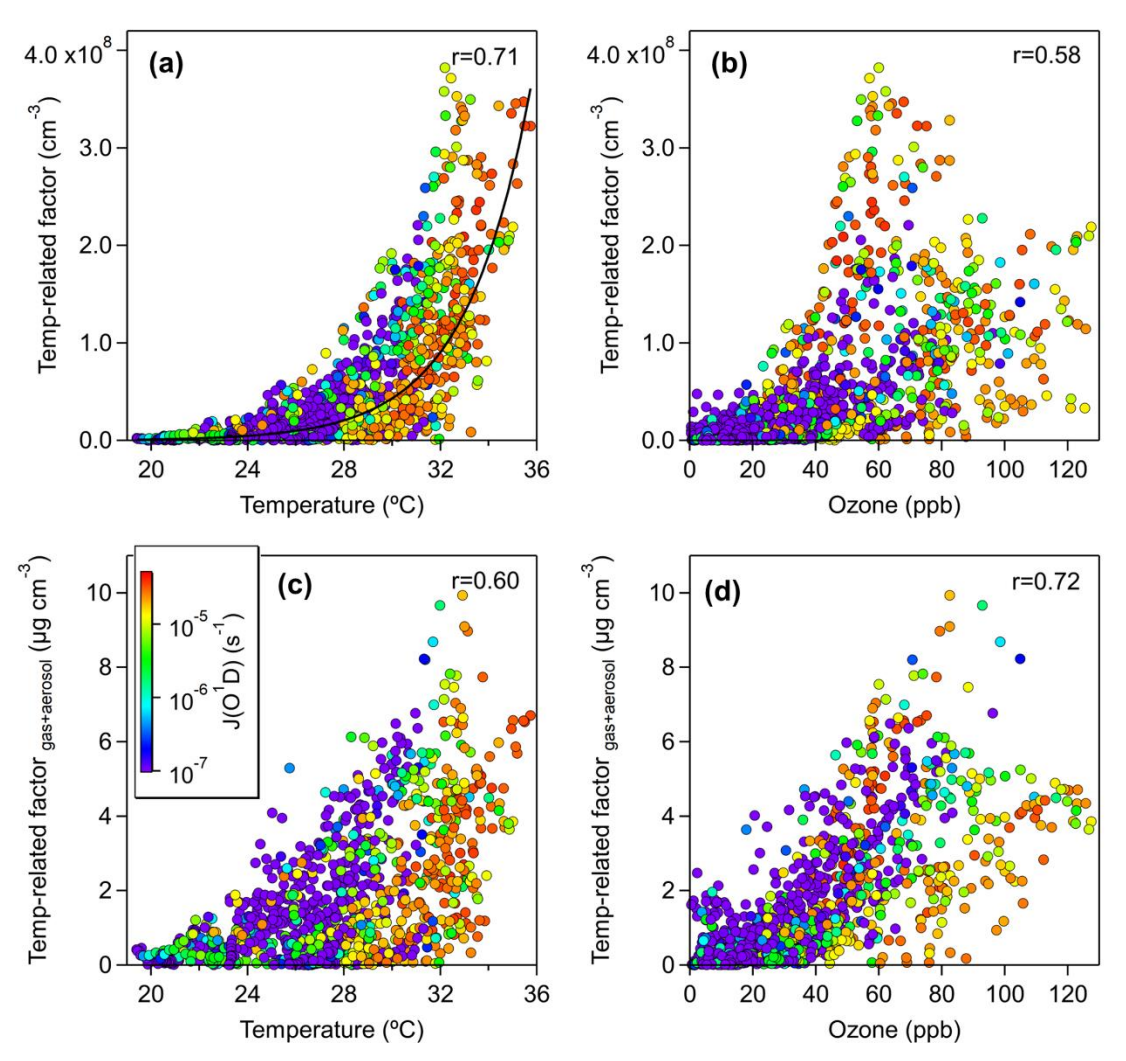


Figure S7. Scatter plots of Temp-related factor with (a) temperature, (b) ozone, the solid black curve in (a) was obtained by e-exponential fitting. All the scatters are colored by $J(O^1D)$, to show the difference between day and night.

S6 Air masses reaching the SORPES station

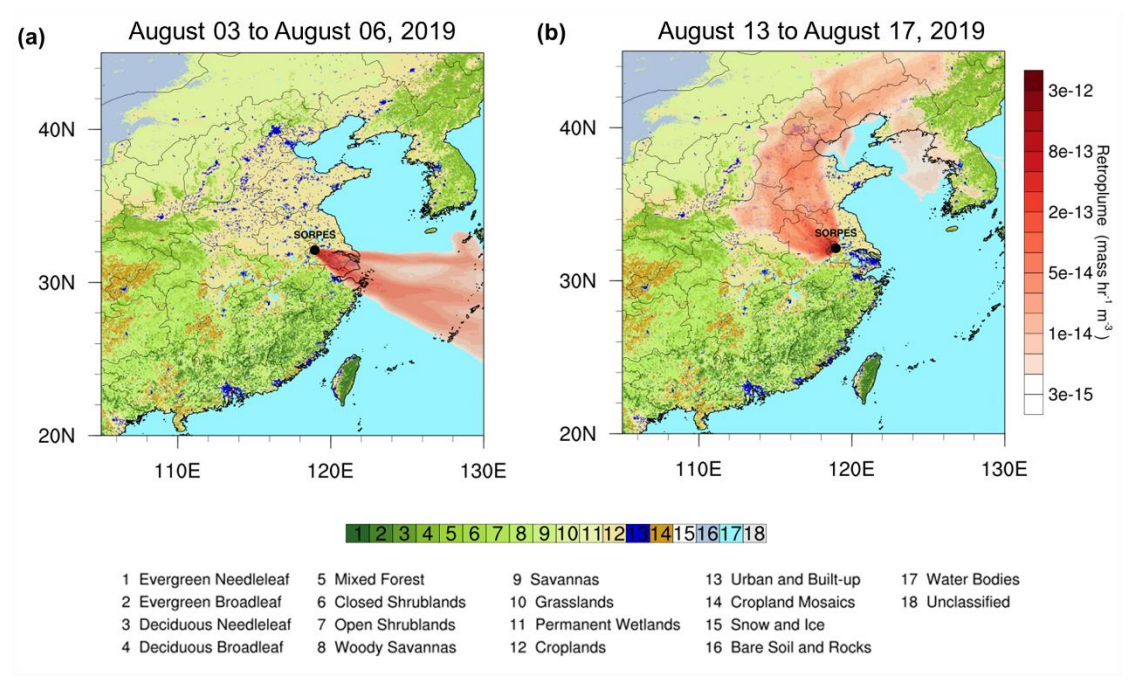


Fig. S8. The averaged retroplumes (i.e., 100 m footprint) based on 3-day backward Lagrangian particle dispersion modeling during (a) August 03 to August 06, 2019, and (b) August 13 to August 17, 2019. Note: Black dot gives the location of the SORPES station. The method of calculating the footprint was developed by (Ding et al., 2013), based on the Hybrid Single-Particle Lagrangian Integrated Trajectory (HYSPLIT) model (Stein et al., 2015). The types of land cover were got from The Terra and Aqua combined Moderate Resolution Imaging Spectroradiometer (MODIS) Land Cover Type (MCD12Q1) (https://lpdaac.usgs.gov/products/mcd12q1v006/, last access: 11 March 2021).

S7 High resolution peak fitting

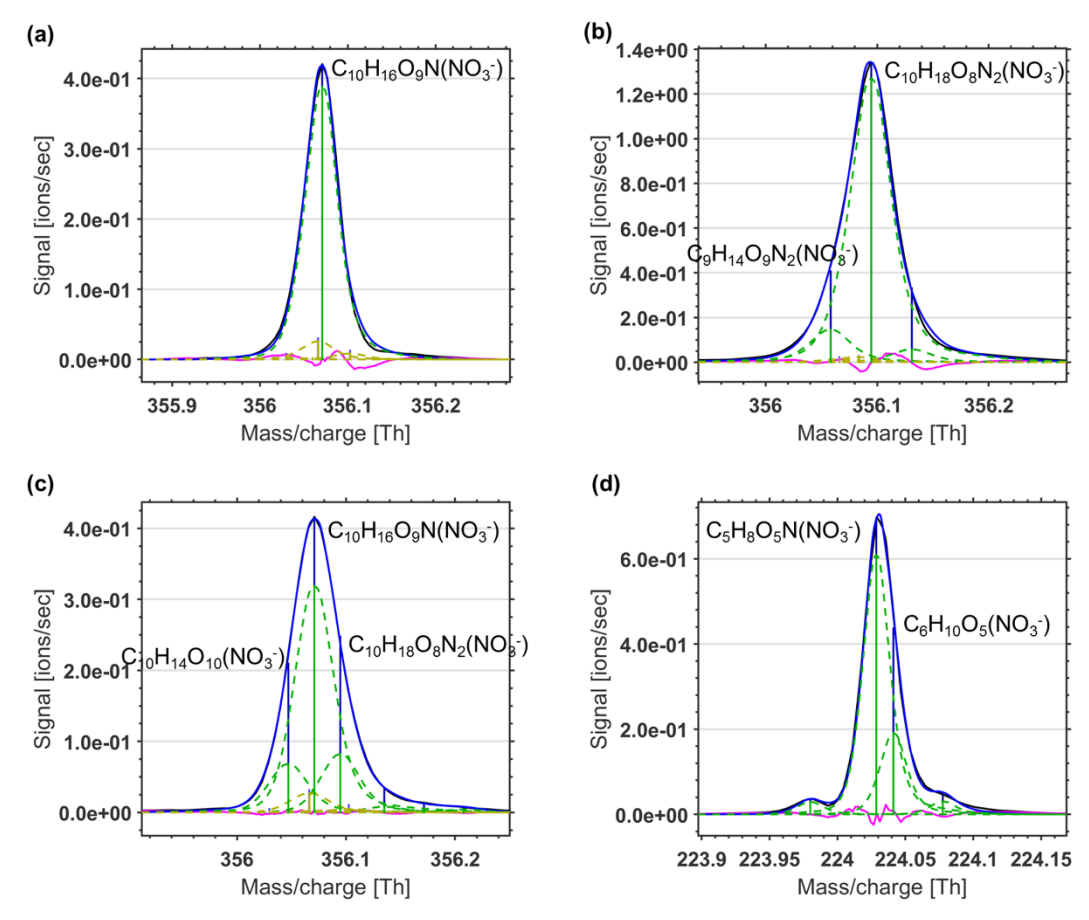


Fig. S9. Examples of peak fitting. Peaks of unit m/z at 356 Th in (a) the BVOC-OOM-I factor, (b) the BVOC-OOM-III factor, and (c) the BVOC-OOM-II factor. Peaks of unit m/z at 224 Th in (d) the BVOC-OOM-II factor. The black solid line is the measured signal, the blue solid line is the total signal of the fitted peaks, the green dashed line denotes the fitted peak, and the purple one is the residual.

Reference

Ding, A., Wang, T., and Fu, C.: Transport characteristics and origins of carbon monoxide and ozone in Hong Kong, South China, Journal of Geophysical Research: Atmospheres, 118, 9475-9488, https://doi.org/10.1002/jgrd.50714, 2013.

Donahue, N. M., Epstein, S. A., Pandis, S. N., and Robinson, A. L.: A two-dimensional volatility basis set: 1. organic-aerosol mixing thermodynamics, Atmospheric Chemistry and Physics, 11, 3303-3318, 10.5194/acp-11-3303-2011, 2011.

Epstein, S. A., Riipinen, I., and Donahue, N. M.: A Semiempirical Correlation between Enthalpy of Vaporization and Saturation Concentration for Organic Aerosol, Environmental Science & Technology, 44, 743-748, 10.1021/es902497z, 2010.

Kroll, J. H., Donahue, N. M., Jimenez, J. L., Kessler, S. H., Canagaratna, M. R., Wilson, K. R., Altieri, K. E., Mazzoleni, L. R., Wozniak, A. S., Bluhm, H., Mysak, E. R., Smith, J. D., Kolb, C. E., and Worsnop, D. R.: Carbon oxidation state as a metric for describing

the chemistry of atmospheric organic aerosol, Nature Chemistry, 3, 133-139, 10.1038/nchem.948, 2011.

Polissar, A. V., Hopke, P. K., Paatero, P., Malm, W. C., and Sisler, J. F.: Atmospheric aerosol over Alaska: 2. Elemental composition and sources, Journal of Geophysical Research: Atmospheres, 103, 19045-19057, https://doi.org/10.1029/98JD01212, 1998. Stein, A. F., Draxler, R. R., Rolph, G. D., Stunder, B. J. B., Cohen, M. D., and Ngan, F.: NOAA's HYSPLIT Atmospheric Transport and Dispersion Modeling System, Bulletin of the American Meteorological Society, 96, 2059-2077, 10.1175/BAMS-D-14-00110.1, 2015.

Stolzenburg, D., Fischer, L., Vogel, A. L., Heinritzi, M., Schervish, M., Simon, M., Wagner, A. C., Dada, L., Ahonen, L. R., Amorim, A., Baccarini, A., Bauer, P. S., Baumgartner, B., Bergen, A., Bianchi, F., Breitenlechner, M., Brilke, S., Mazon, S. B., Chen, D., Dias, A., Draper, D. C., Duplissy, J., El Haddad, I., Finkenzeller, H., Frege, C., Fuchs, C., Garmash, O., Gordon, H., He, X., Helm, J., Hofbauer, V., Hoyle, C. R., Kim, C., Kirkby, J., Kontkanen, J., Kuerten, A., Lampilahti, J., Lawler, M., Lehtipalo, K., Leiminger, M., Mai, H., Mathot, S., Mentler, B., Molteni, U., Nie, W., Nieminen, T., Nowak, J. B., Ojdanic, A., Onnela, A., Passananti, M., Petaja, T., Quelever, L. L. J., Rissanen, M. P., Sarnela, N., Schallhart, S., Tauber, C., Tome, A., Wagner, R., Wang, M., Weitz, L., Wimmer, D., Xiao, M., Yan, C., Ye, P., Zha, Q., Baltensperger, U., Curtius, J., Dommen, J., Flagan, R. C., Kulmala, M., Smith, J. N., Worsnop, D. R., Hansel, A., Donahue, N. M., and Winkler, P. M.: Rapid growth of organic aerosol nanoparticles over a wide tropospheric temperature range, Proc. Natl. Acad. Sci. U. S. A., 115, 9122-9127, 10.1073/pnas.1807604115, 2018.

Yan, C., Nie, W., Äijälä, M., Rissanen, M. P., Canagaratna, M. R., Massoli, P., Junninen, H., Jokinen, T., Sarnela, N., Häme, S. A. K., Schobesberger, S., Canonaco, F., Yao, L., Prévôt, A. S. H., Petäjä, T., Kulmala, M., Sipilä, M., Worsnop, D. R., and Ehn, M.: Source characterization of highly oxidized multifunctional compounds in a boreal forest environment using positive matrix factorization, Atmospheric Chemistry and Physics, 16, 12715-12731, 10.5194/acp-16-12715-2016, 2016.

Zhang, Q., Jimenez, J. L., Canagaratna, M. R., Ulbrich, I. M., Ng, N. L., Worsnop, D. R., and Sun, Y.: Understanding atmospheric organic aerosols via factor analysis of aerosol mass spectrometry: a review, Anal Bioanal Chem, 401, 3045-3067, 10.1007/s00216-011-5355-y, 2011.

Zhang, Y., Peräkylä, O., Yan, C., Heikkinen, L., Äijälä, M., Daellenbach, K. R., Zha, Q., Riva, M., Garmash, O., Junninen, H., Paatero, P., Worsnop, D., and Ehn, M.: A novel approach for simple statistical analysis of high-resolution mass spectra, Atmos. Meas. Tech., 12, 3761-3776, 10.5194/amt-12-3761-2019, 2019.